Master's Theses (2009 -)   Dissertations, Theses, and Professional Projects

Examining the Relationships Among Injury Outcomes, Velocity and Grip Strength During Dynamic Platform Perturbation

Braden Cripe
Marquette University

www.manaraa.com

EXAMINING THE RELATIONSHIPS AMONG INJURY OUTCOMES,
VELOCITY AND GRIP STRENGTH DURING
DYNAMIC PLATFORM
PERTURBATION

by

Braden A. Cripe, B.S.

A Thesis submitted to the Faculty of the Graduate School,
Marquette University,
in Partial Fulfillment of the Requirements for
the Degree of Master of Science

Milwaukee, Wisconsin

August 2011

ABSTRACT
EXAMINING THE RELATIONSHIPS AMONG INJURY OUTCOMES,
VELOCITY AND GRIP STRENGTH DURING
DYNAMIC PLATFORM
PERTURBATION

Braden A. Cripe, B.S.

Marquette University, 2011

Studies examining the relationship between inputs and outputs for simulated models of dynamically perturbed horizontal platforms are scarce. Most of these scenarios include a standing operator with upper extremity grip, oftentimes subjected to lateral impulses, which may lead to occupant injury. While the detailed study of these collision scenarios is sparse, the prevalence of their application is great.

This thesis aims to identify how two input parameters, velocity change (ΔV) and grip strength, affect injury assessment reference values (IARVs). This is accomplished by using Mathematical Dynamic Modeling (MADYMO) software to simulate the scenarios defined by those inputs. In the simulation, an anthropometric test device (ATD) representing the operator is placed in a streamlined quadrilateral model (SQM) representing the dynamic horizontal platform. The SQM is subjected to a deceleration impulse which arrests its motion, causing the ATD to fall and sustain injury.

Results from the series of collision scenarios lend themselves to a modified quadratic regression which adequately predicts head injury criteria (HIC), head angular velocity, neck injury criteria (NIC) shear in the positive direction, and NIC-bending in the negative direction. Quantitative analysis of IARVs shows that high grip strengths tend to protect the occupant from injury, while higher ΔVs do not necessarily correlate to injury exacerbation. Visual examination of the collision series at high ΔVs show the ATD being ejected from the SQM, rebounding off the ground, and rolling onto its back. Following from the visual results, it can be concluded that translational movement parallel to the ground and anterior-posterior impacts to the ATD reduce injury. Ejection from the SQM cabin is not correlated with injury reduction because trials where a lateral constraint (door) was present showed dramatically reduced IARVs at the highest ΔV and lowest grip strength condition.

ACKNOWLEDGMENTS

Braden A. Cripe, B.S.

TABLE OF CONTENTS

LIST OF TABLES

LIST OF FIGURES

LIST OF ACRONYMS

ANSI: American National Standards Institute

AP: Anterior-posterior

ATD: Anthropometric Test Device

BEV: Barrier Equivalent Velocity

BLS: Bureau of Labor Statistics

BOS: Base of Support

CFC: Channel Frequency Class

COG: Center of Gravity

DOF: Degree of Freedom

FE: Finite Element

FMVSS: Federal Motor Vehicle Safety Standard

GSI: Gadd Severity Index

HIC: Head Injury Criterion

IARV: Injury Assessment Reference Value

MADYMO: Mathematical Dynamic Model

MB: Multi-body

MFCL: Multi-functional Control Lever

NEISS: National Electronic Injury Surveillance System

NHTSA: National Highway Traffic Safety Administration

NIC: Neck Injury Criteria

N_{ij}: Neck Injury Predictor

OIICS: Occupational Injury and Illness Classification System

OSHA: Occupational Safety and Health Administration

PA: Posterior-anterior

PIT: Powered Industrial Truck

PIV: Powered Industrial Vehicle

PMHS: Post-mortem Human Surrogate

RITA: Research and Innovative Technology Administration

SDS: Supplementary Data System

SQM: Streamlined Quadrilateral Model

WSTC: Wayne State Tolerance Curve

1   INTRODUCTION

1.1 Background

1.1.1 Overview

Powered industrial vehicles (PIVs), motorized gardening equipment, and public transportation systems are common modes of transport for materials and people. These vehicles require operators to navigate their environments, accomplishing various tasks demanded by their respective occupational duties. Common to all of these vehicles is the prevalence of standing operators or passengers, who may be subjected to unexpected acceleration or deceleration scenarios. Given that there are a possible 1.5 million daily standing users of powered industrial vehicles and motorized gardening equipment, and 35 million standing and sitting users of public transportation systems, injurious situations are common [3, 5, 9, 30, 75, 82].

Two methods have been used to evaluate the consequences of acceleration/deceleration scenarios with standing subjects: postural stability assessment and injury outcome assessment. Postural stability assessment focuses on how well a subject can maintain standing posture during perturbation of a horizontal platform. Seminal work by Hirschfield showed that footing was lost at 0.15g acceleration [35]. Further studies by DeGraaf et al. and Jonkees et al. revealed that subjects are less able to cope with perturbations in the lateral direction as compared to forward or rearward directions [19, 32, 33, 40]. These findings were later corroborated by Harris et al., putting the limits of lateral acceleration between 0.065 and 0.110g [32, 33].

Injury outcome assessment focuses on the biomechanical effects of acceleration/deceleration with respect to selected body parts. Oftentimes, tests for injury

are performed with fresh frozen cadavers or animal models which are scaled to humans [70-73]. Threshold values for injury, called injury assessment reference values (IARVs), are then proposed, which provide a means of comparison for future tests. IARVs serve as a standard of safety that is upheld by government organizations such as the National Highway Traffic Safety Administration (NHTSA) in their Federal Motor Vehicle Safety Standards (FMVSS) [66]. Injury may follow postural stability loss; therefore, the assessment of injury might provide ample information on the given scenario without the additional analysis of postural stability.

When considering injurious situations, collision scenarios are of particular concern. Collision scenarios are indicated when a moving vehicle's motion is arrested by a sudden deceleration caused by contact with an immovable external object. These scenarios are oftentimes too quick for the operator/passenger to apply preventative action for falls as a typical collision may last 100 ms and dynamic reaction time is at least 90 ms [37, 95].

Although the reaction time for an occupant in a collision scenario may be inadequate to prevent falls, operators of industrial equipment and public transit passengers are afforded a safeguard against injury due to upper extremity grip with the vehicle interior. Work by Hausbeck et al. showed that even minimal hand contact with an object improves postural stability in a visually perturbed environment. This improved stability may mitigate subsequent injury [34].

Another factor which may affect injury is velocity change (ΔV) of the vehicle during collision. A higher ΔV will induce greater peak deceleration for a given collision

[95]. The probability of losing grip, falling, and subsequently injuring oneself is expected to be higher with an increased ΔV.

Because the human body mimics an inverted pendulum during fall scenarios, the head and neck experience the largest angular displacement, thereby making them prone to severe injury. Studies of automobile collisions also show that the head and neck are most susceptible to severe injury [53, 87, 94]. Although they are under-represented in forklift accidents, study of the IARVs of the head and neck may provide information on the worst-case scenario injuries to the body.

This thesis aims to interconnect the elements of a side stance collision scenario to better understand how the inputs are related to IARVs. The benefit to this thesis is that it will be entirely performed through computer simulation in Mathematical Dynamic Modeling (MADYMO) software (TASS Americas, Livonia, MI) which has complete reproducibility, therefore making the simulation deterministic [88]. This will afford a more consistent, safe and efficient method to study the relationship of inputs and outputs by removing human interaction components prevalent in live testing. Inputs to the computational model will be ΔV and grip strength and outputs will be selected head and neck IARVs.

MADYMO is designed to provide simulation of complex dynamic systems requiring computational intensity. If the inputs can be successfully mapped to the outputs, then a predictive regression equation might be derived and disseminated, thereby simplifying computation for this application. This equation may provide operational limits for industrial and service vehicles with respect to injury.

1.1.2   Associated Injury Survey

PIVs, motorized gardening equipment (i.e., riding mowers), and public transportation systems have a possible 1.5 million daily standing users and another 35 million standing/sitting users [5, 9-11, 30, 64, 81]. These vehicles share common features such as moving horizontal platforms on which operators or passengers must stand with upper extremity grip. Their extensive applications and inherent environments increase the probability for injuries to either operators or users.

While PIVs may increase the efficiency of production, their misuse or malfunctioning can cause accidents which may lead to injury or fatality. From the number of accidents recorded, collision scenarios represented 41-86% of forklift accidents, which may include collisions with a fixed, moving, or intruding object [16, 46, 78, 86]. Of those collision accidents, 45% resulted in severe injury or fatality [78].

According to the Bureau of Labor Statistics (BLS), from 2005 to 2009 PIVs accounted for an average of 13,540 injuries and 267 fatalities per year [10, 74]. Of those PIVs, forklifts accounted for an annual average of 10,900 injuries and 76 fatalities, although some Occupational Safety and Health Administration (OSHA) estimates put those values at 34,900 injuries and 85 fatalities (Table 1) [10, 74, 78, 86]. Using the BLS data, this amounts to a fatality to injury ratio of 0.70%, as compared to the national average of 0.48% (Table 1) [10]. Of the 568,270 industrial truck and tractor operators working in 2009, injuries were sustained by 1.9% of workers, as compared to the national average of 0.86% (Table 1) [9]. Data for these injuries and fatalities was found using the Supplementary Data System (SDS) for workplace injury and fatality published

by the BLS. Specific searches used the injury source codes for PIVs (85) and forklifts (851) defined by the Occupational Injury and Illness Classification System (OIICS) [11].

The majority of injuries sustained during forklift accidents are to the lower extremities (Table 2) [10]. These occur mostly during forklift tip-over or off-dock scenarios where the operator egresses the compartment and gets pinned/crushed by the falling forklift. Crush injuries are the most common type of injury incurred during forklift accidents [7, 12, 43, 60, 78, 85]. Despite the prevalence of lower extremity crush injuries, head and neck injuries may prove to be more important for study due to their severity. Representing between 5.9 and 12.2% of forklift injuries, head/neck injuries may cause concussions, contusions, spinal cord damage or death , all of which can have more profound, longer lasting effects than lower extremity injuries (Table 2) [10, 12, 26, 48, 53, 85, 87].

An estimated $135 million is attributed to the cost of forklift accidents [13]. Forklift accidents also accounted for 11,040 lost work claims per year, with an estimated 9-16 weeks lost per claim [12, 13, 16]. Given that there are nearly 1 million forklifts driven daily, the mitigation of injuries and lost production could profoundly impact the industries that forklifts serve [13, 86].

Riding mowers provide a more efficient means to landscape, but the same mechanisms which expedite the workload, such as standing platforms and quick-turn maneuverability, may also present injury risks. According to BLS, there were 859,960 landscaping workers in the United States as of May 2009 (Table 1) [9]. Riding mowers accounted for 13,580 injuries and 19 fatalities from 2005 to 2009, although some National Electronic Injury Surveillance System (NEISS) estimates show up to 15,978

annual riding mower injuries (Table 1) [10, 17, 64, 83]. All totaled, riding mowers amount to a 1.6% injury to worker ratio and a 0.14% fatality to injury ratio (Table 1) [5, 9-11, 30, 64, 81].

Of those injuries sustained to riding mower operators, 4.0-22.9% were attributed to falling off the mower [17, 31]. This typically results in lacerations, fractures, contusions, and sprains [17, 31, 83]. While most injuries are to the trunk (30.2%), head and neck injuries comprise 5.4-10.5% of riding mower injuries (Table 2) [10, 31].

Public transportation facilitates commute for people within and outside of their community, but the nature of public transportation systems necessitates frequent random acceleration/deceleration maneuvers. In fact, 34.5-54% of bus injuries are attributed to acceleration/deceleration impulses [23, 30, 75]. These impulsive maneuvers can lead to injury, particularly with standing passengers, who represent 28-55.8% of bus incidents [3, 30, 75, 82].

According to the Research and Innovative Technology Administration (RITA) 8,260 injuries and 125 fatalities are attributed to public transportation systems per year (Table 1) [81]. While the sheer number of injuries and fatalities are comparable to forklifts and riding mowers, the 10.2 billion trips taken by public transit passengers makes the injury risk negligible (Table 1) [81]. However, the injury location, and subsequent mechanism, may be affected by the type of incident: collision or non-collision.

The majority of incidents for passenger buses occur during non-collision scenarios (54-62.6%), with head/neck injuries more prevalent in collision scenarios [8,

30]. Of injuries sustained by bus passengers, 23-39% were to the head/neck (Table 2) [2, 8, 30, 75, 82]. This rate is 6-10 times higher than that for forklifts or riding mowers.

Table 1: Injury and fatality statistics for standing operation and passenger vehicles [5, 9-11, 30, 64, 81]

Source [Occupation]	Source Code [Occupation Code]	Number of Users (from occupation)	Number of Injuries (from source)	Number of Fatalities (from source)	Ratio of Fatality to Injury	Ratio of Injury to Users
All Sources [All Occupations]	- [00-0000]	130,647,610	1,124,036	5,537	0.48%	0.86%
Forklift [Industrial Truck & Tractor Driver]	851 [53-7051]	568,270	10,900	76	0.70%	1.9%
Lawn Mowers - Riding [Landscaping Worker]	3122 [37-3011]	859,960	13,580[†]	19	0.14%	1.6%
Public Transit Systems [Passenger]	- [-]	10.2 billion[‡]	8,260[§]	125[§]	1.5%	~0.0%

Note: all data is taken from 2005-2009 BLS SDS for workplace injury unless otherwise specified
† Data taken from NEISS CSPC 2009 query of powered lawn mowers [64]
‡ Data taken from APTA 2011, relating to number of passenger trips [5]
§ Data taken from RITA 2010 statistics for transit safety [81]

Table 2: Percentage breakdown of injury by body part [8, 10, 30, 82]

Source	Head (%)	Neck (%)	Trunk (%)	Upper Extremity (%)	Lower Extremity (%)
Forklift	5.1	1.3	17.9	13.6	51.7
Lawn Mowers – Riding	2.5	8.0	31.2	15.1	26.6
Public Transit Systems	15[†]	24[†]	13[†]	21[†]	26[†]

Note: all data is taken from 2005-2009 BLS SDS for workplace injury unless otherwise specified
† Data taken from Björnstig et al. 2005 for bus and coach occupants [8, 30, 82]

1.1.3 Variable Velocity and Grip Strength

Vehicle collision studies that include the low velocity operating ranges inherent to PIVs, riding mowers, and low-speed public transit (11.1-16.1 km/h) are typically directed towards seated auto collisions. These cannot adequately capture the injury mechanisms prevalent in standing operation. For the limited studies which do examine standing operation scenarios, those based on government databases lack essential information on quantitative initial parameters, such as velocity. Furthermore, the studies

performed with controlled initial parameters do not systematically increment initial velocity with multiple tests to examine its effect on injury outcome.

Grip strength studies, although informative for human physiological limits of the hand, do not provide information on the application for the data. These studies are simple quantitative measures of grip strength in static scenarios. Dynamic assessment of grip strength could provide more insight into how standing operators/passengers would react in collision scenarios. One study by Hausbeck et al., assessed grip in a dynamic environment, however, this was irrespective of grip strength, and its study outcome was postural stability, not IARVs [34]. Another study by Palacio et al., included grip strength in a dynamic simulation of a public bus, however it did not use variable grip strengths and was only intended for case-specific non-collision scenarios [75].

Inclusion of velocity and grip strength in the study of collision scenarios has yet to be performed with consistency. Incrementing these variables may provide a more systematic approach to assessing how these inputs relate to injury outcomes (i.e., IARV).

1.1.4   *Vehicle Types with Dynamic Horizontal Platform Operation*

Industrial, gardening and public vehicles are used to facilitate occupational duties in the industrial, manufacturing, and service sectors. These vehicles are a means to expedite the process of moving products, altering landscape, or transporting people. Oftentimes the previously mentioned vehicles require the operator or passengers to maintain a standing posture while the vehicle undergoes acceleration, deceleration, braking, and turning maneuvers. Such maneuvers can impose stability difficulties on the

operator or passenger, which can lead to a loss of standing posture, and subsequent contact with either the ground or interior surfaces of the vehicle. Contact with the ground or interior surfaces can cause injury, especially when considering the velocities at which these vehicles can travel and the lack of restraint systems in place to protect against injury. The three categories of vehicles discussed in this paper will include PIVs, motorized garden equipment, and public transportation systems. An example of each type of vehicle is shown in Figure 1 [47, 68, 76].

PIVs including powered industrial trucks (PITs), powered industrial carriers and tractors (a sub-class of powered industrial trucks) are ubiquitous in material handling environments. PIVs are used to transport materials around warehouses, manufacturing plant floors, consumer stores, or outdoor industrial sites. These vehicles are of concern for injury because they can travel up to 12.1 km/h (7.5 mph) oftentimes with a standing operator who may experience obstructed views, difficult steering methods, and few safety measures to prevent egress from the vehicle compartment [18, 62, 68]. While all PIVs may pose injury concerns, PITs are indicated for study in this thesis because of the stand-up operation and upper extremity grip with the vehicle controls.
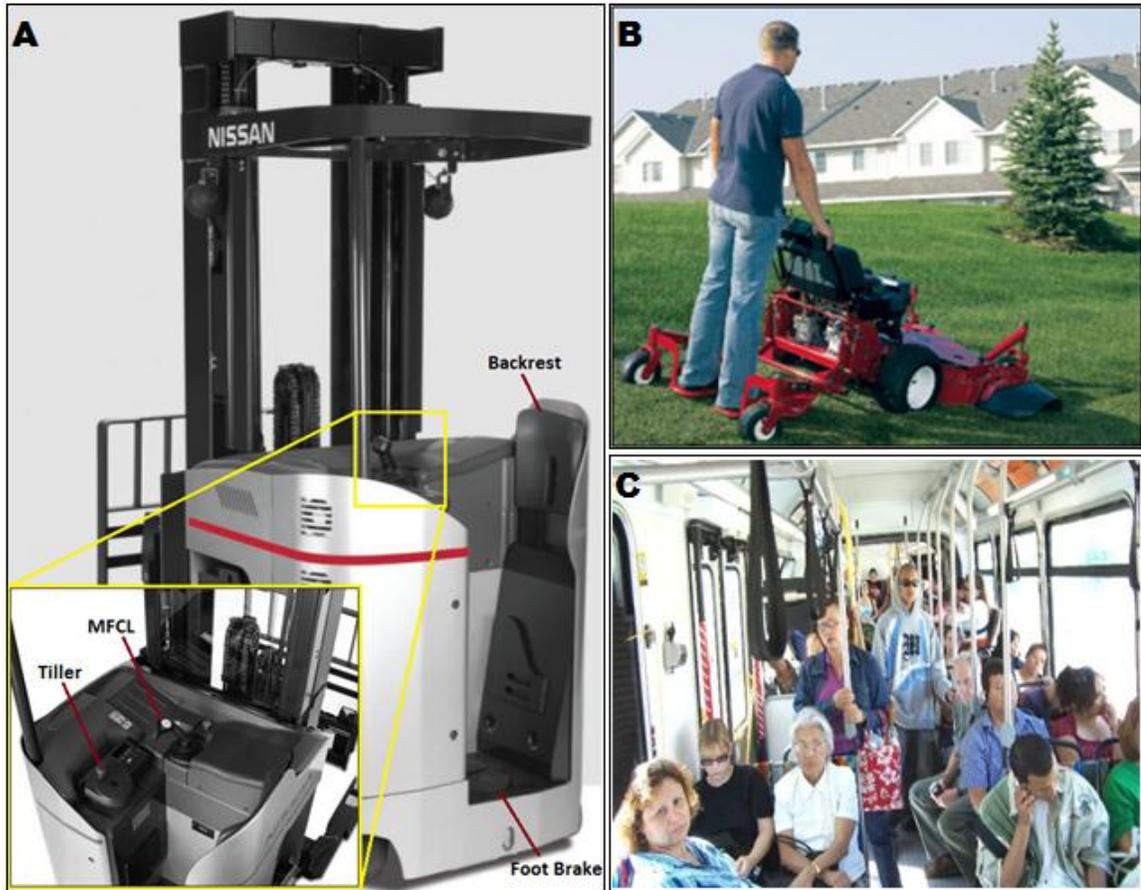
Figure 1: Dynamic horizontal platform vehicle types including: (A) stand-up forklift and control panel with multi-functional control level (MFCL) and tiller used for steering and operation, the backrest for support, and the foot brake pedal for emergency stopping [68]**. Adapted with permission from ©Nissan Forklift. (B) standing sulky attachment for walk-behind mower** [76]**. Reprinted with permission from ©Irrigation & Green Industry. (C) public bus interior with standing passengers** [47]**. Reprinted with permission from ©Light Rail Now**

Specific controls of stand-up PITs (forklifts) necessitating study in this thesis include the multi-functional control lever (MFCL) and tiller used for steering and material handling operation as well as the emergency brake pedal (Figure 1) [20, 68]. An operator will grip the tiller with the left hand, the MFCL with the right hand, and step on the emergency brake with the left foot (excluding brake activation, where the left foot is raised). Some operators also lean against the backrest shown in Figure 1; however, this operator orientation was not studied in this thesis [68].

Forklifts come in a variety of styles according to their application, which have been categorized into seven classes [74]. Classes I-III receive further focus in this thesis because they can travel up to 12.1 km/h (7.5 mph) oftentimes with a standing operator who may experience obstructed views, difficult steering methods, and few safety measures to prevent egress from the vehicle compartment [18, 62, 68].

Concern for operator ejection from the forklift control compartment is particularly important in Class I-III stand-up type forklifts. Operators may be lifting the left foot to engage the emergency brake with only the MFCL, tiller, and backrest as leverage for restraint. Most inexperienced operators use the emergency brake to slow down, thereby invoking a one-leg stance, while more experienced operators use a method called "plugging", where they put the forklift in reverse while it is still progressing forward [41].

Federal regulations for stand-up forklift design promote operator egress from the forklift compartment in an emergency. Section 7.30.3 from the 2009 version of the American National Standards Institute (ANSI) B56.1 safety standard for low lift and high lift trucks states that "operator protection means shall be designed…to permit rapid exit in an emergency" [4]. This requirement is again restated in section 7.36 part b where "operator enclosures…if provided, shall permit easy ingress and egress from the platform" [4]. However, "easy ingress and egress" are not defined in the ANSI B56.1 standard.

In section 7.41 the requisite operator protection mechanisms and enclosures for sit-down vs. stand-up forklifts contradict each other. In the paragraph of section 7.41 pertaining to sit-down forklifts, a "restraint device…is intended to assist the operator in

reducing the risk of entrapment of the operator's head and/or torso between the truck and ground in the event of a tip-over" [4]. Contrarily, stand-up forklifts "shall be designed with open operator compartments to permit easy ingress and egress" and "a free and easy egress from the truck in the event of an imminent tipover or off-the-dock accident" [4]. Recognizing that jumping or ejection from the operator compartment increases injury risk, it seems that current safety standards are at odds with current safety research [7, 86]. As such, considerations for lateral safety restraints such as doors are contraindicated by law for forklifts, which may obligate the operator to maneuver a forklift without maximal possible safety measures.

Garden equipment types, particularly lawn mowers, are of interest for injury because many models are driven and some models allow for stand-up operation. Lawn mowers come in two varieties: walk-behind and riding. Walk-behind mowers are convenient to use because they are cheaper, lightweight, and safer on sloped terrain [91]. For walk-behind mowers, there is an attachment called a sulky that provides a platform on which the operator can ride. This platform permits the operator to either sit or stand allowing for faster mowing and increased productivity (Figure 1) [76, 91]. Riding mowers also include subtypes which allow for standing operation. The rider maintains balance with a stand-on mower by leaning their thighs and hips against a cushion while standing on a suspension platform [91]. Stand-on riding mowers are indicated in this thesis because of their stand-up operation on a horizontal platform and upper extremity grip with mower controls.

Public transportation systems can carry passengers to work, school, social activities, or medical related activities [6]. Modes of public transportation include buses,

streetcars, trolleys, and commuter trains [5, 6, 10]. Transit systems can range from an average speed of 11.6 km/h (7.2 mph) for a trolleybus to 50.2 km/h (31.2 mph) for commuter trains [6]. These high speeds may be experienced on pre-defined tracks with monitored acceleration/deceleration profiles, or on heavily-trafficked city streets with irregular acceleration/deceleration profiles.

1.1.5   Inception of Injury Assessment Reference Values (IARVs)

IARVs are used as quantitative measures of injury to human body segments based on kinetic and kinematic data obtained during experimentation. Proposals for IARVs have been submitted by researchers based on the need to simplify the biomechanical injury outputs of an experiment into a more usable form. As IARVs are proposed, validated, and accepted they become standards in the biomechanical field and can be easily interpreted/analyzed between researchers performing comparable experiments.

For the purposes of this thesis, IARVs for the head and neck will be examined. Head IARVs include head injury criterion (HIC), angular velocity (ω, omega), and angular acceleration (α, alpha). Neck IARVs include neck injury criteria (NIC) and neck injury predictor (N_{ij}).

HIC is the oldest of the IARVs, established in part through the adaptation of previously proposed head injury assessment methods developed over 50 years ago, and is the most widely used IARV [42, 90]. The need for a head injury criterion was originated in response to the number of severe head injuries incurred during motor vehicle accidents [42]. HIC was developed through the modification of two other head

injury assessment methods: the Wayne State Tolerance Curve (WSTC) and the Gadd Severity Index (GSI). As each method was revised, the previous became obviated.

The current HIC was first conceived by Versace in 1971 from a highly critical paper of the GSI and WSTC. Versace identified three major drawbacks to the GSI and WSTC: the conformity and accuracy of data sets used in curve compilation, the scalability of injury, and the chosen exponential weighting factor. In addressing these drawbacks, Versace effectively created the HIC formula (Equation 1) [42, 53, 66, 69, 90, 96].

The HIC formula was soon modified by NHTSA, then implemented as a federal standard for safety in 1972, replacing GSI as the head injury criterion in FMVSS 208 [42, 66]. Later revisions constrained the time window ($t_2 - t_1$) to 36 ms, with an injury threshold value of 1000 for a mid-sized male [66].

$$HIC_{36} = max \left[\frac{1}{t_2 - t_1} \int a(t) \cdot dt \right]^{2.5} (t_2 - t_1) \qquad (1)$$

In Equation 1, $a(t)$ is the acceleration at time t, while t_1 and t_2 are the start and end times of the 36 ms sliding window.

Angular velocity and angular acceleration are useful kinematic measures of inertial (non-contact) head injury. While their formulation was not specific to biomechanical applications, their usage provides information of rotational head injury. Angular velocity and acceleration can be defined from the rotational motion of a body, without respect to any single point or reference to the center of rotation [63]. Angular velocity can be determined by tracking the linear velocity of two points on a non-

deformable (rigid) body given the distance between those points (Equation 2) [63]. The angular acceleration can be derived from the angular velocity (Equation 3) [63].

$$\omega = \frac{(V_A - V_B)}{r} \tag{2}$$

$$\alpha = \frac{\frac{d}{dt}(V_A - V_B)}{r} \tag{3}$$

In Equation 2 and Equation 3, ω is angular velocity, α is angular acceleration, V_A and V_B are linear velocities of points on the rigid body, and r is the distance between those points.

If the center of rotation is assumed, then only one point needs tracking. For the head, the assumed center of rotation is the midpoint between the occipital condyles, which lie at the juncture of the basilar skull, and the C1 vertebra (atlas vertebra) [56]. When considering neck kinetics, which will be discussed later, the occipital condyles are commonly used as the fulcrum for rotation between the head and neck [56].

Rotation of the head during non-contact scenarios is probable considering that the fulcrum of the head-neck complex will cause the head to rotate unless the torso and head are translated at the same velocity in the same direction (i.e., rigid translation of the upper body) [63]. Contact scenarios will cause angular acceleration unless the impact locus is directed towards or away from the center of rotation [26]. Any imposed angular acceleration will rotate the brain with respect to the skull, straining the brain stem and spinal cord, which has been found as a typical cause of concussions and closed head injuries [28, 29, 48, 84, 98].

Injury thresholds for angular velocity and acceleration widely differ in the biomechanical field. Seminal work on primate whiplash testing by Ommaya et al. in 1971 showed that chimpanzees suffered concussions at an angular velocity tolerance limit of 70 rad/s, while squirrel monkeys had a limit of 300 rad/s [72]. To associate impact results with human tests, Ommaya et al. developed an angular acceleration scaling factor based on brain mass ratio of the human to the primate (Equation 4) [73]. When using an integrated version of the scaling factor shown in Equation 5, the concussive tolerance limit for humans was found to be between 18.6 rad/s and 37.0 rad/s (Table 3) [72, 73]. Furthermore, Ommaya et al. found the angular acceleration tolerance limit to be 1800 rad/s^2 (Table 3) [72].

$$\ddot{\theta}_h = \ddot{\theta}_p \left(\frac{M_p}{M_h}\right)^{\frac{2}{3}} \tag{4}$$

$$\dot{\theta}_h = \dot{\theta}_p \left(\frac{M_p}{M_h}\right)^{\frac{2}{3}} \tag{5}$$

In Equation 4 and Equation 5, $\dot{\theta}_h$ and $\ddot{\theta}_h$ are the angular velocity and acceleration of the human head, $\dot{\theta}_p$ and $\ddot{\theta}_p$ are the angular velocity and acceleration of the animal surrogate head, M_p is the mass of the animal surrogate brain, and M_h is the mass of the human brain. For reference, the rhesus monkey brain is 70-100g, the squirrel monkey (20-27g), the chimpanzee (350-500g) and the human (1300g) [72, 73].

Tests of cadaver head impacts performed by Löwenhielm in 1974 found that closed head injury will likely occur at angular accelerations above 4500 rad/s^2 and/or

angular velocities above 50 rad/s (Table 3) [49, 50]. These angular acceleration thresholds were nearly three times smaller than values observed by Unterharnscheidt and Higgins and nearly three times larger than values observed by Ommaya et al. (Table 3) [49, 50, 72, 92, 93]. Later work by Löwenhielm revised the angular velocity values to increase the threshold to 70 rad/s (Table 3) [49]. Human volunteer tests performed by Ewing et al. in 1975 found that angular accelerations below 1700 rad/s^2 and angular velocities below 32 rad/s produced no head injury (Table 3) [22, 67].

While rotational kinematics can be linked to serious head injury, precaution must be taken when considering these measures for study. The angular velocities and accelerations derived from rotational dynamics are dependent on the assumption that the body in motion (i.e. the head) is rigid. However, injury mechanisms of the head rely on incongruent motion of different portions of the head, acknowledging that it is deformable (not rigid) [63]. When using rotational kinematic measures, the disparate nature of injury mechanism and injury assessment should be recognized and accounted for if possible.

Table 3: Historical threshold values for angular velocity (rad/s) and angular acceleration (rad/s^2) [49, 50, 72, 92, 93]

Author, Date	ω Threshold [rad/s]	α Threshold [rad/s^2]
Unterharnscheidt and Higgins, 1969	N/A	9,300-15,000
Ommaya et al., 1971	18.6-37.0	1800
Löwenhielm, 1974	50	4500
Löwenhielm, 1975	70	N/A
Ewing, 1975	32	1700

Neck Injury Criteria (NIC) is the second oldest established IARV, next to HIC, with preliminary work developing this criteria dating back 40 years. Injury to the neck, including fractured cervical vertebrae

and hemorrhages in the brain stem, has been shown to cause severe impairment, paralysis or death [45, 55].

NIC assesses the axial and shear forces of the neck as well as the bending moment about the occipital condyles. Axial forces on the neck can occur in either tension (forces pulling the head superiorly) or compression (forces pushing the head inferiorly), and shear forces can occur perpendicular to the neck in either the anterior or posterior direction. Bending of the neck can either occur in flexion (anterior bending) or extension (posterior bending) can affect the measurement outcome, considering that neck flexion will be limited by contact between the chin and chest [42, 56].

Seminal work by Mertz and Patrick in 1967 analyzed the kinematics and kinetics of the head (assumed to be a rigid body); noting that motion of the head is controlled by forces in the neck [56, 57]. Using Newtonian mechanics, the forces acting on the head can be resolved into a resultant force and torque at the occipital condyles; the occipital condyle force can be further resolved into axial and shear components [56, 57]. Hyperextension and hyperflexion of the neck, as shown in Figure 2, can be solved for torque (Equation 6) and force at the occipital condyles (Equation 7) [56, 57]. Hyperflexion of the neck involves an additional contact force at the chin as shown in. Variables defined for the following equations are shown in Table 4 [56].
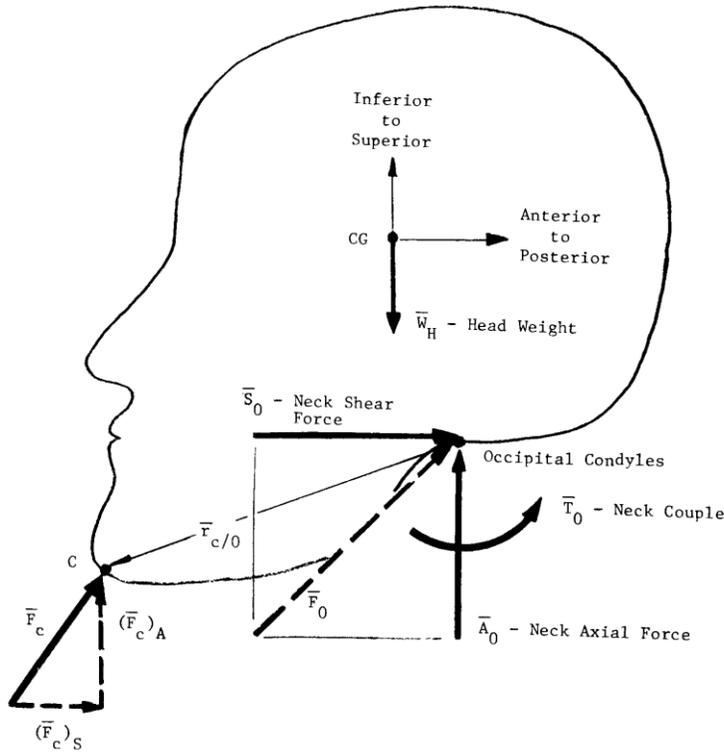
Figure 2: Free body diagram for hyperextension/hyperflexion of the neck, where hyperflexion scenarios include forces at the chin [56]**. Reprinted by permission of the Stapp Association.**

$$\bar{T}_O + \bar{r}_{G/O} \times \bar{W}_H + \bar{r}_{C/O} \times \bar{F}_C = I_G \bar{\alpha} + m_H \bar{r}_{G/O} \times \bar{a}_G \tag{6}$$

$$\bar{F}_O + \bar{F}_C + \bar{W}_H = m_H \bar{a}_G \tag{7}$$

Table 4: Variable defined for torques and forces incurred by hyperextension and hyperflexion of the neck [56]

Variable	Definition
$\bar{T}_O$	Torque about the occipital condyles
$\bar{r}_{G/O}$	Distance from the head COG to the occipital condyles
$\bar{W}_H$	Weight of the head
I_G	Mass moment of inertia of the head
$\bar{\alpha}$	Angular acceleration of the head
m_H	Mass of the head
$\bar{a}_G$	Linear acceleration of the head
$\bar{F}_O$	Force at the occipital condyles
$\bar{r}_{C/O}$	Distance from the chin to the occipital condyles
$\bar{F}_C$	Contact force at the chin

Current threshold standards, as required by FMVSS 208 (2010), are taken from the compiled works of Mertz et al. and Nyquist et al. [56-58, 69]. FMVSS 208 states that the safety threshold for belted automobile occupants is 4170 N in axial tension and 4000 N in axial compression [66]. For unbelted passengers the threshold limit for flexion is 190 Nm, extension (57 Nm), axial tension

(3.3 kN), axial compression (4.0 kN), and fore-aft shear (3.1kN) [66]. Graphs of the

axial tension and shear force limits vs. time are shown in Figure 3, and a graph of the

compression force vs. time is shown in Figure 4 [38, 90].
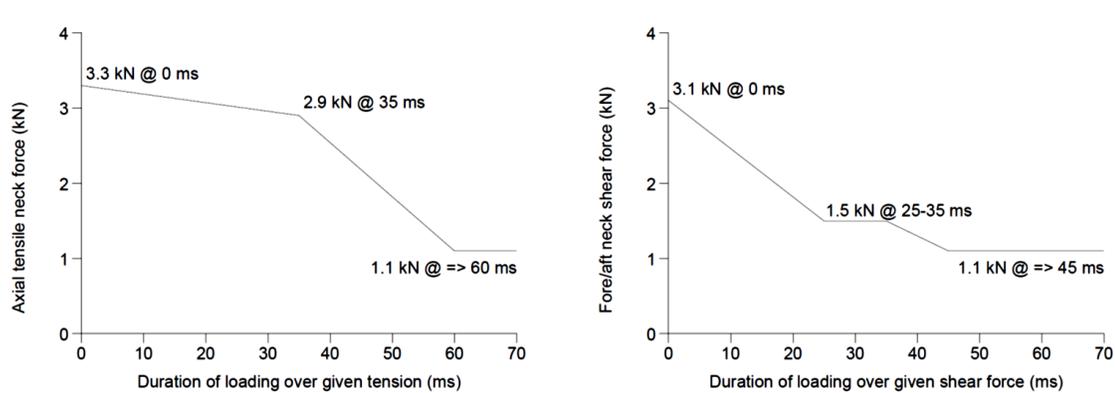
Figure 3: (Left) neck tension, and (right) neck shear force performance criteria with lower force limits for longer loading durations [38, 90]**. Reprinted with permission from the Insurance Institute for Highway Safety.**
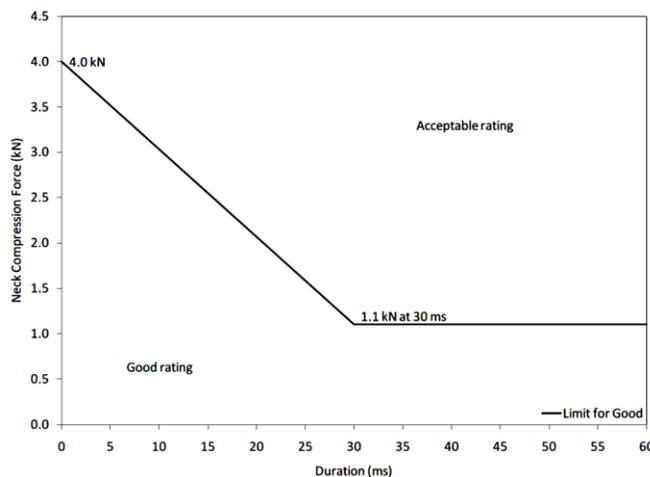
Figure 4: Neck compression force performance criteria [38]**. Reprinted with permission from the Insurance Institute for Highway Safety.**

The neck injury predictor (N_{ij}) is a collection of four predictive equations for

neck injury based on combinations of axial force (tension/compression) and bending

moment (flexion/extension). Although shear force is not explicitly included in the

predictive equations, it is used to formulate the effective moment at the occipital

condyles [42]. In essence, N_{ij} has merged the NIC outputs to devise more useful predictive injury indicators. These predictive indicators are neck tension-extension (NTE), tension-flexion (NTF), compression-extension (NCE), and compression-flexion (NCF) [42, 90].

Prasad and Daniel were the first to consider linearly combining axial force and bending moment to formulate a composite injury indicator [42, 63, 77]. The N_{ij} criteria place more stringent constraints on the composite values, whereas before, the FMVSS 208 regulation only required the mutually exclusive axial force and bending moment to fall within a box defined by tension/compression and flexion/extension limits [42].

Mertz et al. used the method proposed by Prasad and Daniel to fit equations to the constant stress lines on the graph of axial tension vs. extension moment [42, 58, 63]. Using data from Mertz et al. and Prasad and Daniel, the Alliance of Automobile Manufacturers proposed an injury risk curve to evaluate the combined tension-extension neck response [1, 54, 59, 63]. The injury risk curve was able to provide information pursuant to determining the normalized stress ratio (i.e., N_{ij}), which could then be related back to the linear combination of the normalized axial force and bending moment [42, 63]. Resulting from these calculations is the equation of N_{ij} in its final form (Equation 8) [38, 42, 63, 66, 90].

$$N_{ij} = \left| \frac{F_z}{F_{zc}} \right| + \left| \frac{M_y}{M_{yc}} \right| \tag{8}$$

In Equation 8, F_z is the measured axial load, F_{zc} is the axial load critical value, M_y is the effective flexion/extension moment at the occipital condyles, and M_{yc} is the flexion/extension critical value.

Critical values had been proposed by Kleinberger et al. during the development of N_{ij} in 1998, but the current FMVSS 208 regulation has set the limits for axial tension at 6806 N, axial compression (6160 N), flexion moment (310 Nm), and extension moment (135 Nm) [38, 66]. Because the N_{ij} is normalized, if any one of the four predictive equations or their sum is above 1, then injury is probable [42, 66, 90].

1.1.6   *Mathematical Dynamic Modeling (MADYMO) Software*

MADYMO is used to simulate the dynamic interaction of an anthropometric test device (ATD) and vehicle within a user-defined 3D environment. Typically, the software is used for collision scenarios, assessing the injury incurred by the ATD [90]. These injury outcomes are readily available in pre-defined output files.

MADYMO allows for multi-body systems (gross motion systems) to be seamlessly incorporated with finite element (structural) modules, although inclusion of both modeling methods is not required (Figure 5) [63, 90]. Whether using multi-body systems, finite element modules, or both, a reference space must be specified, from which all other system motion (i.e. multi-body motion) is defined [63, 90]. A multi-body (MB) system is a system of rigid bodies connected by kinematic joints. Rigid bodies require only specification of mass, center of gravity locus, and inertial properties; surfaces may be attributed to rigid bodies if contact is desired between multiple bodies. Motion of the rigid body is defined by the orientation of its local coordinate system relative to the reference space coordinate system. Kinematic joints restrict the motion of the bodies they link and come in various types, all of which are further described in the MADYMO Theory Manual [90]. Contacts can be defined between bodies with

associated surfaces which allow interaction between the surfaces, and subsequently cause the IARVs specified within MADYMO. A myriad of pre-programmed IARVs are supplied by MADYMO, including HIC, NIC, and N_{ij} [90]. Restraints, such as belts, can be implemented for points, joints, or between bodies. Tensile forces in the belt can be monitored using sensors to ensure that the belt segment is responding adequately to the imposed loads.
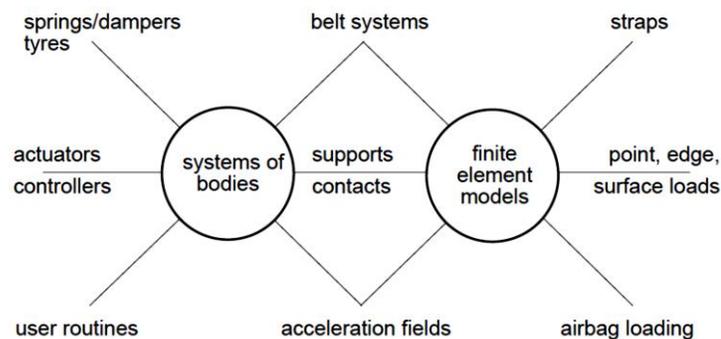
Figure 5: MADYMO environment structure [90]. **Reprinted with permission from ©TASS Americas.**

Model simulation is performed by integrating the second time derivatives of the joint degrees of freedom, typically with 4th order Runge-Kutta methods. Prior to running the simulation, initial joint positions and velocities must be specified, and appropriate joint stiffness, damping, and friction can be applied.

ATDs, commonly referred to as dummies, are mechanical surrogates to human testing designed to be biofidelic and fitted with extensive instrumentation [63]. Biofidelity signifies that the ATD is comparable to a human in anthropometry such as size, shape and stiffness, and mechanical response such as kinematic movement, kinetic response, body segment articulation, and injury outcome [63, 94]. Instrumentation supplies information on the kinematics and kinetics experienced by the ATD.

A special version of the Hybrid III 50th percentile male ATD, which was developed and validated by MADYMO to mimic standing posture, was used in this thesis (Figure 6) [89]. The ATD's standing posture was accomplished by straightening the pelvis and lumbar spine as well as increasing stiffness in the hips, knees, and ankles [89]. The standing Hybrid III 50th percentile male MADYMO supplied ATD has a height and weight of 66.8" and 171.9 lbs, respectively.

Figure 6: Standing Hybrid III 50th percentile male [89]**. Reprinted with permission from ©TASS Americas.**

1.2 Thesis Aims

This thesis aims to relate input parameters to injury outcomes in side-stance collision scenarios of a perturbed horizontal platform. The input variables for study will be ΔV of the platform and grip strength of the standing Hybrid III 50th percentile male ATD where the hands contact the simulated controls. Collision of the platform with an external object will be modeled with a scaled 100 ms haversine impulse applied to the platform. Injury outcomes will be selected head and neck IARVs, including HIC, ω, α, NIC, and N_{ij}.

The value of this thesis is linked to its use of a computer-simulated dynamic model (MADYMO). This allows for complete reproducibility of the collision scenario, systematic assessment of the input parameters with incremental changes, and a method to evaluate injury without compromising human safety. Design of the platform model in

MADYMO facilitates efficiency while maintaining comparable results to more complex computational or live models.

While the MADYMO model is efficient, safe, and consistent, it can be computationally intensive. This thesis will model the relationship between inputs and outputs using a regression equation which may adequately predict injury outcome based on the initial parameters (ΔV and grip strength). This equation can be disseminated freely to permit other institutions to predict injury in these scenarios without the requisite computational intensity of MADYMO.

2   METHODS

2.1   Methods Summary

This section outlines the methods used to build and position the MADYMO models, implement their interaction in a dynamic environment, and analyze the resulting data. Descriptions of the SQM design, ATD positioning, dynamic environment setup, and analysis methods are provided.

The SQM is a representative summation of the average stand-up forklift design which contains the fewest possible surface elements necessary to provide the basic architecture for dynamic contact scenarios. The ATD was arranged in the SQM to mimic operator stance and upper body posture during an impending contact scenario. One-leg stance was implemented to simulate emergency brake activation, where the left leg was raised (to engage the brake). Upper body grip with the controls was modeled to simulate typical hand position under normal operation. Dynamic perturbation of the SQM was modeled with a 100 ms haversine waveform which slows the moving SQM to a stop in a manner similar to frontal auto collisions. Data analysis was performed via nonlinear regression, which maps the input parameters (ΔV and grip strength) onto the outputs. This provides an equation to predict IARVs using only the supplied inputs, without having to re-run the MADYMO model.

2.2   Streamlined Quadrilateral Model (SQM) Design

2.2.1   SQM Description

The quadrilateral forklift model used in this work is a streamlined design of a forklift derived from the characterization of fully realized models. Measurements of the

fully realized modeled were taken and simplified to provide only the essential components of a forklift. This model maintains the basic functional and geometric integrity of the fully realized models while requiring fewer elements. A reduction in elements is expected to reduce computational time and provide a future standard for similar forklift modeling. While a fully realized model may contain over 100 elements, the SQM has only 16 elements.

2.2.2   *Reasoning for Surface Inclusion*

Surface inclusion was based on the necessity for ATD interaction with the environment. The floor provides a horizontal surface for foot contact, allowing the ATD to stand. The overhead guard, although not contacted in this work, is at the appropriate distance from the floor. This is crucial when analyzing forklift upset scenarios including left tip over, right tip over, and off-dock. Outer walls provide the geometric scaffolding for the operator compartment. Of particular importance is the right side outer wall which may be considered as back support for the ATD. Walls on either side of the door complete the operator compartment, and are dimensioned such that the door is properly positioned with respect to the SQM. The right side door wall may also provide a means to prevent operator egress from the compartment during dynamic perturbation. The door, which is included only for trials which require a fully enclosed compartment, has dimensions commensurate to the fully realized models and may be used to prevent operator egress from the compartment. The inner compartment wall and control panel are possible contact surfaces for the lower body, while the posts are contact surfaces for the upper body and head. Tiller and MFCL surface elements allow for upper extremity

grip with the controls in the appropriate position. Relevant surfaces selected for

inclusion in the SQM are as follows and their positioning is shown in Figure 7.
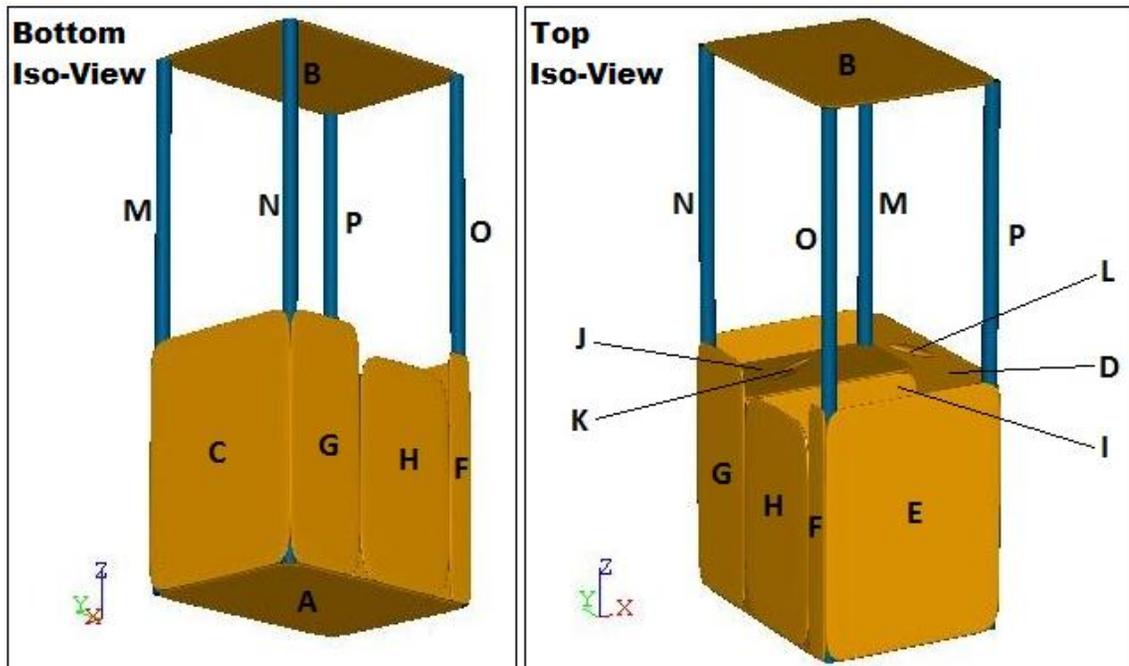
Figure 7: Isometric view of SQM with component labeling; (A) floor, (B) overhead guard, (C) left side outer wall, (D) back outer wall, (E) right side outer wall, (F) right side door wall, (G) left side door wall, (H) door, (I) inner compartment wall, (J) control panel, (K) tiller, (L) MFCL, (M-P) posts 1-4

2.2.3   Representative Dimensions, Geometries, Positions and Orientations

Table 5: Contact points for upper extremity grip

Contact Point (Hand)	Position (X,Y,Z) [mm]
Tiller Point (left)	(-348,-36,1270)
MFCL Point (right)	(-715,-50,1263)

Representative dimensions, positions, and orientations of the elements used were

chosen to replicate the geometry of the fully realized model without compromising or

altering the expected interaction between the ATD and the material handling

environment. Tiller and MFCL controls contact points are shown in Table 5.

Dimensions for included surface elements are shown in Table 6.

Table 6: Surface element dimensions, positions and orientations where clockwise is positive

Surface Element [Label]	Semi-axes (X,Y,Z) [mm]	Position (X,Y,Z) [mm]	Orientation (X,Y,Z) [deg]
Floor [A]	(375,500,6.3)	(-525,-50,245)	
Overhead guard [B]	(375,500,6.3)	(-525,-50,2400)	
Left outer wall [C]	(375,6.3,500)	(-525,-550,745)	
Back outer wall [D]	(6.3,500,500)	(-900,-50,745)	
Right outer wall [E]	(375,6.3,500)	(-525,450,745)	
Right door wall [F]	(6.3,60,500)	(-150,390,745)	
Left door wall [G]	(6.3,190,500)	(-150,-360,745)	
Door [H]	(6.3,250,450)	(-150,80,695)	
Inner compartment wall [I]	(375,6.3,427.5)	(-525,-170,672.5)	
Control panel [J]	(375,190,6.3)	(-525,-360,1100)	
Tiller [K]	(16.3,40,170)	(-349,-0.180,1.186)	(120.3,0.0,85.9)
MFCL [L]	(16.3,40,105)	(-805,-50,1226)	(0.0,69.9,0.0)
Post 1 [M]	(1077.5,30,30)	(-870,-520,1322.5)	(0.0,90.0,0.0)
Post 2 [N]	(1077.5,30,30)	(-180,-520,1322.5)	(0.0,90.0,0.0)
Post 3 [O]	(1077.5,30,30)	(-180,420,1322.5)	(0.0,90.0,0.0)
Post 4 [P]	(1077.5,30,30)	(-870,420,1322.5)	(0.0,90.0,0.0)

2.3   Dummy (ATD) Description

The anthropometric model used in this work is a variant of the standard Hybrid III 50th percentile male, which has been made to stand. As mentioned earlier, the standing Hybrid III has been validated for joint angle ranges, and increased joint stiffness.

MADYMO has specified which type of modeled joint corresponds to each anatomical joint. Because of this, some upper and lower extremity joints may only have motion about certain axes. For the lower extremities, the knees are revolute joints and the hips and ankles are spherical joints. This means the knees have one degree of freedom (DOF), while the hips and ankles have three DOF. For the upper extremities, the shoulders, elbows, and wrists are universal joints, each having two DOF.

2.3.1 Dummy (ATD) Position and Orientation

The ATD needed to be repositioned to represent a standing forklift operator with emergency brake activation and upper extremity grip with the controls. Brake activation modeling required the left leg to be raised about 152.4 mm (6 inches) from the floor pan, with associated hip, knee, and ankle joint rotations to keep the foot roughly at its initial X- and Y-position. Upper extremity joint positioning was performed to match the ATD hands with their respective controls at the contact points specified in Table 5. The only further alteration made to the standing Hybrid III ATD was to specify contact between the arms and body.

Table 7: Dummy (ATD) position

Dummy position and orientation are

Joint Name	Position (X,Y,Z) [mm]
Dummy Attachment	(400,-180,1168)

specified based on the body orientation of a forklift user under normal operating conditions. The location of the ATD in the reference space is specified by the dummy attachment joint which allows rigid body movement; its position for this application is shown in Table 7. The initial orientations of altered joints are shown in Table 8.

Table 8: Joint orientations for standing Hybrid III forklift ATD where orientations are local (relative to the joint) and N/A denotes a nonexistent joint constraint

Joint Name	Initial Orientation (R1,R2,R3) [deg]	R1 Positive Joint Angle Movement	R2 Positive Joint Angle Movement	R3 Positive Joint Angle Movement
Left Hip	(0.0,-39.0,0.0)	Abduction	Extension	External Rotation
Right Hip	(0.0,0.0,0.0)	Adduction	Extension	Internal Rotation
Left Knee	(-5.2,---,---)	Flexion	N/A	N/A
Right Knee	(-83.1,---,---)	Flexion	N/A	N/A
Left Ankle	(0.0,0.0,-1.1)	External Rotation	Pronation	Plantar-flexion
Right Ankle	(0.0,0.0,4.6)	Internal Rotation	Supination	Plantar-flexion
Left Shoulder	(10.9,24.1,---)	Flexion/Posterior	Abduction	N/A
Right Shoulder	(20.6,-14.9,---)	Flexion/Posterior	Adduction	N/A
Left Elbow	(-36.7,-100.8,---)	External Rotation	Extension	N/A
Right Elbow	(-21.2,-98.5,---)	Internal Rotation	Extension	N/A
Left Wrist	(-63.0,0.0,---)	External Rotation	Extension	N/A
Right Wrist	(74.5,0.0,---)	Internal Rotation	Flexion	N/A

2.3.2 *Dummy (ATD) Posture Verification in a Gravity Environment*

Gravity environment testing was performed on the standing Hybrid II 50th percentile male ATD in its supplied anatomical position and with user-specified joint positioning. This was done to verify the dummy biofidelic response in a static environment.

For the anatomical positioning trial, the ATD was positioned upright in a gravitational field with both feet on the reference space and no altered joint angles. This test was performed to verify that the ATD could stand upright in gravity for two seconds without additional supports.

Initial orientations of the joints were tested in a static gravity environment to ensure that the angles chosen were within appropriate operating ranges. The time duration of these tests was at least two seconds to allow for settlement of the joints, or aberrant movement of the ATD surface elements. Each joint was adjusted separately to encompass the angle ranges likely to be experienced by the joint. Starting angles for the joint range findings were taken from those supplied by MADYMO; those angles facilitated the ATD's upright posture in a gravity environment and may not necessarily be zero. Lower extremity joints were only tested for the left side, and upper extremity angles were referenced to the left side, however both upper extremity limbs were positioned together. The test ranges are shown in Table 9, and fall within the validated ranges provided by MADYMO [90].

Table 9: Joint angle range finding in static gravity environment

Joint Name (Axis)	Starting Angle [deg]	Ending Angle [deg]	Corresponding Anatomic Range (Direction) [deg]
Hip (R2)	0.0	-45.0	0° to 45° (flexion)
Knee (R1)	-83.1	6.9	0° to 90° (flexion)
Ankle (R3)	4.6	-17.9	0° to 22.5° (dorsi-flexion)
Shoulder (R1)	22.5	-45.0	22.5° (flexion) to 45° (extension)
Shoulder (R2)	9.0	54.0	0° to 45° (abduction)
Elbow (R1)	-45.0	45.0	45° (internal rotation) to 45° (external rotation)
Elbow (R2)	0.0	-105.0	0° to 105° (flexion)
Wrist (R1)	0.0	-90.0	0° to 90° (internal rotation)

2.4   Dynamic Trials

Dynamic trials of the SQM and standing ATD were performed to examine the interaction of the two multi-body models. These required additional constraints on the models pertinent to their dynamic movements including contact specifications, initial velocities, deceleration impulses, and grip between the SQM controls (tiller and MFCL) and the ATD hands. Analysis of the dynamic trials can be performed with visual inspection, time series plots, descriptive statistics, and regression equations which are iteratively built to map the inputs to the outputs.

2.4.1   Parameters Defining the System

Contact between the SQM and ATD was specified such that the reciprocal action between these two MB systems could be modeled. This means that when a surface element of the ATD contacts an element of the SQM, there is an inherent elastic deformation which imparts energy onto the ATD, causing subsequent injury. A contact list is established to identify relevant surface elements in both MB systems for inclusion in these dynamic interactions. For trials where a door is absent, the door and front posts

are excluded from the contact list, allowing the ATD to freely pass through the SQM entrance.

Values for ΔV during the collisions ranged from 3.2 to 16.1 km/h (2-10 mph) in increments of 3.22 km/h (2 mph). The fastest stand-up forklifts have a maximum speed of 12.1 km/h (7.5 mph), so these velocities represented normal operational limits and excessive speeds. Prescribed ΔVs were attributed to the main SQM joint, from which all surface elements were defined. Movement of this joint displaces all corresponding surface elements (floor pan, door, etc.) concurrently. The same ΔV was attributed to the main ATD joint called the dummy attachment joint, which has similar function to the SQM joint. When the SQM and ATD are prescribed identical ΔVs they move together until a deceleration impulse impedes that translation.

Verification of the ΔV was performed by monitoring the linear velocity of points on the SQM and ATD. This provided certainty that the prescribed ΔVs were indeed correct in the implementation of the model.

The acceleration impulses used for the SQM model were 100 ms scaled haversine waveforms applied in the opposite direction of SQM translation (i.e., decelerating the SQM). These waveforms are magnitude scaled based on the imposed ΔV. The equation for a haversine is shown in Equation 9, and the array of scaled impulses can be seen in Figure 8 [95]. Scaling of the haversine waveform is accomplished with a function in MADYMO and can be verified analytically via Equation 10, which relates peak acceleration to the velocity change [95].

$$a = P \sin^2 \frac{\pi t}{T} \tag{9}$$

$$P = \frac{2\Delta V}{T} \tag{10}$$

In Equation 9, *a* is the acceleration at any time point, *t*, over the impulse

duration, *T*, given the peak acceleration, *P*. In Equation 10, the peak acceleration is

related to *ΔV*, the change in velocity from initial velocity to zero velocity.

Haversine Acceleration Impulses
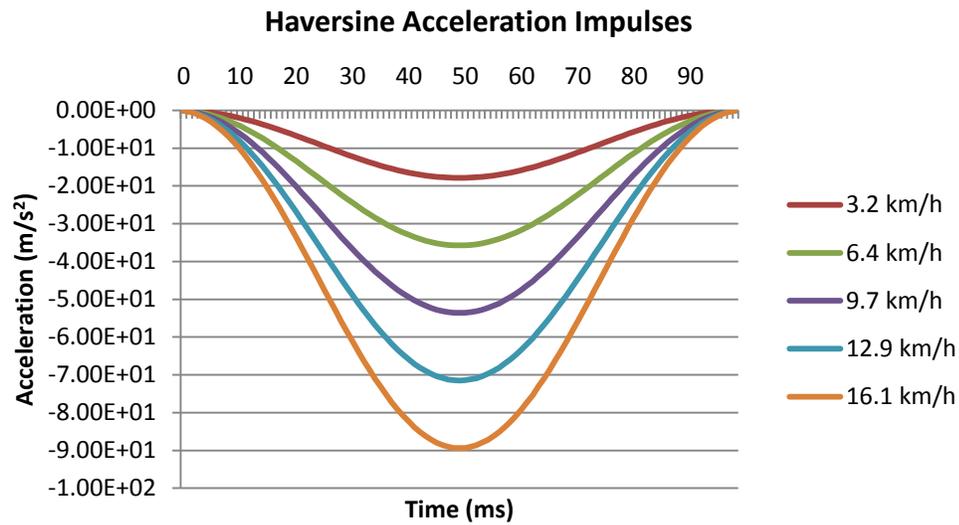
Figure 8: Array of haversine impulses used in the dynamic trials

Verification of the haversine impulse was performed by monitoring the linear

position, velocity, and acceleration of a point on the SQM. This ensured that the

prescribed haversine impulse was implemented properly in the model. Results of the

haversine integrity verification for a representative mid-range ΔV (9.7 km/h) condition

are shown in the *Results* section.

Grip between the SQM controls (tiller and MFCL) and ATD hands was

simulated with belt elements. The belt elements connected the ATD hands at external

points on their respective surfaces to the contact points shown in Table 5. Belts were set

to an array of break strengths based on grip strength performance standards identified by Rantanen et al. [79]. Grip strengths included for study in this thesis were the average grip strength found by Rantanen et al., 384.6 N (86.2 lbf), two standard deviations below, five standard deviations above, and a zero grip condition [79]. For the nonzero conditions, this gave a range of 266.8 N (59.8 lbf) to 678.9 N (152.2 lbf) in increments of 58.9 N (13.2 lbf).

Verification of the grip strength was performed by monitoring the tensile force of the belt elements with tensile sensors. This ensured that the belts (simulated grip strength) ruptured at their intended limits. Results of the belt rupture strength verification for minimum (266.8 N), middle (443.4 N), and maximum (678.9 N) values at a representative 9.7 km/h (6 mph) condition are shown in the *Results* section.

2.4.2 *Dynamic Model Analysis Methods*

Based on the five ΔV conditions and nine grip conditions, there are a possible 45 collision scenarios. For each of these scenarios, ten IARVs are assessed to determine injury risk. This produces a possible 450 injury risk matrices with two inputs (ΔV and grip strength) and one output (the specific IARV). The dynamic trials can be analyzed visually for fall progression, temporally for IARV advancement over time, statistically for general descriptive values, and with regression modeling of IARVs vs. inputs, analyzed as surfaces. All of the aforementioned methods can reduce the raw data into a more usable form.

Fall progression analysis tracked the movement of the ATD at discrete time points. This was accomplished by taking snapshots of the dynamic environment and

placing these pictures adjacent to one another. Multiple ΔV series of fall progressions were juxtaposed to better identify the differences between trials.

Time series plots of the IARVs over the trial duration show the temporal characteristics of the collision scenarios. These values are directly supplied in continuous time plots for angular velocity, angular acceleration, NIC, and ΣN_{ij}. For HIC, the value is found by the maximum integral of the linear acceleration over a 36 ms time window.

Descriptive statistics give a basic overview of the results of the dynamic trials. Included in the descriptive statistics are minimum, maximum, mean, and standard deviation values for each measured IARV.

Nonlinear regression of the input/output (I/O) interaction was performed by relating the I/O in a linear fashion and iterating to yield higher correlation. First, a linear form of the I/O relation was assumed, as shown in Equation 13, and its coefficient of determination (R^2) and adjusted R^2 ($\overline{R}^2$) were found with Matrix Laboratory (MATLAB) software (MathWorks, Natick, MA) [44, 52, 61, 80]. Calculation of R^2 and $\overline{R}^2$ are shown in Equation 11 and Equation 12, respectively, where $\overline{R}^2$ accounts for the number of terms used [44, 61, 80]. These regression statistics measure the goodness of fit of a regression model to its observed data, and their outcomes can be defined as the percent of variation explained by the regression (ex. $R^2 = 0.75$ is 75% variation explained) [44, 61, 80].

$$R^2 \equiv 1 - \frac{SS_{err}}{SS_{tot}} \equiv \frac{\sum_i(y_i - f_i)^2}{\sum_i(y_i - \bar{y})^2} \tag{11}$$

$$\bar{R}^2 \equiv 1 - \frac{VAR_{err}}{VAR_{tot}} \equiv 1 - \frac{SS_{err}}{SS_{tot}}\frac{df_t}{df_e} \equiv 1 - (1 - R^2)\frac{n-1}{n-p-1} \tag{12}$$

In Equation 11, R^2 is the coefficient of determination, SS_{err} and SS_{tot} are the residual sum of squares and total sum of squares, y_i are the observed values, f_i are the predicted values, and $\bar{y}$ is the observed mean. In Equation 12, $\bar{R}^2$ is the adjusted coefficient of determination, VAR_{err} and VAR_{tot} are the statistically unbiased variances of errors and observations, df_t and df_e are the degrees of freedom estimates for dependent variable population variance and underlying error population variance, n is the sample size, and p is the number of regressors excluding constant terms.

Secondly, analysis of the residuals (predicted – observed values) was performed by plotting the residuals against their inputs (i.e. ΔV or grip strength). If the $\bar{R}^2$ was considered low (below 0.5) and the residual plots showed any nonlinear trends, such as a quadratic nature, then higher order terms (i.e., x^2) or interaction terms (i.e., $x \cdot y$) could be added to the equation [44, 61]. This process was iterated to produce a nonlinear equation such as that shown in Equation 14 [44, 61, 80].

$$z = a + bx + cy \tag{13}$$

$$z = a + bx + cy + dx^2 + exy + fy^2 \tag{14}$$

In Equation 13 and Equation 14, z is the IARV output as it relates to ΔV, x, and grip strength, y. Additional terms, such as a through f, are regression coefficients which weight the terms according to their influence on the output.

3   RESULTS

3.1 Results Summary

Results from MADYMO simulations can be analyzed with pictorial representations, time series graphs, basic descriptive statistics, and regression modeling. Frame-by-frame pictures of the fall progression of the anthropometric test device (ATD) show the nature of the fall and may provide insight into subsequent injury. Time series plots show the continuous IARVs of the head/neck through the duration of the trials. Basic descriptive statistics give an overview of the IARVs, which can be compared to previous literature of similar scenarios. Regression models of the scenarios provide predictive equations mapping inputs (ΔV and grip strength) onto outputs (IARVs), thereby circumventing the use of MADYMO for these particular scenarios. Predictive equations can simplify the analysis of the collision scenario and provide any easily assessable resource for others to predict injury.

Preliminary results from simulations including a lateral constraint (door) showed that no head/neck injury occurred when the ATD was subjected to worst-case initial parameters (i.e., ΔV at 16.1 km/h without grip). As such, all of the following results are specific to collision scenarios involving a streamlined quadrilateral model (SQM) without a door. Results from the fully enclosed SQM (with door) trials are shown in Appendix A.

3.2   Input Parameter Integrity Verification

3.2.1   *Haversine Verification*
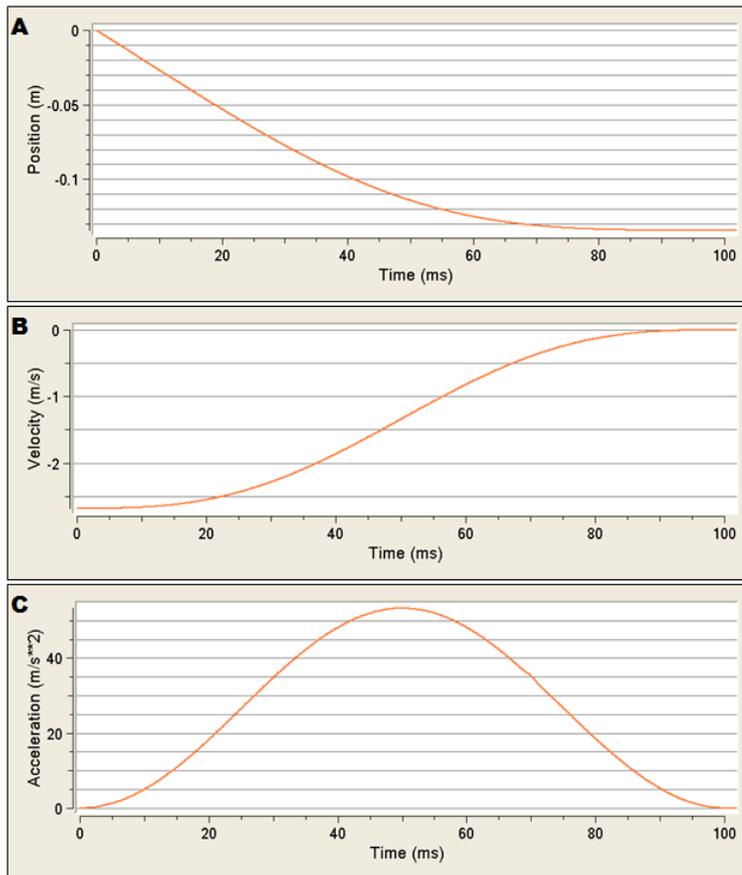
Figure 9: Haversine waveform verification at the representative 9.7 km/h (6 mph) condition for (A) position, (B) velocity, and (C) acceleration

Results for the haversine position, velocity, and acceleration verification at a representative ($\Delta V = 9.7$ km/h) condition are shown in Figure 9. The measured haversine acceleration graph for 9.7 km/h (6 mph) has a bell shape and shows a peak at 53.6 m/s^2, which is in accordance with the expected haversine waveform for 9.7 km/h. Trials at other ΔVs yielded similar findings, scaled to the appropriate magnitude based on their ΔV.

3.2.2   Belt Rupture Strength Verification

Table 10: Belt rupture strength verification at a representative (9.7 km/h) condition

Expected rupture strength [N]	**Measured tiller belt rupture strength (left hand) [N]**	**Measured MFCL belt rupture strength (right hand) [N]**	**Tiller belt simulation error [%]**	**MFCL belt simulation error [%]**
266.8	274.2	275.8	2.7	3.3
443.4	463.2	458.3	4.5	3.4
678.9	706.5	701.5	4.1	3.3

Belt rupture strength verification at minimum, middle, and maximum values for a representative ΔV (9.7 km/h) condition are shown in Table 10. From these results, the belt rupture strength induced up to 4.5% error in the simulation. Trials at other ΔVs and grip strengths yielded similar results.

3.3   Fall Progression

Once subjected to the dynamic perturbations applied to the computational model, the ATD tends to progress its movement outside of the SQM operator compartment (cabin) and onto the reference surface (ground). This movement varies slightly from trial to trial, but seems to follow a similar pattern within each velocity grouping, and a more generalized pattern for all trials. The generalized pattern shows the ATD move towards the cabin entrance while still maintaining upper extremity grip during the start of the trial. If grip is maintained, then the ATD will slump forward and rotate its shoulders clockwise, held in place by only its arms. If grip is not maintained, then the ATD will fall sideways through the cabin door and may even fall slightly forward if there is latent grip loss. Movement progression from this point causes the ATD to continue its fall, striking the ground with its left shoulder, followed by head contact with the ground. Depending on initial velocity parameters, the ATD may rebound away from the SQM,

sustaining multiple shoulder-ground and head-ground contacts. It will eventually roll to either its front or back side while it comes to rest. An example of the fall progressions for each ΔV at a representative (mid-range) grip strength (443.4 N) is shown in Figure 10.
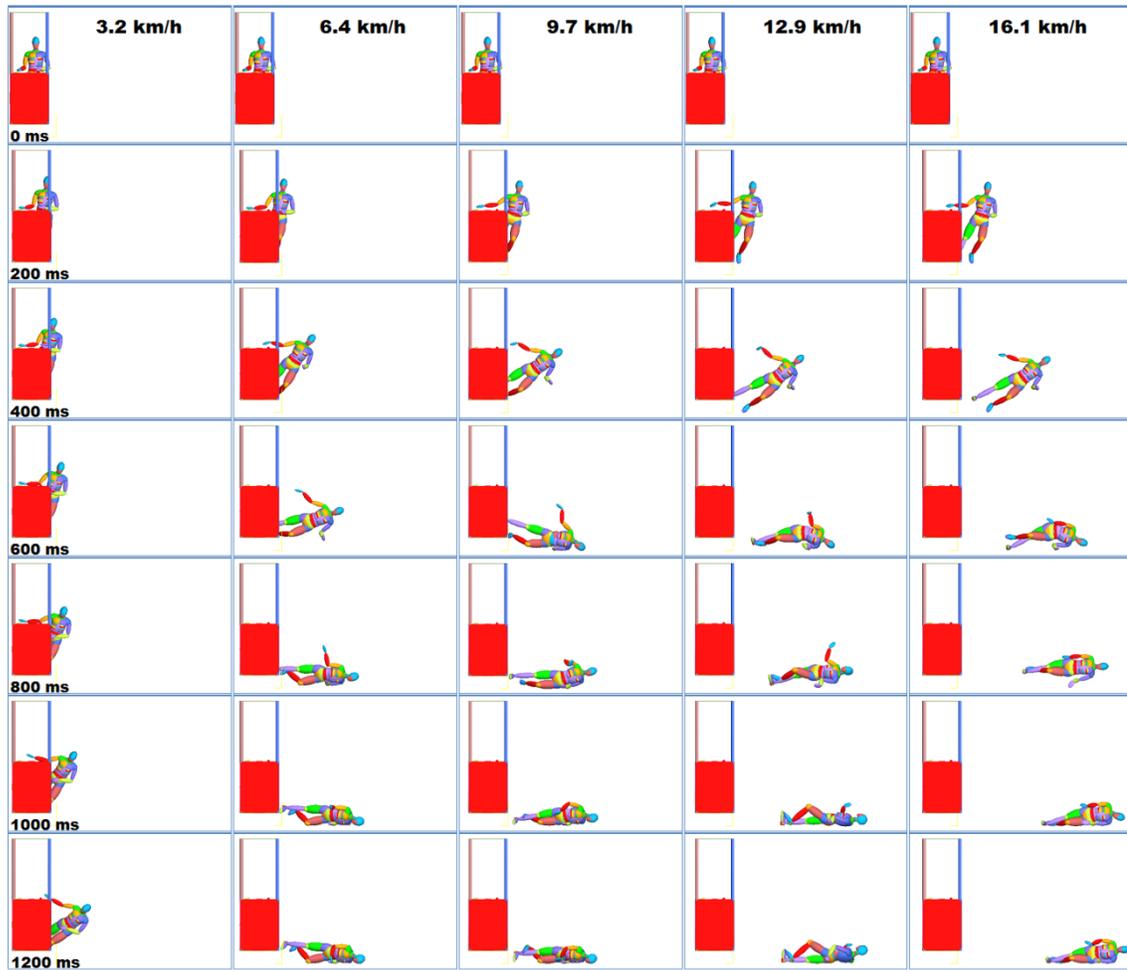
Figure 10: Fall progression for all ΔVs (3.2-16.1 km/h) at a representative (mid-range) grip strength (443.4 N)

3.4 Time Series Plots of IARVs

Example times series plots for the IARV conditions are provided below. These plots are from representative collision scenarios at the mid-range grip strength (443.4 N) and all ΔVs.

3.4.1 HIC Time Series

Representative scenarios of time series plots for resultant linear acceleration of the head at the mid-range grip (443.4 N) is shown in Figure 11, from which HIC can be determined. For this series, the linear accelerations peak progressively earlier with each increasing ΔV, with the highest HIC (1020) incurred at 9.7 km/h (6 mph).
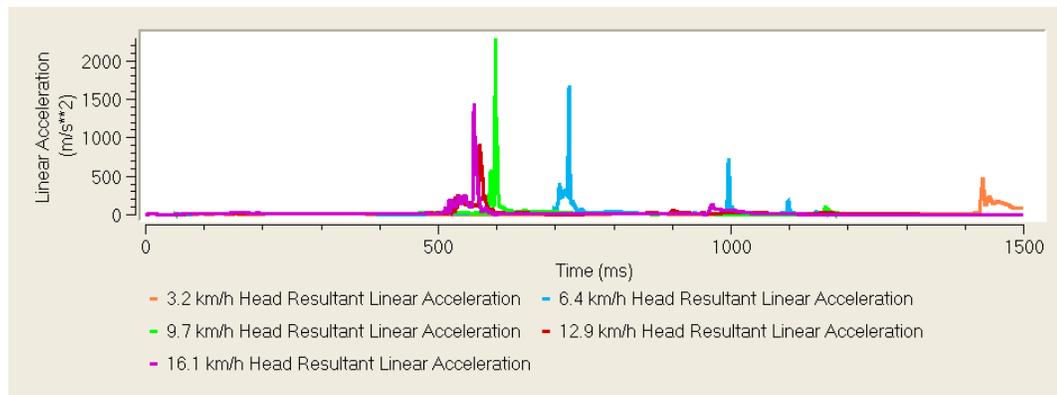
Figure 11: Linear acceleration [m/s^2] time series plots of representative collision scenarios at 443.4 N grip strength and all ΔVs, where (orange) is 3.2 km/h, (blue) is 6.4 km/h, (green) is 9.7 km/h, (red) is 12.9 km/h, and (purple) is 16.1 km/h

3.4.2 Angular Velocity (ω) and Acceleration (α) Time Series

Representative time series plots for ω and α of the head at the mid-range grip (443.4 N) are shown in Figure 12 and Figure 13, respectively. Similar to HIC, for these

series the ω and α peak progressively earlier with each increasing ΔV, with the highest ω

(56 rad/s) incurred at 9.7 km/h (6 mph) and the highest α (21,454 rad/s^2) incurred at 9.7

km/h (6 mph).
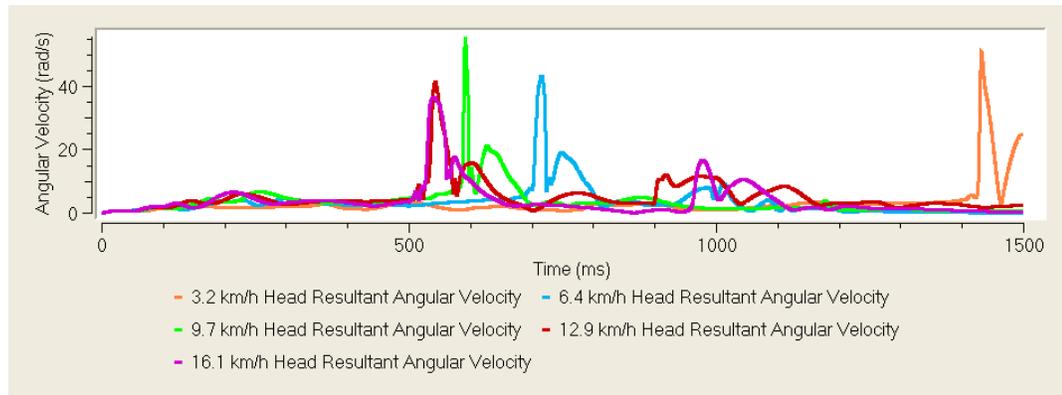
Figure 12: Angular velocity [rad/s] time series plots of representative collision scenarios at 443.4 N grip strength and all ΔVs, where (orange) is 3.2 km/h, (blue) is 6.4 km/h, (green) is 9.7 km/h, (red) is 12.9 km/h, and (purple) is 16.1 km/h
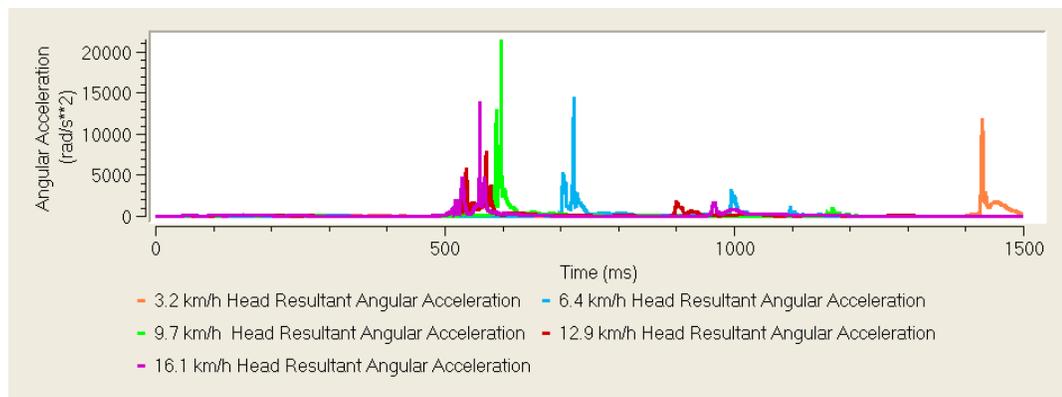
Figure 13: Angular acceleration [rad/s^2] time series plots of representative collision scenarios at 443.4 N grip strength and all ΔVs, where (orange) is 3.2 km/h, (blue) is 6.4 km/h, (green) is 9.7 km/h, (red) is 12.9 km/h, and (purple) is 16.1 km/h

3.4.3   NIC Time Series

Representative time series plots for NIC tension, shear, and bending in the

negative and positive directions at the mid-range grip (443.4 N) are shown in Figure 14

through Figure 19. In these plots, the forward and backward motions are plotted, relating to tension/compression, anterior-posterior (AP)/posterior-anterior (PA) shear, and flexion/extension bending for the tension, shear, and bending plots, respectively. Again, the NIC forces and moments peak earlier with each increasing ΔV.
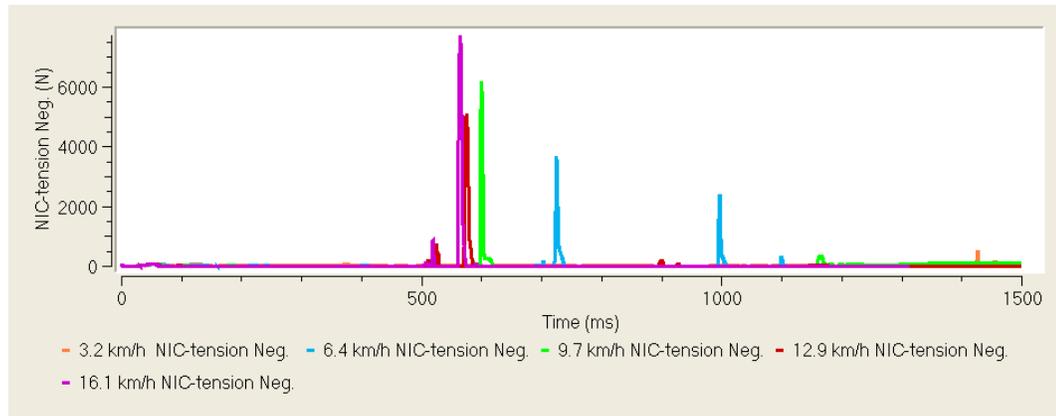
Figure 14: NIC-tension negative [N] time series plots of representative collision scenarios at 443.4 N grip strength and all ΔVs, where (orange) is 3.2 km/h, (blue) is 6.4 km/h, (green) is 9.7 km/h, (red) is 12.9 km/h, and (purple) is 16.1 km/h
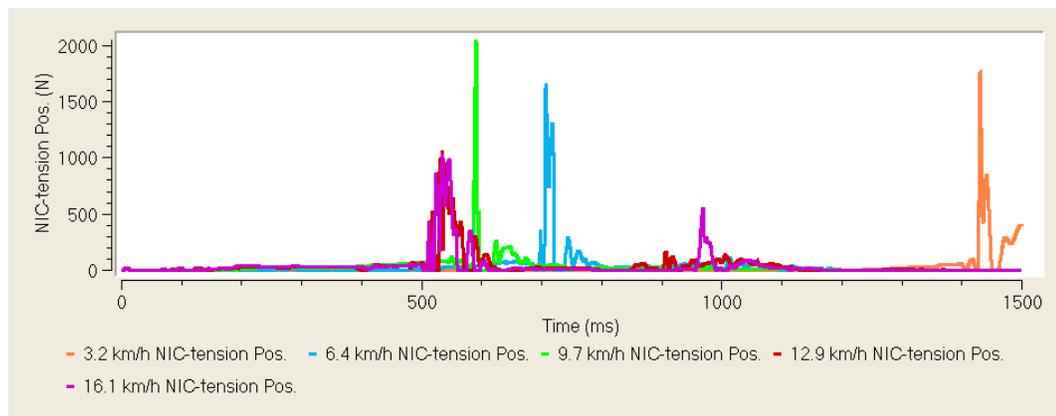
Figure 15: NIC-tension positive [N] time series plots of representative collision scenarios at 443.4 N grip strength and all ΔVs, where (orange) is 3.2 km/h, (blue) is 6.4 km/h, (green) is 9.7 km/h, (red) is 12.9 km/h, and (purple) is 16.1 km/h
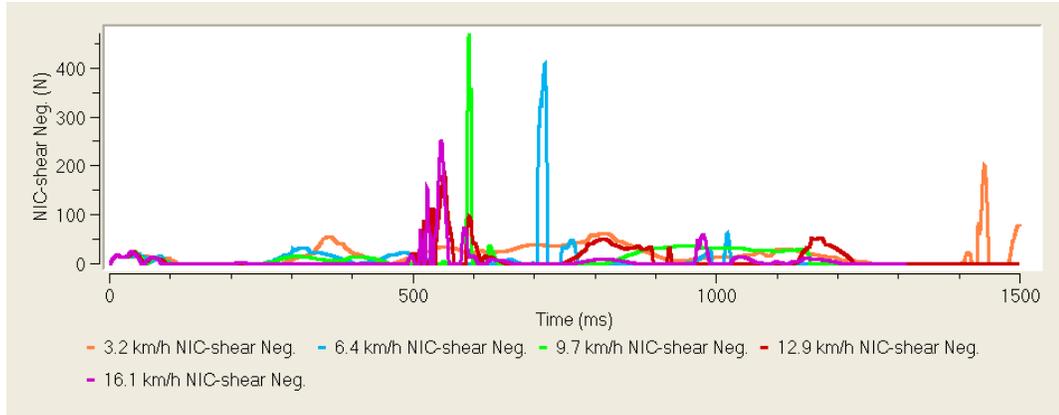
Figure 16: NIC-shear negative [N] time series plots of representative collision scenarios at 443.4 N grip strength and all ΔVs, where (orange) is 3.2 km/h, (blue) is 6.4 km/h, (green) is 9.7 km/h, (red) is 12.9 km/h, and (purple) is 16.1 km/h
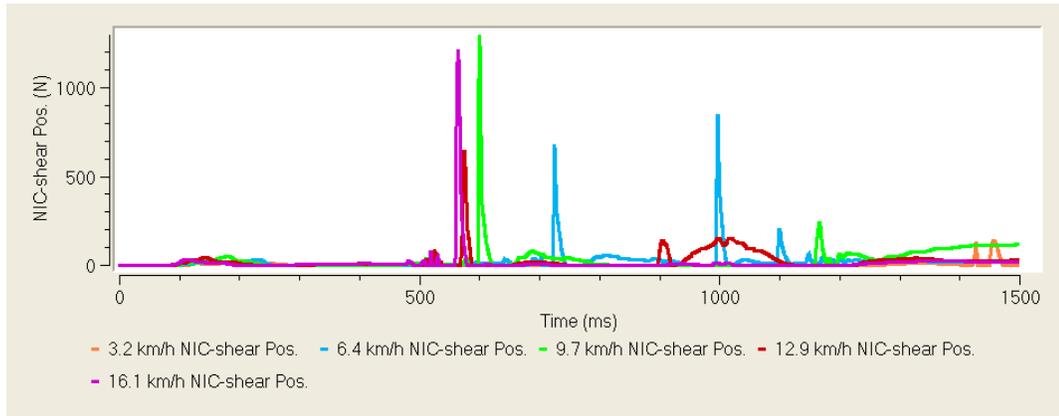
Figure 17: NIC-shear positive [N] time series plots of representative collision scenarios at 443.4 N grip strength and all ΔVs, where (orange) is 3.2 km/h, (blue) is 6.4 km/h, (green) is 9.7 km/h, (red) is 12.9 km/h, and (purple) is 16.1 km/h
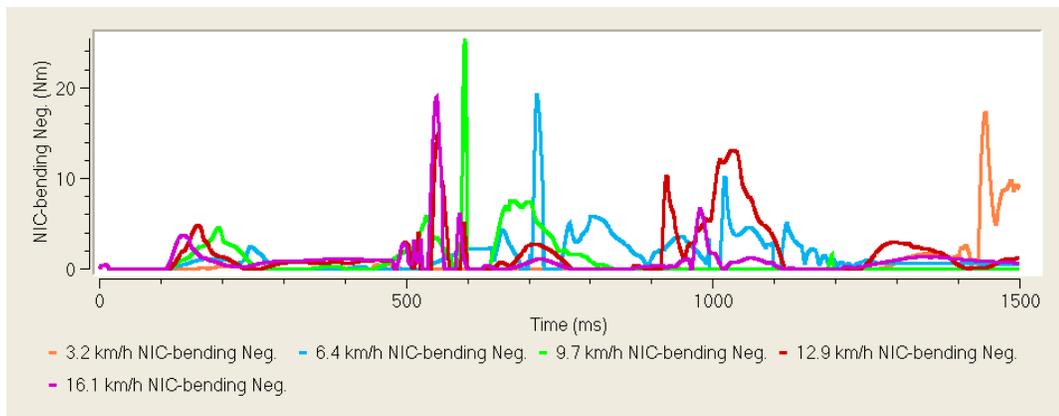
Figure 18: NIC-bending negative [Nm] time series plots of representative collision scenarios at 443.4 N grip strength and all ΔVs, where (orange) is 3.2 km/h, (blue) is 6.4 km/h, (green) is 9.7 km/h, (red) is 12.9 km/h, and (purple) is 16.1 km/h
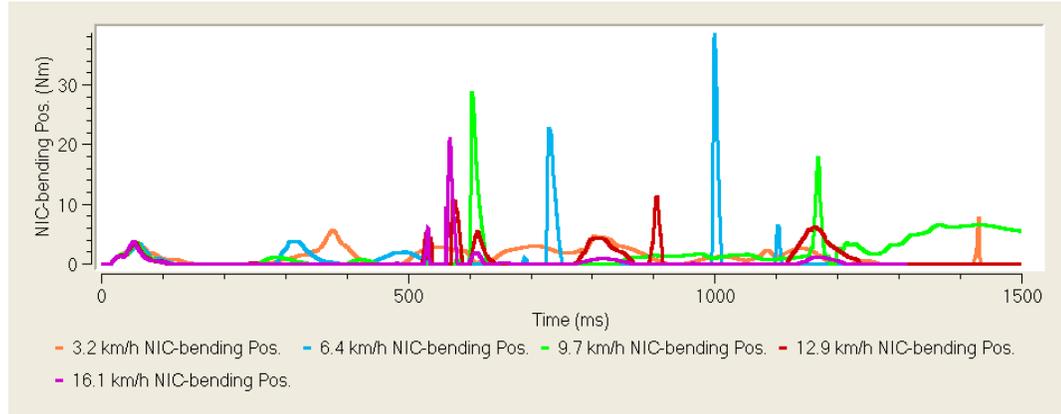
Figure 19: NIC-bending positive [Nm] time series plots of representative collision scenarios at 443.4 N grip strength and all ΔVs, where (orange) is 3.2 km/h, (blue) is 6.4 km/h, (green) is 9.7 km/h, (red) is 12.9 km/h, and (purple) is 16.1 km/h

3.4.4 N_{ij} Time Series

A representative time series plot for ΣN_{ij} at the mid-range grip (443.4 N) are

shown in Figure 20, including all combinations of tension/compression and

flexion/extension. For these particular scenarios, the sum of the maximum values is

highest ($\Sigma N_{ij} = 2.8$) in the 16.1 km/h (10 mph) condition.
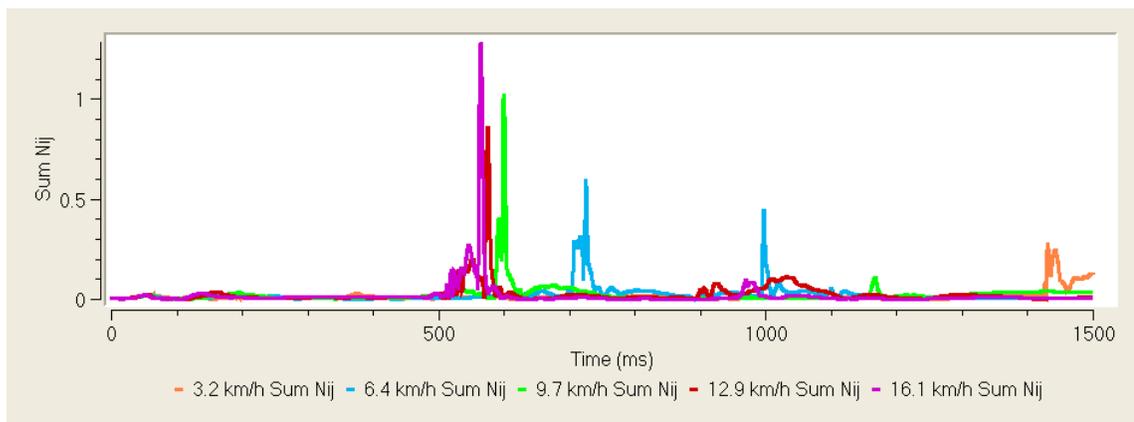
Figure 20: ΣN_{ij} time series plots of representative collision scenarios at 443.4 N grip strength and all ΔVs, where (orange) is 3.2 km/h, (blue) is 6.4 km/h, (green) is 9.7 km/h, (red) is 12.9 km/h, and (purple) is 16.1 km/h

3.5   Descriptive Statistics

3.5.1   Statistical Summary

Table 11: IARV descriptive statistics including minimum, maximum, mean, and standard deviation for all ΔVs (3.2-16.1 km/h) and all grip strengths (0-678.9 N) with the respective injury threshold limits included

IARV	Min	Max	Mean	Std Dev	Limit
HIC_{36}	0	1,435	368	114	1,000
Omega [rad/s]	3	59	41	9	32
Alpha [rad/s^2]	73	25,056	10,981	2,626	1,700
NIC-tension neg. [N]	83	8,441	3,534	691	1,100
NIC-tension pos. [N]	19	2,406	1,423	406	1,100
NIC-shear neg. [N]	59	476	288	57	1,100
NIC-shear pos. [N]	16	2,013	685	146	1,100
NIC-bending neg. [Nm]	0.4	53.6	20.0	2.9	57.0
NIC-bending pos. [Nm]	4.4	66.3	20.1	4.7	57.0
ΣN_{ij}	0.0	3.2	1.4	0.3	1.0

The minimum, maximum, mean, and standard deviations were found for each of the ten IARVs examined for all 45 trials (Table 11). Mean values that exceeded their injury thresholds include angular velocity (41 rad/s), angular acceleration (10981 rad/s^2), NIC-tension negative (3534 N), NIC-tension positive (1423 N), and ΣN_{ij} (1.4). Mean values that were within injury thresholds include HIC (368), NIC-shear negative (288 N), NIC-shear positive (685 N), NIC-bending negative (20.0 Nm), and NIC-bending positive (20.1 Nm).

3.5.2   Results Grouped by Velocity

Groupings of median IARVs by velocity are shown in Table 12, with minimum and maximum values included in error bars. Specific IARV outcomes for the varied ΔVs are shown in Figure 21 through Figure 27. Graphs of the IARVs by ΔVs show a general triangular-shaped trend with IARVs peaking at 9.7 km/h, and oftentimes dropping off at the 12.9 km/h scenarios.

Table 12: Median IARVs by ΔV for all grip strengths with the respective injury threshold limits included

ΔV [km/h]	**3.2**	**6.4**	**9.7**	**12.9**	**16.1**	**Limit**
HIC_{36}	69	417	1,029	221	337	1,000
Omega [rad/s]	30	45	53	41	37	32
Alpha [rad/s²]	6,462	13,243	21,118	6,855	10,195	1,700
NIC-tension neg. [N]	568	3,338	6,176	4,710	6,174	1,100
NIC-tension pos. [N]	990	1,657	2,203	1,117	1,032	1,100
NIC-shear neg. [N]	166	393	412	189	225	1,100
NIC-shear pos. [N]	138	824	1,297	579	958	1,100
NIC-bending neg. [Nm]	10.1	19.4	20.9	14.9	20.5	57.0
NIC-bending pos. [Nm]	9.0	36.4	30.4	12.1	14.0	57.0
ΣN_{ij}	0.5	1.2	2.6	1.3	1.6	1.0
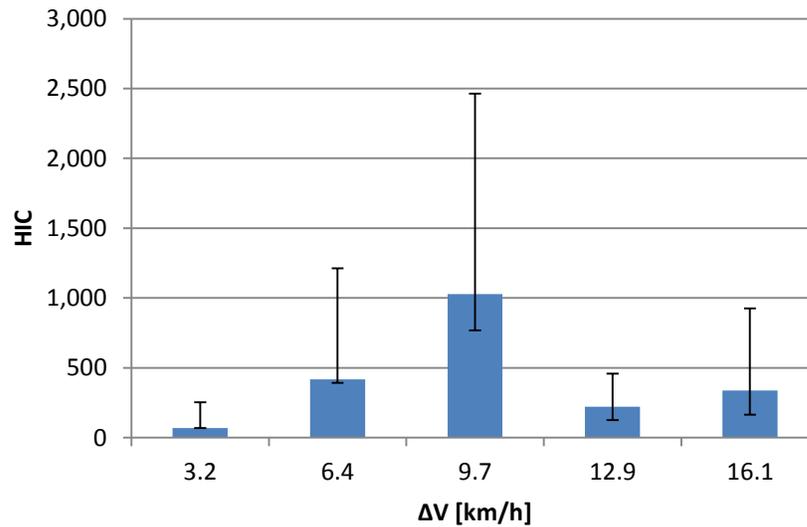
Figure 21: Median HIC vs ΔV for all grip strengths (0-678.9 N) with a limit of 1000 and error bars included

Median Head Angular Velocity vs. ΔV
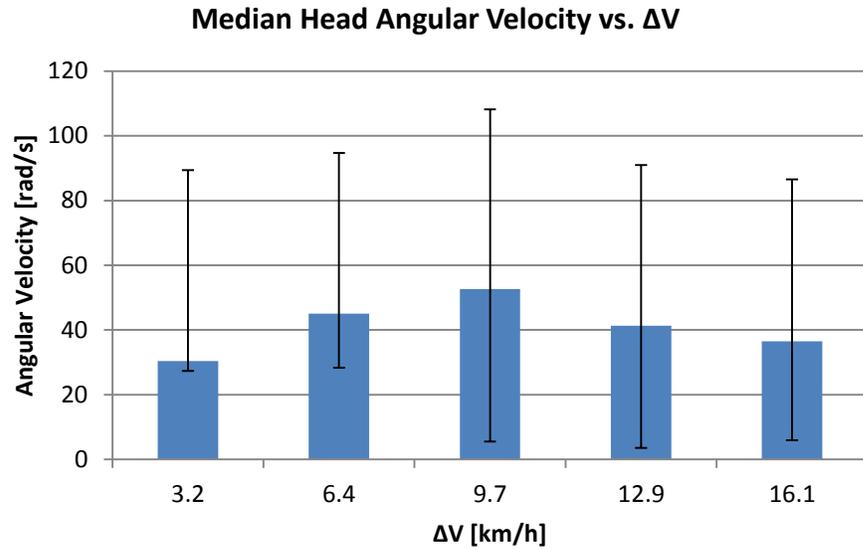
Figure 22: Median head angular velocity vs. ΔV for all grip strengths (0-678.9 N) with a limit of 32 rad/s and error bars included

Median Head Angular Acceleration vs. ΔV
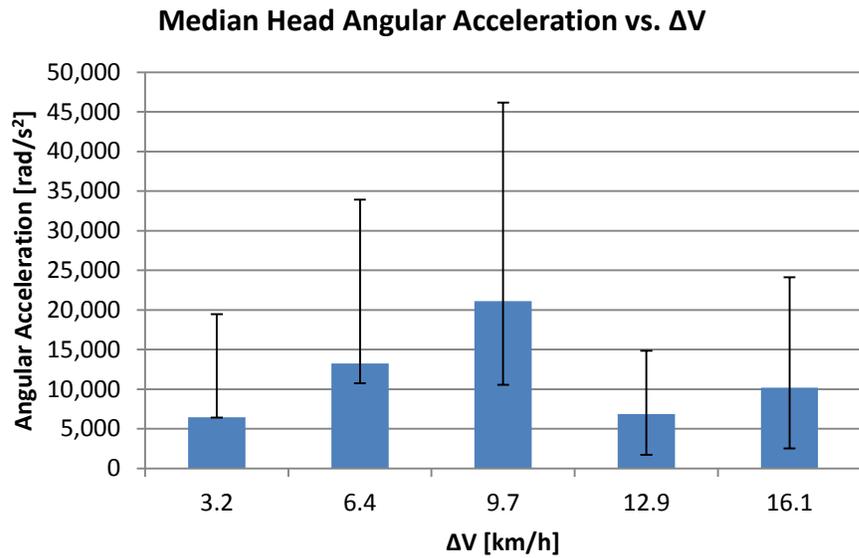
Figure 23: Median head angular acceleration vs. ΔV for all grip strengths (0-678.9 N) with a limit of 1700 rad/s^2 and error bars included

Median NIC Tension vs. ΔV
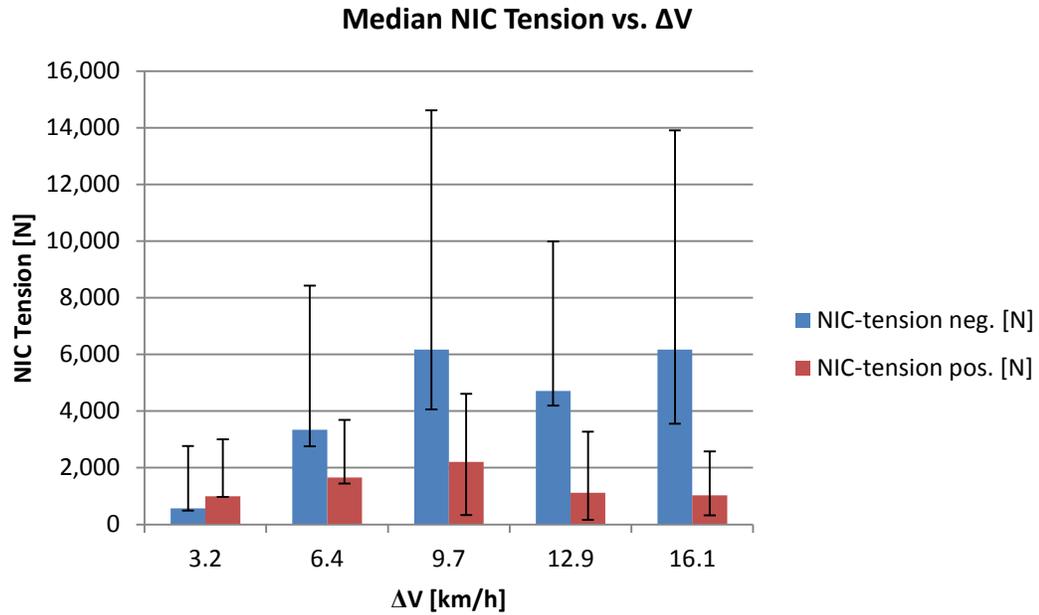
Figure 24: Median NIC tension vs. ΔV for all grip strengths (0-678.9 N) with a limit of 1.1 kN and error bars included

Median NIC Shear vs. ΔV
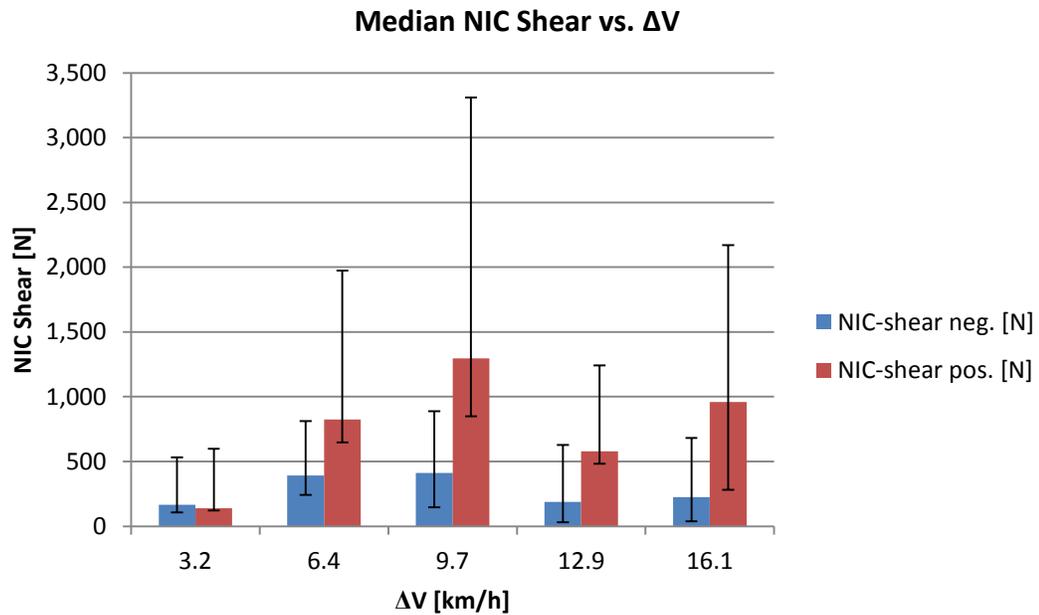
Figure 25: Median NIC shear vs. ΔV for all grip strengths (0-678.9 N) with a limit of 1.1 kN and error bars included

Median NIC Bending vs. ΔV
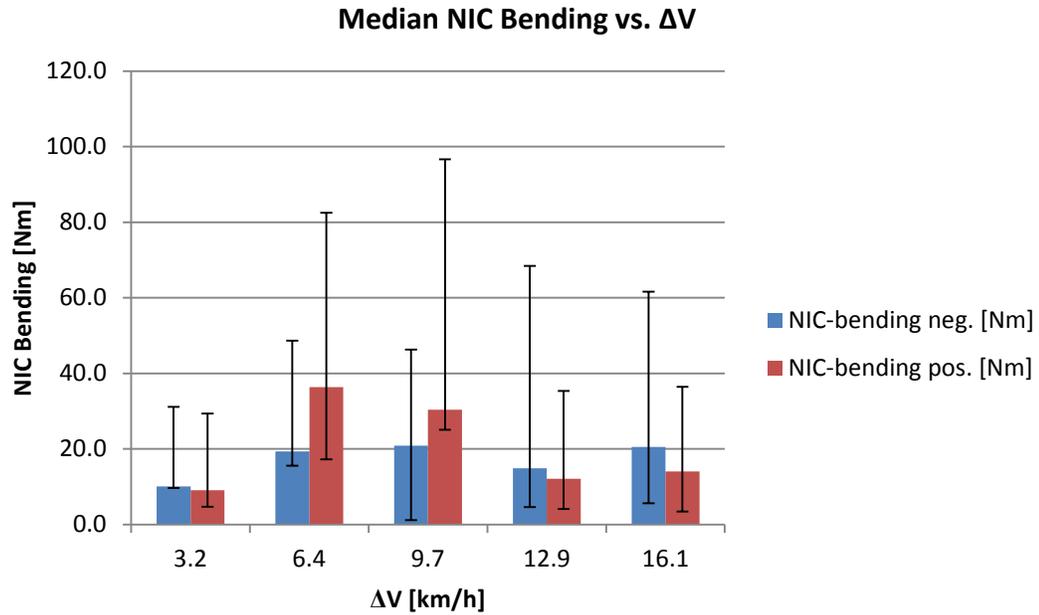
Figure 26: Median NIC bending vs. ΔV for all grip strengths (0-678.9 N) with a limit of 57.0 Nm and error bars included

Median ΣN$_{ij}$ vs. ΔV
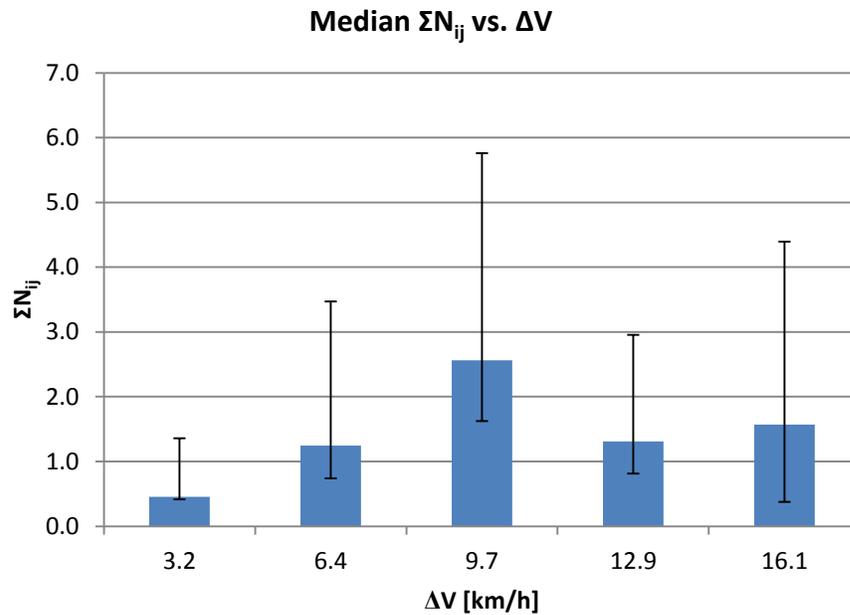
Figure 27: Median ΣN$_{ij}$ vs. ΔV for all grip strengths (0-678.9 N) with a limit of 1.0 and error bars included

3.5.3 Results Grouped by Grip Strength

Groupings of median IARVs by grip strength are shown in Table 13, with

minimum and maximum values included in error bars. Specific IARV outcomes for the

varied grip strengths are shown in Figure 28 through Figure 34. Graphs of the IARVs by

grip strength show two general trends: a triangular-shaped trend with IARVs peaking at

384.6-443.4 N, and a decreasing trend with the highest IARVs at 0 N and lowest IARVs

at 678.9 N.

Table 13: Median IARVs by grip strength for all ΔVs (3.2-16.1 km/h) with the respective injury threshold limits included

Grip [N]	**0.0**	**266.8**	**325.7**	**384.6**	**443.4**	**502.3**	**561.1**	**620.0**	**678.9**	**Limit**
HIC_{36}	172	217	213	313	525	236	414	231	221	1,000
Omega [rad/s]	49	49	50	45	43	40	38	31	31	32
Alpha [rad/s^2]	10,576	9,042	12,331	11,849	13,905	10,793	12,594	6,855	6,713	1,700
NIC-tension neg. [N]	2,865	2,624	3,439	5,099	5,094	4,970	4,833	2,119	2,312	1,100
NIC-tension pos. [N]	2,011	1,754	1,848	1,545	1,657	1,068	980	822	708	1,100
NIC-shear neg. [N]	397	393	330	379	254	247	225	173	315	1,100
NIC-shear pos. [N]	635	677	785	822	848	614	604	579	472	1,100
NIC-bending neg. [Nm]	21.0	19.9	19.4	17.5	18.9	17.9	20.5	17.4	23.2	57.0
NIC-bending pos. [Nm]	13.1	20.3	13.2	18.0	21.2	14.0	20.6	15.9	12.1	57.0
ΣN_{ij}	1.4	1.2	1.3	1.4	1.6	1.3	1.3	1.1	0.9	1.0

Median HIC vs Grip Strength
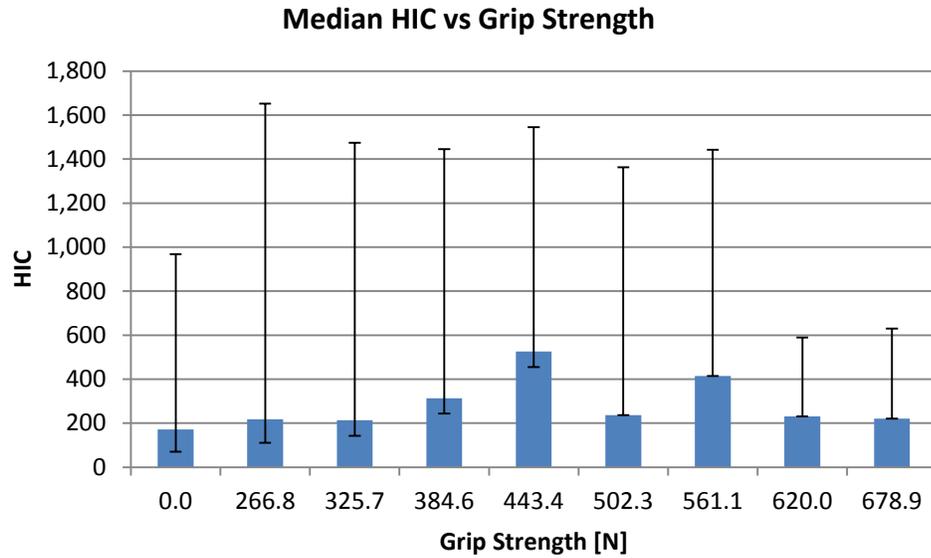
Figure 28: Median HIC vs. grip strength for all ΔVs (3.2-16.1 km/h) with a limit of 1000 and error bars included

Median Head Angular Velocity vs. Grip Strength
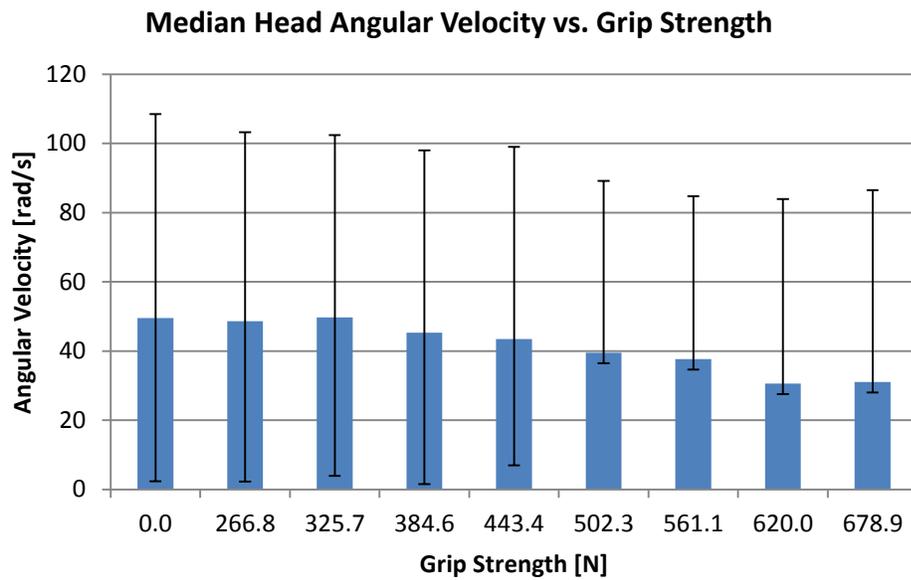
Figure 29: Median head angular velocity vs. grip strength for all ΔVs (3.2-16.1 km/h) with a limit of 32 rad/s and error bars included

Median Head Angular Acceleration vs. Grip Strength
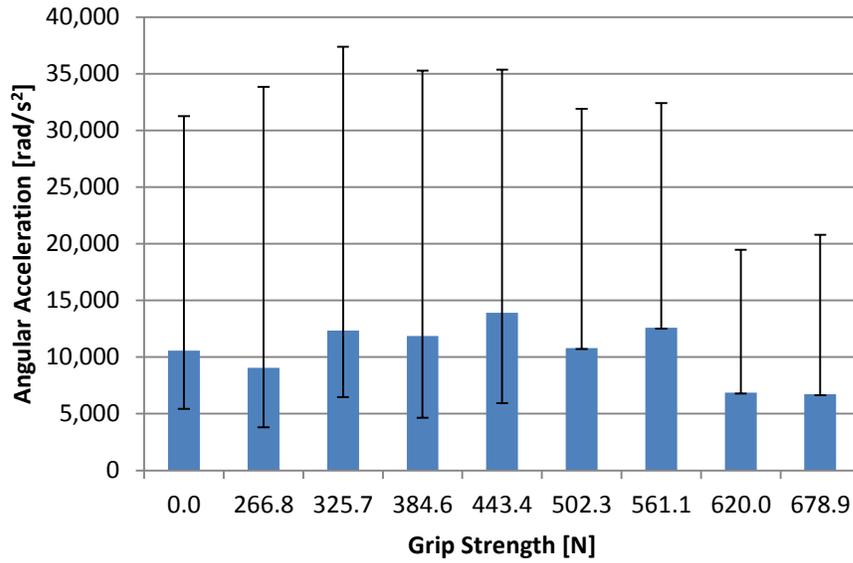
Figure 30: Median head angular acceleration vs. grip strength for all ΔVs (3.2-16.1 km/h) with a limit of 1700 rad/s² and error bars included

Median NIC Tension vs. Grip Strength
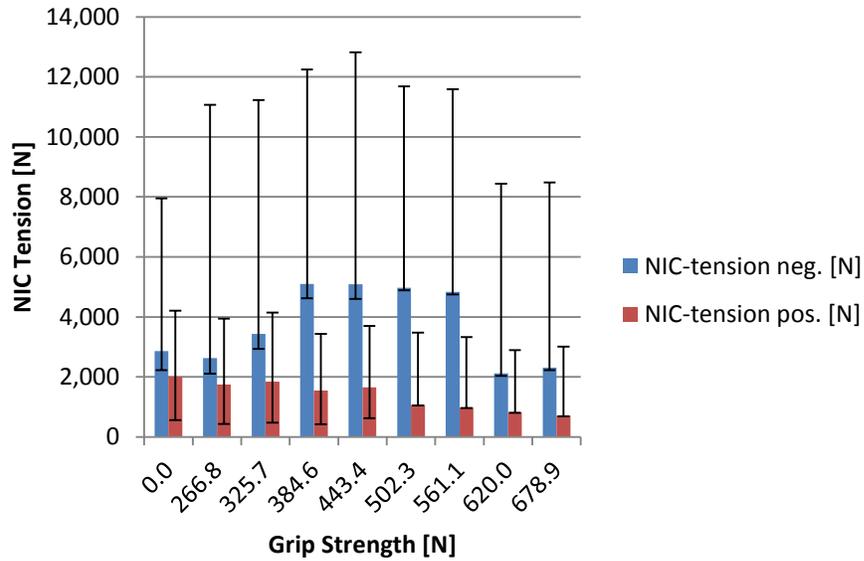
Figure 31: Median NIC tension vs. grip strength for all ΔVs (3.2-16.1 km/h) with a limit of 1.1 kN and error bars included
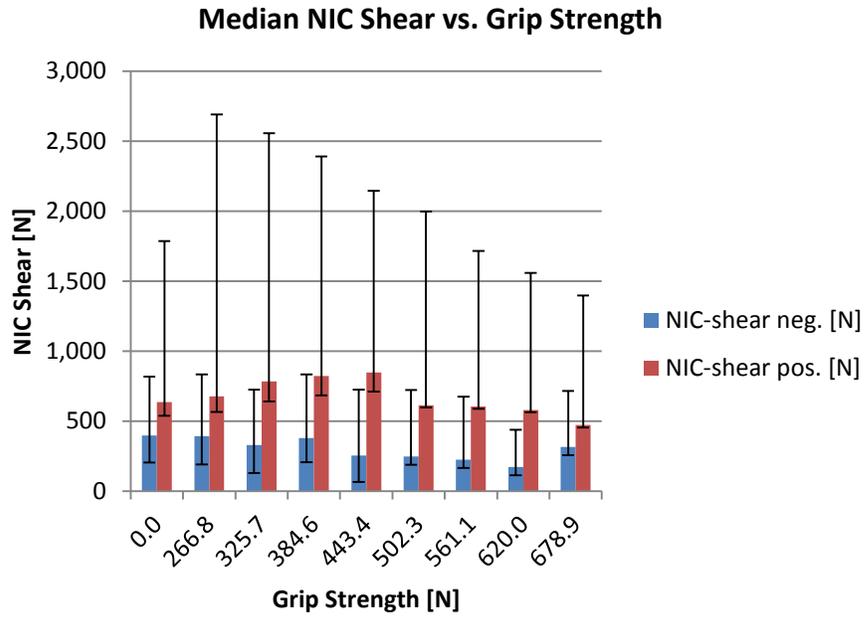
Figure 32: Median NIC shear vs. grip strength for all ΔVs (3.2-16.1 km/h) with a limit of 1.1 kN and error bars included
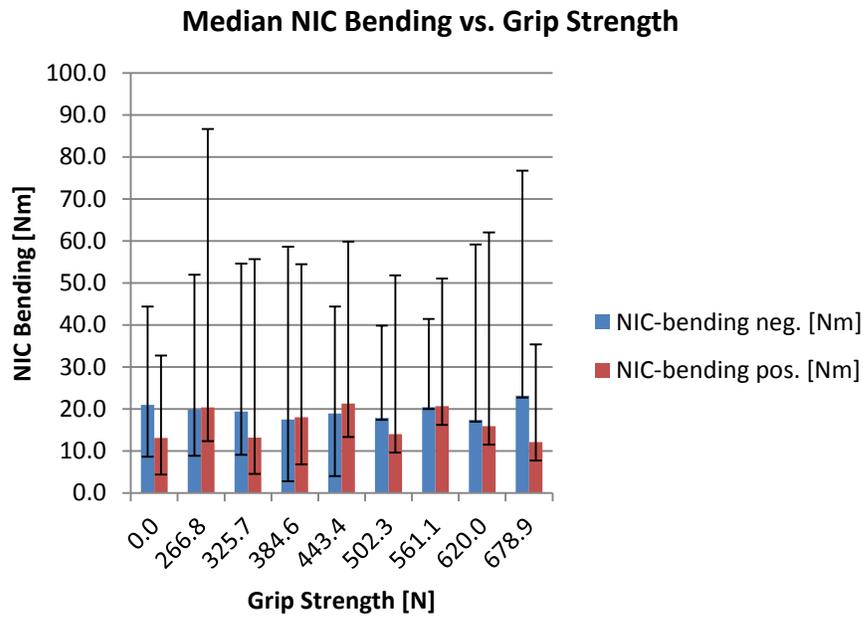
Figure 33: Median NIC bending vs. grip strength for all ΔVs (3.2-16.1 km/h) with a limit of 57.0 Nm and error bars included
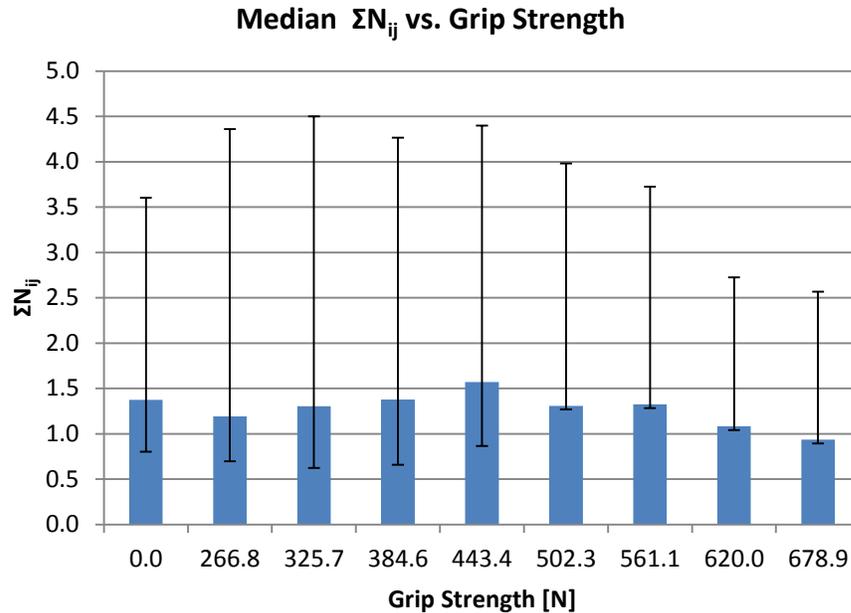
Figure 34: Median ΣN$_{ij}$ vs. grip strength for all ΔVs (3.2-16.1 km/h) with a limit of 1.0 and error bars included

3.6 Regression Modeling

Analysis of the IARV data as compared to the input parameters can yield predictive equations. The predictive equations used in this thesis are linear and nonlinear, allowing for higher order interaction of input terms. The iterative process for creating these equations starts with analysis of the linear regression equation.

3.6.1 Linear Regression

The general form of linear regression fit is shown in Equation 15. An example of a linear regression fit to the data is shown in Figure 35, where a surface map is created to best-fit the IARV data points. Graphs for all IARVs can be found in Appendix A.

$$z = a + bx + cy \tag{15}$$

Figure 35: Linear regression surface fit for HIC outputs with color scale, predictive equation (x_1 is ΔV and x_2 is grip), and adjusted R^2 value
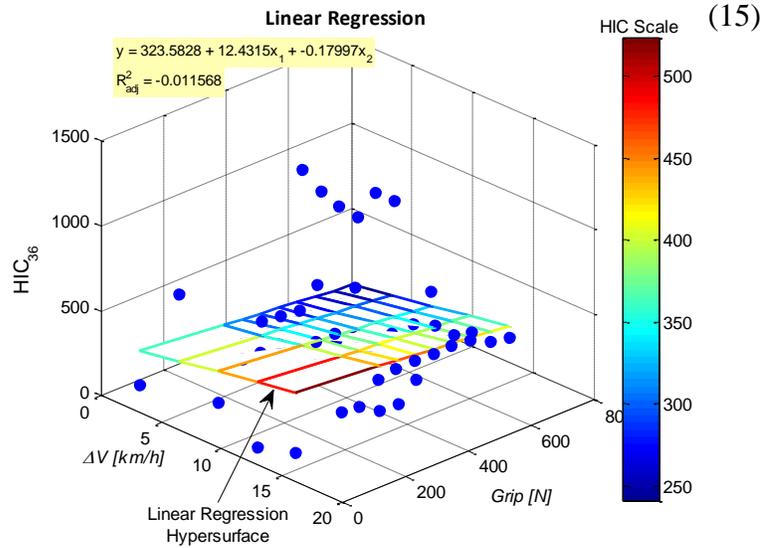
In Equation 15, the output IARV, z, is related to the velocity, x, and grip strength, y, using scaling on each term with regression coefficients, a-c.

Table 14: Linear regression results for predicted IARVs including the regression coefficients (a-c) and the goodness of fit measurements (R^2 and $\overline{R}^2$)

IARV	a	b	c	R^2	$\overline{R}^2$
HIC_{36}	3.2E+02	1.2E+01	-1.8E-01	0.03	-0.01
Omega [rad/s]	5.1E+01	6.7E-01	-3.9E-02	0.31	0.28
Alpha [rad/s^2]	1.3E+04	1.0E+02	-7.5E+00	0.06	0.02
NIC-tension neg. [N]	2.0E+02	3.2E+02	5.2E-01	0.35	0.32
NIC-tension pos. [N]	2.1E+03	8.5E+00	-1.8E+00	0.26	0.22
NIC-shear neg. [N]	3.6E+02	2.4E+00	-2.2E-01	0.14	0.10
NIC-shear pos. [N]	4.0E+02	4.2E+01	-2.9E-01	0.17	0.13
NIC-bending neg. [Nm]	1.0E+01	9.7E-01	-5.9E-04	0.19	0.15
NIC-bending pos. [Nm]	2.4E+01	-1.5E-01	-5.3E-03	0.01	-0.04
ΣN_{ij}	8.1E-01	8.2E-02	-5.5E-04	0.22	0.18

Coefficients of determination (R^2) and adjusted R^2 ($\overline{R}^2$) from the linear regression results were considered low ($R^2 < 0.5$, $\overline{R}^2 < 0.5$), as shown in Table 14. Despite the low correlation, residual plots for velocity and grip strength did not show nonlinear trends as exemplified in Figure 36 and Figure 37, respectively. Therefore, a higher order regression equation is indicated for use based only on the low correlation. Additional plots for linear regression and residual tables can be found in Appendix A.
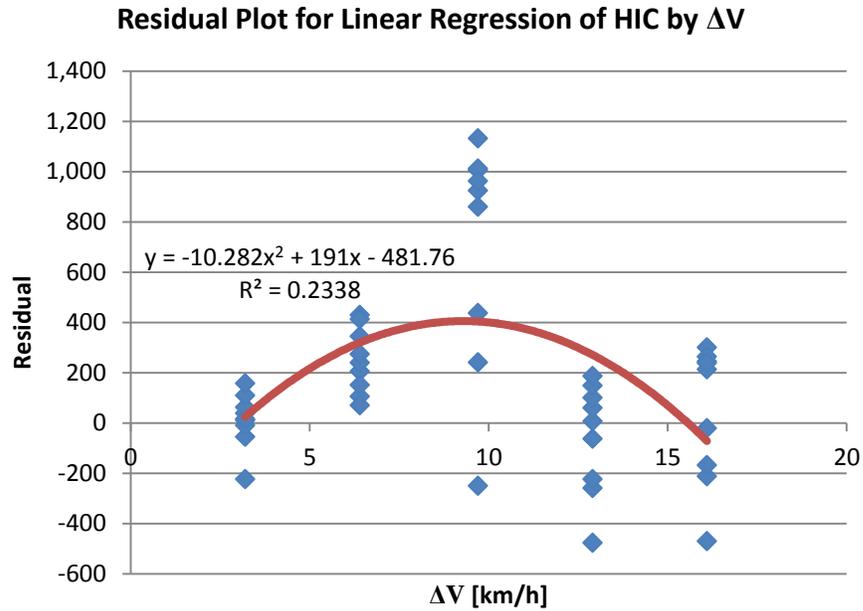
Figure 36: Residual plot for linear regression of HIC by ΔV for all grip strengths (0-678.9 N)
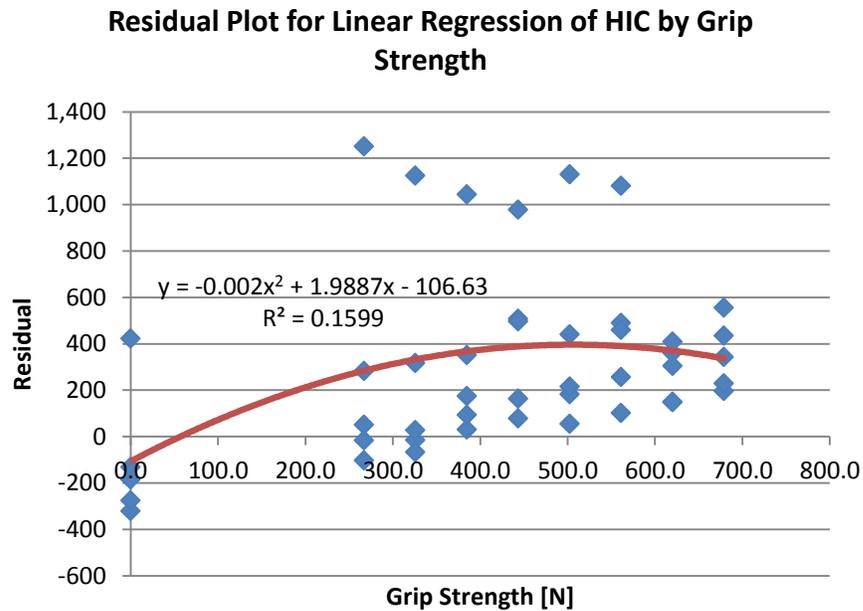
Figure 37: Residual plot for linear regression of HIC by grip strength for all ΔVs (3.2-16.1 km/h)

3.6.2   *Quadratic Regression*

Quadratic regression models of the IARV data showed high correlation for IARVs. In particular, quadratic regression models without linear or interaction terms showed very high correlation for HIC ($\overline{R}^2$=0.83), angular velocity ($\overline{R}^2$=0.88), NIC-shear positive ($\overline{R}^2$=0.85), and NIC-bending negative ($\overline{R}^2$=0.85). The modified equation for a quadratic model without linear or interaction terms is shown in Equation 16. An example of a modified quadratic fit to the data is shown in Figure 38, where a surface map is created to best-fit the IARV data points. Quadratic regression results without linear or interaction terms are shown in Table 15.

$$z = a + bx^2 + cy^2 \tag{16}$$

Figure 38: Modified quadratic regression surface fit for HIC outputs with color scale, predictive equation (x_1 is ΔV and x_2 is grip), and adjusted R^2 value

In Equation 16, the output IARV, *z*, is related to the velocity, x, and grip strength, *y*, using scaling on each term with regression coefficients, *a-c*.
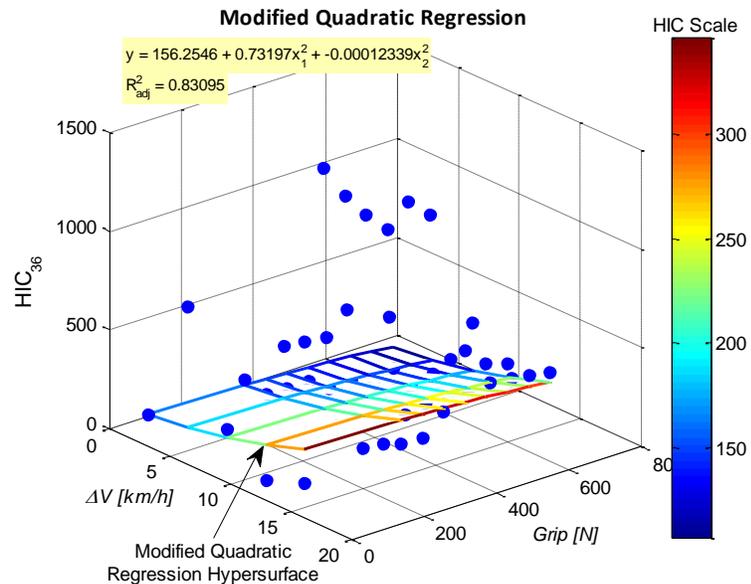
Table 15: Modified quadratic regression results without linear or interaction terms for predicted IARVs including the regression coefficients (a-c) and the goodness of fit measurements (R^2 and $\overline{R}^2$)

IARV	a	b	c	R^2	$\overline{R}^2$
HIC_{36}	1.6E+02	7.3E-01	-1.2E-04	0.84	0.83
Omega [rad/s]	5.2E+01	-7.0E-03	-4.1E-05	0.89	0.88
Alpha [rad/s^2]	1.3E+04	-5.5E+00	-7.6E-03	0.07	0.03
NIC-tension neg. [N]	1.7E+03	2.2E+01	-2.6E-03	0.20	0.16
NIC-tension pos. [N]	2.1E+03	-1.6E+00	-2.3E-03	0.26	0.23
NIC-shear neg. [N]	4.3E+02	-3.8E-01	-3.5E-04	0.02	-0.03
NIC-shear pos. [N]	2.7E+02	2.8E+00	-2.1E-04	0.86	0.85
NIC-bending neg. [Nm]	1.9E+01	7.5E-03	-1.7E-06	0.86	0.85
NIC-bending pos. [Nm]	2.0E+01	-2.3E-02	5.9E-07	-0.02	-0.07
ΣN_{ij}	8.8E-01	3.8E-03	-6.8E-07	0.11	0.07

Further regression analysis was performed on the data; however no models (up to 3rd order) produced higher overall correlation coefficients than the modified quadratic model. Additional tables, figures and equations for regression results can be found in Appendix A.

MATLAB code for generation of regression results can be found in Appendix B.

4   DISCUSSION

443.4, and 678.9 N) broke above their intended rupture strengths. The highest simulation error for these trials was 4.5%. Although the particular origin of this error is uncertain, it is likely due to simulation error in the MADYMO system itself. This must be accounted for when considering the accuracy of the model.

4.2.2   *Biofidelity of the ATD*

The ATD used for these trials was a MADYMO supplied standing Hybrid III 50th percentile male dummy. Modifications were made within MADYMO which permitted the ATD to stand, including straightened and stiffened lower extremity joints. These same modifications were previously implemented using manual methods by other researchers [60, 75, 100]. The overly stiffened joints introduce a lapse in biofidelity which might profoundly affect the results of the collision trials. Although examination of ATD biofidelity was not a main focus of this thesis, it may prove to explain certain fall mechanics which will be discussed later.

One user modification to the MADYMO supplied ATD was included on the basis of promoting biofidelity in the ATD. The modification included contact between the arms and the body of the ATD. During input integrity verification trials in a gravity environment it was recognized that the arms were free to move through the body (i.e., no contact was defined). The verification trials were re-run with appropriate upper extremity contact definitions, and this modified ATD was used for all future trials. Because of the added contact between the arms and upper body, the arms were restricted in movement, illuminating another biofidelic issue of the ATD: joint type selection.

The joint types of the shoulders, elbows, and wrists are all universal joints, however these joint types might not be appropriate for the dynamic scenarios encountered in this thesis. During examination of the video for the various collision scenarios it was recognized that the arms could rotate externally at the elbows in a manner unbefitting of physiological movement. If the shoulders were changed to spherical joints and the elbows to revolute joint, then this issue might not occur. However, for these trials the arms were kept as supplied with the joint types initially specified, and the outcome of the trials was not presumed to be affected.

4.2.3 *Haversine Impulse Peak and Its Relation to Postural Stability*

The lowest peak acceleration for the haversine impulse was set at 17.9 m/s^2 (1.82g). This value greatly exceeded the published limits for postural stability in the lateral direction. Postural stability is defined by the center of gravity (COG) projection staying with the perimeter of all contact points of the body [99]. The area within these points of contact is called the base of support (BOS) [99]. Seminal work by Jonkees et al. in 1942 set the limits of postural stability for forward, backward, and lateral accelerations at 0.049g, 0.076g, 0.034g, respectively [40]. These limits were later corroborated by DeGraaf et al. and Harris et al., who found the lateral acceleration threshold for postural stability to be between 0.046g and 0.11g [19, 32, 33]. It would stand to reason that the accelerations experienced by the ATD in the SQM trials would cause stability loss and subsequent injury, however this was not the case. In trials at a ΔV of 3.2 km/h (2 mph, a_{peak} = 1.82g), upper extremity contact between the ATD and SQM was retained at grip strengths above 502.3 N (112.6 lbf), and for trials at a ΔV of

6.4 km/h (4 mph, $a_{peak} = 3.64g$) and grip above 561.1 N (139.0 lbf), grip loss was delayed. In both of these scenarios, the postural stability was not lost or the subsequent fall was delayed, thereby mitigating the injury. Further analysis of the means by which the ATD fell may provide better insight into the injuries sustained by the ATD.

4.3   Fall Progression

Visual analysis of the fall progression can demonstrate how the ATD fell and perhaps link that to the injury mechanisms likely to be experienced by real operators. In the progression of the fall (if the ATD fell), there were three characteristics unique to this application: latent grip loss, rolling/rebounding body, and lack of reflexive movements. Grip was lost for the majority of the trials, causing the ATD to fall outside the SQM. However, sometimes a latent grip loss altered the mechanisms of the fall and produced adjusted IARVs. Rolling and rebounding of the body was experienced seemingly at random, again causing different injury mechanisms. Lack of reflexive movement was inherent in the setup, as the ATD was not designed with a muscle model. This was to be expected, but physiological study of fall protection mechanisms may provide insight as to how the real operator may react in a collision scenario similar to the ones simulated in this thesis.

4.3.1   Latent Grip Release

Some of the collision trials experienced phenomena in which the ATD retained grip for longer than usual, altering the subsequent fall pattern and temporal

characteristics of the simulation. As mentioned earlier, grip was retained longer for ΔVs of 3.2-6.4 km/h (2-4 mph) at higher grip strengths in which the impact force was not sufficient to break the belts connecting the hands and controls; body inertia was need to break the belts. This altered the fall pattern of the ATD where it would swing its left shoulder inward and lean gently out of the SQM compartment causing it to fall not only laterally (as typically seen) but also forward. Because of the leaning of the ATD, it would not fall as far to the ground, mitigating almost all IARVs experienced. Drastic reduction in IARVs with latent grip loss is shown in the full simulation results in Appendix A.

When the ATD loses grip it has also lost postural stability because its BOS is outside its COG, however the results of the latent grip loss trials elucidate a disparity between postural instability and injury. For applications where an upper extremity grip is present, examination of postural stability alone is not enough to predict injury. Sufficient grip strength can anchor the body with respect to the environment, keeping the COG within the total BOS, although the COG may lie outside the feet-defined BOS [97].

Considerations for grip release must take into account the operation of a live forklift. While the controls in the model do not actually direct the SQM, the controls steer the forklift in live operation. If a live operator were to maintain grip or experience latent grip release, the forklift would change direction and perhaps encounter a different collision scenario and injury outcomes than those modeled.

4.3.2   Rolling and Rebounding Body

Settlement of the ATD after initial contact with the ground was dramatically different between trials. Some trials experienced the ATD rolling onto its front or back or rebounding off the ground incurring multiple contacts. Examination of these particular scenarios may provide explanations as to the attenuated IARV outcomes experienced at the 12.9 and 16.1 km/h conditions. For the higher ΔV scenarios and all grip strengths, the ATD rebounded off the ground at least once, ultimately rolling onto its back. This reduced almost all IARVs as compared to the low ΔV scenarios (< 9.7 km/h). However, it is unclear whether the rolling of the ATD is due to natural biomechanical phenomena or because the overly stiffened lower extremities hit the ground and force the ATD to roll. It seems in these scenarios that the ATD was launched out of the SQM thereby roughly translating about its long axis and never incurring the full force of the fall in the head and neck because initial contact was absorbed by the shoulder.

4.3.3   Altered Operator Orientation

Following from the fall mechanisms which lead to a rolling and rebounding body is the orientation which may cause those phenomena. Data from mid-range ΔV (9.7 km/h) and grip strength (443.4 N) which contains varied orientations of the ATD at ± 4 degrees transverse rotation in 2 degree increments shows that the orientation does have a dramatic effect on the injury outcome. Those orientations which place the ATD in an off-perpendicular position tend to produce lower IARVs, such that the transverse

rotation is inversely proportional to IARV. Data from these trials can be seen in
Appendix A.

4.3.4 *Absence of Reaction Mechanism*

The limitations of the ATD used for this thesis precluded neuromuscular reflexes
of the standing ATD during the collision trials. These reactions would be seen with real
operators in a live environment, but are difficult to mimic in a computer environment. A
distinction must be made between postural reflexes (those that prevent falls or regain
balance) and protective reflexes (those that mitigate injury) [37]. Postural reflexes to
recover balance have a 90 ms reaction time, which is barely below the 100 ms haversine
impulse duration used in the dynamic trials [37]. This would lead one to believe that
balance recovery might be just enough to prevent the vehicle operator from being
ejected from the vehicle compartment. Furthermore, foundational work by Hsiao et al.
on protective movements for falls while standing discovered that 78% of subjects were
able to avoid lateral falls, suggesting that perhaps the operator might recover balance
and not fall at all [36]. But the mechanisms which prevent falling are contraindicated for
dynamic horizontal platform scenarios. The most common fall avoidance mechanism is
stepping, which attempts to expand the BOS such that the COG again falls within the
BOS [36, 97]. However, reflexive stepping would cause the operator to step outside the
vehicle compartment and propagate the fall that was initiated [36]. Upon fall progression
protective reflexes of the upper extremity tend to injure the wrist as the subject extends
the arm to mitigate the fall impact to the hip and pelvis [36]. For the scenarios indicated

by the simulation run in this thesis, injury would be even greater due to the added height of the platform on which the operator stands.

4.4   Time Series

Temporal analysis of the IARVs can provide information on how the ATD incurs injury over time. Of particular note are the submaximal peaks of the time series plots and how the peaks relate to the visual analysis of the fall progression. Submaximal peaks may present more complex injuries not identified by only examining the peak IARV values. Concurrent analysis of the time series IARV peaks with the fall progression can link the quantitative data to the qualitative data.

4.4.1   Submaximal Peaks and Their Importance

The submaximal peaks of the time series plots show possible injuries that were not identified by the peak IARVs reported. For the trials of ΔV at 6.4 km/h (4 mph), there were often double peaks that were nearly commensurate in magnitude. Sometimes the second peak (latent contact) would surpass the first, identifying a situation where the peak IARVs reported were not specific to one time point. The double contact situations could affect the physiological response of the head/neck complex, perhaps even creating resonant injury mechanisms otherwise hidden by the peak IARV results.

For all ΔV conditions, the angular velocity time series plots show a steep primary peak followed by a smoother secondary peak. This suggests that the head is experiencing successive peaks in speed, likely in opposite directions which may give

more credence to a resonance of the soft tissue matter in the head. As expected, these dual angular velocity peaks are complimented with singular steep angular acceleration peaks. Based on seminal work by Gurdjian et al. in 1953-1954, the high accelerations suggest intracranial pressures which are indicative of concussions [25, 27].

4.4.2   Peak IARV Comparison to Fall Progression

Concurrent analysis of the peak IARVs and fall progression may provide a fuller picture of the injury mechanisms experienced by the ATD, which might not be distinguishable from separate analyses of both. In all cases, the higher ΔVs show visual ATD contact with the ground earlier, which is corroborated by the time series plots of the IARVs. Of interesting note is that the 12.9 km/h and 16.1 km/h conditions show multiple ground contacts, but only the 12.9 km/h (8 mph) condition shows multiple large peaks for the time series plots, much like the 6.4 km/h (4 mph) condition, but with smoother slopes. Upon further examination of the fall progression videos, it can be seen that the 12.9 km/h (8 mph) trials have the ATD roll onto its back earlier than the 16.1 km/h (10 mph) trials, perhaps causing the multiple weak peaks which would be encountered at the back of the head and in almost pure neck flexion/extension. These results suggest that anterior-posterior movement of the body protects against head/neck injury better than lateral body movement.

4.5   Application Comparison to Literature

Direct comparison of the SQM outcomes to other dynamic horizontal platform model, their resulting IARVs, and their use of IARVs can elucidate the similarities and differences between previous studies and the current study. Forklift-derived models or other dynamic horizontal platform studies show how a standing operator/passenger responds to a sudden perturbation. Those studies typically end in injury, which can be compared to the IARVs found in this thesis and their supposed mechanisms.

4.5.1   Dynamic Horizontal Platform Models and Fall Protection

Previous studies on the injuries incurred by PITs and public transportation can be related to the findings from the SQM. These share the commonalities of a standing user on a dynamic horizontal platform with upper extremity grip. Data from modeling studies and live surveys can be compared.

Simulated PIT (forklift) models for tip-over and off-dock scenarios run by Zoghi-Moghadam et al. and Meyer et al. experienced maximum HIC values between 423 and above 2,200 [60, 100]. The maximum HIC from this thesis was 1,435, which falls within the range reported by the aforementioned literature. When considering trials where a lateral constraint (door) was present, results from this thesis show much lower IARVs than those trials without a door. These findings are in agreement with Meyer et al. and opposed by Zoghi-Moghadam. However, the study by Zoghi-Moghadam does not explicitly state the assessment of both door and no-door trials [60, 100]. Database surveys performed by Railsback et al. and Berry as well as live testing performed by

Carlin and Sances Jr. agree with the findings of Meyer et al. and this thesis in that doors tend to prevent the operator from being ejected from the forklift compartment and suffering greater injury [7, 14, 15, 60, 78]. However, all of the aforementioned studies except Zoghi-Moghadam et al. do not account for ΔV, so the results may differ with a series analysis of ΔVs as compared to injury. A comparison of the door vs. no door scenario is shown in **Error! Reference source not found.**, which shows a clear arresting of lateral movement leading to dramatically lowered IARVs.
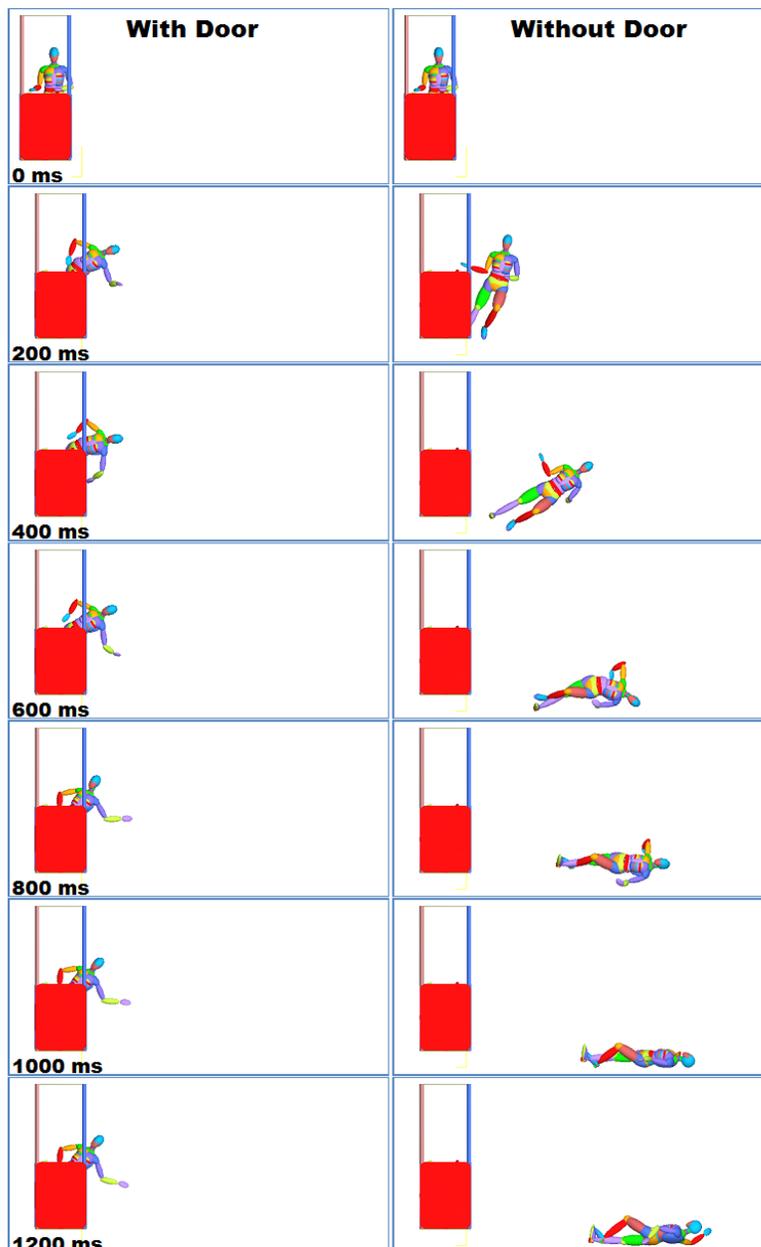
Figure 39: Fall progression comparison of door and no door trials for ΔV of 16.1 km/h (10 mph) and no grip

A simulated public bus model performed by Palacio et al. showed a maximum HIC value of 758 [75]. This is in general accordance with the HIC values found in this thesis. One note from

Palacio et al. suggests that hand supports placed at hip level are not as protective as supports placed above the head [75]. This would follow that the extremity controls present in the SQM (and subsequently in a live forklift) do not provide an ideal arrangement to mitigate injury in a harsh deceleration scenario; however, forklift controls placed above the head would not be ideal for operation. Because the Palacio et al. study does not consider varied grip strengths, it is impossible to determine how grip strength might affect the ideal hand contact positioning.

4.5.2   Reversed Operator Positioning in Forklift

The position of the operator in the SQM (representative forklift) for this thesis was based on numerous forklift models wherein the operator's left side faces the forklift entrance. This necessitates left foot brake activation, left hand tiller grip, and right hand MFCL grip. However, an example of a forklift model provided by Washington State Department of Labor and Industries shows the opposite orientation, thereby calling into question the effect of side dominance in forklift operation (Figure 40) [21].
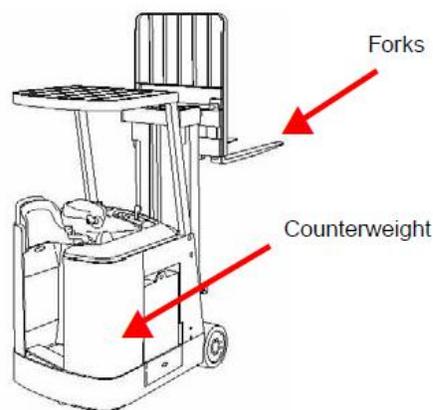
Figure 40: Example of a class I stand-up electric forklift [21]**. Reprinted with permission from Washington State Department of Labor & Industries**

The mechanics of the upper extremity grips and lower extremity stance in this thesis were irrespective of upper or lower extremity side dominance.

However, a more realistic scenario may show preference to a particular side of the body for grip or stance. Work by Incel et al. on hand dominance showed that the non-dominant hand averages 68.0 N less grip strength than the dominant hand [39]. An alternate forklift-operator orientation, wherein the right side faces the forklift entrance, may have drastically different results due to operator side dominance for live operators with active response mechanisms.

4.5.3   *IARV Evolutions and Their Adaption to Applications*

IARVs were created for ease of injury assessment in specific scenarios, and have since been adapted to fit the needs of a myriad of studies. While their standardization provides a basis for comparison between studies, their use must be examined with regard to their inception, certifying that they are either appropriate for use or understanding the limitations for contraindicated use. In this thesis, IARVs were typically lower for those trials which saw the ATD roll upon impact, suggesting that the IARVs are directionally dependent.

HIC was originally developed by Versace in 1971 in response to head impact criteria that lacked a solid foundation [96]. The criteria that prompted the development of HIC were based mainly from cadaveric and animal tests impacting the front of the skull as shown in Figure 41 [48]. Since then HIC has been adopted by many researchers including Zoghi-Moghadam et al., Meyer et al. and Palacio et al. for tests which may include lateral or rear impacts, however, the threshold that estimates injury and the determination of HIC is still founded from frontal impacts.

Accelerometer

Pressure gages

A

59 7/8"

14 1/2"

D

Floor
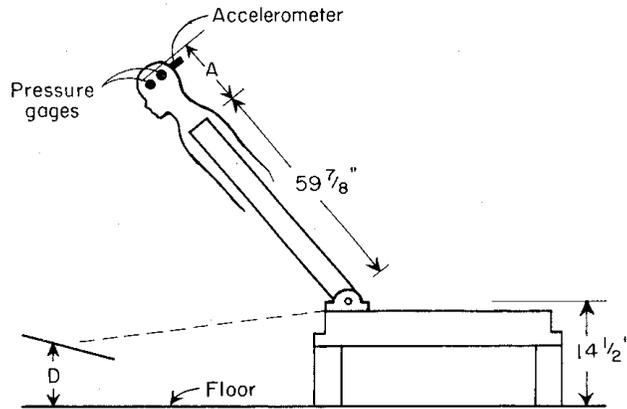
Figure 41: Head impact apparatus for human cadaver [48]**. Reprinted with permission from the Journal of the American College of Surgeons, formerly Surgery Gynecology & Obstetrics.**

While HIC has yet to be revised, it has been highly criticized for its inability to correlate injury to kinematics, describe continuous injury severity, and account for varied impact location [24, 51, 65]. Also, HIC is only valid for contact scenarios involving linear acceleration of the head, while the rotational response of the head has been shown to cause injury as well [90].

Angular velocity (ω) and acceleration (α) are rarely found in literature relating to applications for collision scenarios. While seminal work performed by Ommaya et al., Unternharnsheidt et al. and Löwenhielm to determine the thresholds for ω and α was exhaustive, few applications have adapted these IARVs, yet these IARVs consider rotational motion which has been identified as causing shear stress, and subsequent concussion [49, 50, 72, 73, 92]. However, the rotational motion of the study subjects was purely in the sagittal plane, neglecting lateral motion.

NIC and N_{ij} were also formed on the basis of studies which considered only sagittal motion of the head/neck. These are also scarce in their application, as evidenced by their paucity in literature. The tension/compression and flexion/extension motion, however, is well described within the sagittal plane. Given the understanding of the IARV evolution precaution should be taken when applying HIC, ω, α, NIC, and N_{ij} assessment to lateral impact scenarios. Until a new injury criterion which accommodates

lateral impact scenarios is widely adopted, the current IARVs will continue to be used and compared amongst researchers.

4.6   Regression Modeling

Regression models can simplify a complicated system into an equation containing a limited number of inputs and one output. These equations can be used in lieu of the full system (i.e., MADYMO) to predict the outputs based on the input parameters. For this thesis, a modified quadratic regression equation was determined to be the best applicable for HIC, ω, NIC-shear positive, and NIC-bending negative. An understanding of the benefits and drawbacks to the regression model should be employed before applying the model to a new dataset.

4.6.1   Where Regression Models are Useful

Regression models are useful for relating input variables to an output in a simple format. The regression model used in this thesis relates ΔV and grip strength inputs to the IARV outputs. A high correlation, in this case adjusted coefficient of determination ($\overline{R}^2$), is generally a measure of the goodness of fit of the model to the data. In the case of $\overline{R}^2$, it measures the explained variance in the model and accounts for additional terms that would increase the coefficient of determination (R^2) while increasing the complexity of the model [80]. The modified quadratic model is useful because it maintains a high $\overline{R}^2$ for HIC, ω, positive NIC-shear, and negative NIC-bending with only three terms. The simplicity of the regression equations for the indicated IARVs

should make them widely applicable for industries utilizing forklifts or similar dynamic horizontal platform vehicles.

4.6.2 Drawbacks of the Regression

While the modified quadratic regression is widely applicable for the IARVs indicated, it does not extend to all IARVs. Further analysis could be performed to produce a better regression model which garners high $\overline{R}^2$ for all IARVs on the basis of the total data reprinted in Appendix A. When considering regression models for use, it must be understood that they do not imply causation, but merely demonstrate the goodness of fit for that particular model to the data. Moreover, the $\overline{R}^2$ does not denote whether the appropriate regression was used, as residual plots can [61].

4.6.3 Additional Uses for Regression Data

The data for the previously mentioned regression models has already been collected, and can be analyzed without additional MADYMO simulations. While cluster analysis was not performed in this thesis, it may help to identify trend groups. Analysis of the data excluding trials where the ATD either fell out late or not at all might better separate those scenarios where major injury is likely, and those where minor injury is likely. With further study of industrial efficiency, the current regression model (or any future improvement thereof) could identify the operating conditions maximizing safety and efficiency.

4.7   Future Opportunities

Modifications to the ATD, including orientation adjustments, anthropometric scaling, and biofidelity improvements, may allow for a more accurate model. Orientation, height, and weight of the ATD may have an effect on the egress from the SQM compartment and subsequent injury, if ejected. Short (5th percentile) or tall (95th percentile) operators may also contact portions of the SQM upon egress which would otherwise have been avoided. Biofidelity improvements such as full-body muscle models and reflex reactions for the ATD could better liken the ATD to live subjects. If these were implemented, considerations should be made for postural stability and fall avoidance maneuvers. Lastly, a validation of these ATDs in a side stance position would be required, and should be considered even if biofidelity improvements are not implemented.

5   CONCLUSION

This thesis provided a regression equation predicting IARV outcomes based on ΔV and grip strength inputs for a collision scenario involving a dynamic horizontal platform supporting a lateral standing operator with upper extremity grip. A modified quadratic regression equation was used to correlate the inputs to IARV outputs including HIC, ω, positive NIC-shear, and negative NIC bending with $\overline{R}^2$ values above 0.5. Supplemental to the regression equation was a comparison of peak input accelerations to those found in literature as well as visual and quantitative analysis of the trials simulated in MADYMO. Peak input accelerations from the haversine impulse series were far greater than those found to cause lateral stability loss in standing subjects, while maintaining relatively low injury outcomes. This suggests that the upper extremity grip afforded to the ATD allows for injury mitigation. Visual analysis of the trials demonstrated that higher ΔVs will cause the ATD to be ejected from the SQM compartment irrespective of grip strength. This will lead to the ATD rebounding off the ground and rolling onto its back. Quantitative data showed that ATDs which rolled onto their backs earlier sustained lesser injuries, perhaps indicating that anterior-posterior movement in collision scenarios is less injurious. Trials where a lateral constraint (door) was present on the SQM showed dramatically reduced IARVs suggesting that doors should be implemented as safety measures for forklifts and other dynamic horizontal platforms.

The work performed in this thesis represents a basis for experimentation and analysis in the application of dynamic horizontal platforms supporting a standing operator with upper extremity grip. Future directions for this work may include refined input series, regression models, IARVs, and ATDs.

A refined series of ΔVs and grip strengths would provide more precision for the collision trials, which should increase the statistical strength of the study. If a principle component analysis were to be performed on the data, clusters of similarly behaving outcomes might be identified and individually analyzed to produce piecewise regression models which better fit the data. The additional data points and principle component analysis may be able to better characterize the IARVs pertinent to the study. As a tangent to better characterized IARVs, new IARVs might be developed which account for lateral movements and impacts.

BIBLIOGRAPHY

[1] AAMA, 1998, "Proposal for Dummy Response Limits for FMVSS 208 Compliance Testing,"

[2] Albertsson, P., 2005, "Occupant Casualties in Bus and Coach Traffic," pp. 1-65.

[3] Albertsson, P., and Falkmer, T., 2005, "Is there a Pattern in European Bus and Coach Incidents? A Literature Analysis with Special Focus on Injury Causation and Injury Mechanisms," Accident Analysis & Prevention, **37**(2) pp. 225-233

[4] ANSI, and ITSDF, 2009, "Safety Standard for Low Lift and High Lift Trucks: Powered and Nonpowered Industrial Trucks, Effective 10-1-2010," **ANSI B56.1**

[5] APTA, 2011, "Transit Facts," **2011**(April 14)

[6] APTA, 2010, "2010 Public Transportation Fact Book," **2011**(April 27) pp. 40.

[7] Berry, T. A., 2006, "A risk based study of tipover and off-dock accidents involving stand-up lift trucks," ASME International Mechanical Engineering Congress and Exposition, Anonymous ASME, pp. 85-91.

[8] Björnstig, U., Albertsson, P., Björnstig, J., 2005, "Injury Events among Bus and Coach Occupants," IATSS Research, **29**(1) pp. 79

[9] BLS et al., 2009, "May 2009 National Occupational Employment and Wage Estimates," **2011**(April 14)

[10] BLS, and US Department of Labor, 2009, "Occupational Injuries and Illnesses: Industry Data,"

[11] BLS, and US Department of Labor, 2008, "Occupational Injury and Illness Classification System (OIICS)," **2011**(April 6)

[12] Born, C. T., Ross, S. E., Aron, B., 1996, "Patterns of Injury and Disability Caused by Forklift Trucks," The Journal of Trauma, **40**(4) pp. 636

[13] Bostelman, R., 2009, "Towards improved forklift safety: white paper," Proceedings of the 9th Workshop on Performance Metrics for Intelligent Systems, Anonymous ACM, pp. 297-302.

[14] Carlin, F., and Sances Jr, A., 2000, "Head Injury in Fork Lift Upsets,"

[15] Carlin, F. H., and Sances Jr, A., 2000, "Fork lift overturns and head injury," Engineering in Medicine and Biology Society, 2000. Proceedings of the 22nd Annual International Conference of the IEEE, Anonymous IEEE, **4,** pp. 2711-2725.

[16] Collins, J. W., Smith, G. S., Baker, S. P., 1999, "Injuries Related to Forklifts and Other Powered Industrial Vehicles in Automobile Manufacturing," American Journal of Industrial Medicine, **36**(5) pp. 513-521

[17] Costilla, V., and Bishai, D. M., 2006, "Lawnmower Injuries in the United States: 1996 to 2004," Annals of Emergency Medicine, **47**(6) pp. 567-573

[18] Crown Equipment Corporation, 2004, "Specifications: RR5200 Series Narrow-Aisle Reach Truck," **2011**(April 6) pp. 6.

[19] DeGraaf, B. D., and Weperen, W. V., 1997, "The Retention of Balance: An Exploratory Study into the Limits of Acceleration the Human Body can Withstand without Losing Equilibrium," Human Factors, **39**(1) pp. 111-118

[20] DOSH, and Washington State Department of Labor & Industries, 2010, "Safe Operation of Forklifts and Other Powered Industrial Trucks (PITs)," **2011**(April 7) pp. 54.

[21] DOSH, and Washington State Department of Labor & Industries, 2007, "Forklift Safety Guide," **2011**(April 7) pp. 42.

[22] Ewing, C. L., Thomas, D. J., Lustick, L., 1975, "The effect of the initial position of the head and neck on the dynamic response of the human head and neck to -Gx impact acceleration," Proceedings of the 19th Stapp Car Crash Conference, SAE, ed. Society of Automotive Engineers, Warrendale, PA,

[23] Fruin, J., Huang, H. F., Zegeer, C. V., 1994, "Recommendations for Reducing Noncollision Bus Passenger Injuries," pp. 41-48

[24] Greenwald, R. M., Gwin, J. T., Chu, J. J., 2008, "Head Impact Severity Measures for Evaluating Mild Traumatic Brain Injury Risk Exposure," Neurosurgery, **62**(4) pp. 789

[25] Gurdjian, E. S., Lissner, H. R., Latimer, F. R., 1953, "Quantitative Determination of Acceleration and Intracranial Pressure in Experimental Head Injury; Preliminary Report," Neurology, **3**(6) pp. 417-423

[26] Gurdjian, E. S., Lissner, H. R., and Patrick, L. M., 1963, "Concussion mechanism and pathology," Proceedings of the 7th Stapp Car Crash Conference, AAAM, ed. Association for the Advancement of Automotive Medicine, Des Plaines, IL, pp. 470-482.

[27] Gurdjian, E. S., Lissner, H. R., Webster, J. E., 1954, "Studies on Experimental Concussion: Relation of Physiologic Effect to Time Duration of Intracranial Pressure Increase at Impact," Neurology, **4**(9) pp. 674-681

[28] Gurdjian, E. S., Webster, J. E., and Lissner, H. R., 1958, "Mechanisms of Scalp and Skull Injuries, Concussion, Contusion and Lacerations," Journal of Neurosurgery, **15**(2) pp. 125-128

[29] Gurdjian, E. S., Webster, J. E., and Lissner, H. R., 1955, "Observations on the Mechanism of Brain Concussion, Contusion, and Laceration," Surgery, Gynecology & Obstetrics, **101**(6) pp. 680-690

[30] Halpern, P., Siebzehner, M. I., Aladgem, D., 2005, "Non-Collision Injuries in Public Buses: A National Survey of a Neglected Problem," Emergency Medicine Journal, **22**(2) pp. 108

[31] Hammig, B., Childers, E., and Jones, C., 2009, "Injuries Associated with the use of Riding Mowers in the United States, 2002-2007," Journal of Safety Research, **40**(5) pp. 371-375

[32] Harris, G. F., and DeRosia, J., 2003, "Dynamic Postural Stability Testing during Standup Forklift (Lift Truck) Operation," Proceedings of IMECE'03,

[33] Harris, G. F., and DeRosia, J., 2003, "Occupant Protection and Standup Forklift (Lift Truck) Dynamics," Proceedings of IMECE'03,

[34] Hausbeck, C. J., Strong, M. J., Tamkei, L. S., 2009, "The Effect of Additional Hand Contact on Postural Stability Perturbed by a Moving Environment," Gait & Posture, **29**(3) pp. 509-513

[35] Hirshfield, C. F., 1932, "Disturbing Effects of Horizontal Acceleration," Electric Railway President's Conference Committee,

[36] Hsiao, E. T., and Robinovitch, S. N., 1997, "Common Protective Movements Govern Unexpected Falls from Standing Height," Journal of Biomechanics, **31**(1) pp. 1-9

[37] Hyde, A.S., 1996, "Accidental falls: their causes and their injuries: fundamentals of slipping, stumbling, tumbling, and crumpling," HAI, Key Biscayne, FL, pp. 251.

[38] IIHS, 2009, "Frontal offset crashworthiness evaluation - guidelines for rating injury measures," Insurance Institute for Highway Safety, Arlington, VA

[39] Incel, N. A., Ceceli, E., Durukan, P. B., 2002, "Grip Strength: Effect of Hand Dominance," Singapore Medical Journal, **43**(5) pp. 234-237

[40] Jonkees, L. B. W., and Groen, J. J., 1942, "De Stadnvastigheid Van De Mens [the Steadfastness of Humans]," Nederlands Tiidschrift Voor Geneeskunde, **86**pp. 1401-1407

[41] Keough, J., "Discussion of Nissan SRX 35N Forklift," **Personal Interview**

[42] Kleinberger, M., Sun, E., Eppinger, R., 1998, "Development of improved injury criteria for the assessment of advanced automotive restraint systems," National Highway Traffic Safety Administration, Washington, DC, pp. 122.

[43] Larsson, T. J., and Rechnitzer, G., 1994, "Forklift Trucks--Analysis of Severe and Fatal Occupational Injuries, Critical Incidents and Priorities for Prevention," Safety Science, **17**(4) pp. 275-289

[44] Ledolter, J., and Hogg, R.V., 2010, "Applied statistics for engineers and physical scientists," Pearson/Prentice Hall, Upper Saddle River, NJ, pp. 591.

[45] Lenox, J. B., Stalnaker, R. L., White, C. D., 1982, "Development of neckinjurytolerancecriteria in human surrogates ~ static tensile loading in the baboon neck ~ preliminary observations," Ninth International Technical Conference on Experimental Safety Vehicles, NHTSA, ed. National Highway Traffic Safety Administration, Washington, D.C., pp. 279.

[46] Lifschultz, B. D., and Donoghue, E. R., 1994, "Deaths due to Forklift Truck Accidents," Forensic Science International, **65**(2) pp. 121-134

[47] Light Rail Now Production Team, 2006, "Los Angeles "Orange Line" Busway - Part 4 - Buses and Interior Space," **2011**(May 25)

[48] Lissner, H. R., Lebow, M., and Evans, F. G., 1960, "Experimental Studies on the Relation between Acceleration and Intracranial Pressure Changes in Man," Surgery, Gynecology & Obstetrics, **111**pp. 329-338

[49] Löwenhielm, P., 1975, "Brain susceptibility to velocity changes, relative and absolute limits for brain tissue tolerance to trauma and their relation to actual traumatic situations," Proceedings of the International Interdisciplinary Symposium on Traffic Speed and Casualties, Anonymous

[50] Löwenhielm, P., 1974, "Strain Tolerance of the Vv. Cerebri Sup.(Bridging Veins) Calculated from Head-on Collision Tests with Cadavers," International Journal of Legal Medicine, **75**(2) pp. 131-144

[51] Margulies, S. S., and Thibault, L. E., 1992, "A Proposed Tolerance Criterion for Diffuse Axonal Injury in Man," Journal of Biomechanics, **25**(8) pp. 917-923

[52] MathWorks, 2010, "MATLAB," **R2010bSP1**

[53] McElhaney, J., 1976, "Head Injury Criteria," Mechanics of Composite Materials, **12**(3) pp. 411-429

[54] Mertz, H. J., Driscoll, G. D., Lenox, J. B., 1982, "Responses of animals exposed to deployment of various passenger inflatable restraint system concepts for a variety of collision severities and animal positions," Proceedings of the Ninth International Technical Conference on Experimental Safety Vehicles, Anonymous Society of Automotive Engineers, Warrendale, PA, pp. 352-368.

[55] Mertz, H. J., Hodgson, V. R., Thomas, L. M., 1978, "An Assessment of Compressive Neck Loads Under Injury-Producing Conditions," Physician and Sports Medicine, **6**(11)

[56] Mertz, H. J., and Patrick, L. M., 1971, "Strength and response of the human neck," Proceedings of the 15th Stapp Car Crash Conference, SAE, ed. SAE International, Warrendale, PA,

[57] Mertz, H. J., and Patrick, L. M., 1967, "Investigation of the kinematics and kinetics of whiplash," Proceedings of the 11th Stapp Car Crash Conference, Anonymous SAE International, **670919,**

[58] Mertz, H. J., Prasad, P., and Irwin, A. L., 1997, "Injury risk curves for children and adults in frontal and rear collisions," Proceedings of the 41st Stapp Car Crash Conference, SAE, ed. Society of Automotive Engineers, Warrendale, PA, pp. 13-30.

[59] Mertz, H. J., and Weber, D. A., 1982, "Interpretations of the impact responses of a 3-year-old child dummy relative to child injury potential," Proceedings of the Ninth International Technical Conference on Experimental Safety Vehicles, Anonymous Society of Automotive Engineers, Warrendale, PA, pp. 1-4.

[60] Meyer, A. R., Fritz, J. M., and Harris, G. F., 2009, "Biomechanical Model to Assess Injury Reduction during Impact," 31st Annual International Conference of the IEEE EMBS, pp. 5267-5270

[61] Mickey, R.M., Dunn, O.J., and Clark, V., 2004, "Applied statistics: analysis of variance and regression," Wiley-Interscience, Hoboken, N.J., pp. 448.

[62] Mitsubishi Forklift Trucks, 2009, "2500-4500 Lbs Capacity 24V and 36V Reach Trucks," **2011**(March 12) pp. 20.

[63] Nahum, A.M., and Melvin, J.W., 2002, "Accidental injury: biomechanics and prevention," Springer, New York, NY, pp. 637.

[64] NEISS, and CPSC, 2009, "NEISS Query Results: Riding Power Lawn Mowers," **2011**(April 27)

[65] Newman, J. A., 1980, "Head injury criteria in automotive crash testing," Proceedings of the 24th Stapp Car Crash Conference, SAE, ed. SAE International, Warrendale, PA, **89,**

[66] NHTSA, and US DOT, 2011, "Occupant Crash Protection," Federal Motor Vehicle Safety Standards, **49 CFR 571.208**pp. S6.2-S6.6.

[67] NHTSA, and US DOT, 1983, "Head and neck injury criteria: a consensus workshop," U.S. Dept. of Transportation, National Highway Traffic Safety Administration, Washington, D.C., pp. 253.

[68] Nissan Forklift, 2009, "SRX Platinum Series: Rider Reach, Rider Double Reach," **2011**(April 3) pp. 8.

[69] Nyquist, G. W., Begman, P. C., King, A. I., 1980, "Correlation of Field Injuries and GM Hybrid III Dummy Responses for Lap-Shoulder Belt Restraint," Journal of Biomechanical Engineering, **102**pp. 103

[70] Ommaya, A. K., Faas, F., and Yarnell, P., 1968, "Whiplash Injury and Brain Damage," JAMA: The Journal of the American Medical Association, **204**(4) pp. 285

[71] Ommaya, A.K., Fisch, F.J., Mahone, R.M., 1993, "Biomechanics of Impact Injury and Injury Tolerances of the Head-Neck Complex,"Society of Automotive Engineers, Warrendale, PA., pp. 265-274, Chap. 3

[72] Ommaya, A. K., and Hirsch, A. E., 1971, "Tolerances for Cerebral Concussion from Head Impact and Whiplash in Primates," Journal of Biomechanics, **4**(1) pp. 13-21

[73] Ommaya, A. K., Yarnell, P., Hirsch, A. E., 1967, "Scaling of Experimental Data on Cerebral Concussion in Sub-Human Primates to Concussion Threshold for Man," Proceedings of the 11th Stapp Car Crash Conference, SAE, ed. SAE International, Warrendale, PA

[74] OSHA, and US Department of Labor, 2008, "Powered Industrial Trucks (Forklifts)," **2011**(April 6)

[75] Palacio, A., Tamburro, G., O'Neill, D., 2009, "Non-Collision Injuries in Urban Buses--Strategies for Prevention," Accident Analysis & Prevention, **41**(1) pp. 1-9

[76] Peterson, R., 2006, "Mow Down the Competition," Irrigation & Green Industry,

[77] Prasad, P., and Daniel, R. P., 1984, "A biomechanical analysis of head, neck, and torso injuries to child surrogates due to sudden torso acceleration," Anonymous SAE International,

[78] Railsback, B. T., and Ziernicki, R. M., 2008, "Hazard analysis and risk assessment for the operators of stand-up forklifts," ASME International Mechanical Engineering Congress and Exposition, Anonymous ASME, pp. 237-242.

[79] Rantanen, T., Guralnik, J. M., Foley, D., 1999, "Midlife Hand Grip Strength as a Predictor of Old Age Disability," Journal of the American Medical Association, **281**(6) pp. 558

[80] Rawlings, J.O., Pantula, S.G., and Dickey, D.A., 1998, "Applied regression analysis: a research tool," Springer, New York, pp. 657.

[81] RITA et al., 2010, "National Transportation Statistics," **2011**(April 27)

[82] Robert, T., Beillas, P., Maupas, A., 2007, "Conditions of Possible Head Impacts for Standing Passengers in Public Transportation: An Experimental Study," International Journal of Crashworthiness, **12**(3) pp. 319-327

[83] Robertson Jr, W. W., 2003, "Power Lawnmower Injuries," Clinical Orthopaedics and Related Research, **409**pp. 37-42

[84] Schneider, R. C., Reifel, E., Crisler, H. O., 1961, "Serious and Fatal Football Injuries Involving the Head and Spinal Cord," The Journal of the American Medical Association, **177**(6) pp. 362

[85] Stout-Wiegand, N., 1987, "Characteristics of Work-Related Injuries Involving Forklift Trucks," Journal of Safety Research, **18**(4) pp. 179-190

[86] Swartz, G., 2001, "When PITs Strike People and Objects," Professional Safety, **46**(3) pp. 25-30

[87] Tarrière, C., Leung, Y.C., Fayon, A., 1993, "Biomechanics of Impact Injury and Injury Tolerances of the Head-Neck Complex,"Society of Automotive Engineers, Warrendale, PA, pp. 699-712, Chap. 5

[88] TASS Americas, 2008, "MADYMO," **7.0**

[89] TASS Americas, 2008, "MADYMO Model Manual," **7.0**

[90] TASS Americas, 2008, "MADYMO Theory Manual," **7.0**

[91] The Lawn Advisor, 2005, "Commercial Lawn Mowers," **2011**(April 14)

[92] Unterharnscheidt, F., and Higgins, L. S., 1969, "Pathomorphology of Experimental Head Injury due to Rotational Acceleration," Acta Neuropathologica, **12**(2) pp. 200-204

[93] Unterharnscheidt, F., and Higgins, L. S., 1969, "Traumatic Lesions of Brain and Spinal Cord due to Nondeforming Angular Acceleration of the Head," Texas Reports on Biology and Medicine, **27**(1) pp. 127-166

[94] Van Don, B., Van Ratingen, M., Bermond, F., 2003, "Biofidelity impact response requirements for an advanced mid-sized male crash test dummy," Proceedings of 18th International Technical Conference on Enhanced Safety of Vehicles, Anonymous

[95] Varat, M. S., and Husher, S. E., 2003, "Crash pulse modeling for vehicle safety research," 18th International Technical Conference on the Enhanced Safety of Vehicles, Anonymous

[96] Versace, J., 1971, "A review of the severity index," Proceedings of the 15th Stapp Car Crash Conference, SAE, ed. SAE International, Warrendale, PA,

[97] Vincent, M.L., and Moreau, T.M., 2008, "Accidental falls: causes, prevention and intervention," Nova Science Publishers, New York, pp. 366.

[98] Votaw, C.L., 1993, "Biomechanics of Impact Injury and Injury Tolerances of the Head-Neck Complex,"Society of Automotive Engineers, Warrendale, PA, pp. 27-39

[99] Winter, D.A., 2009, "Biomechanics and motor control of human movement," Wiley, Hoboken, N.J., pp. 370.

[100] Zoghi-Moghadam, M., Sadegh, A., Watkins, C. B., 2008, "Biodynamics Model for Operator Head Injury in Stand-Up Lift Trucks," Computer Methods in Biomechanics and Biomedical Engineering, **11**(4) pp. 397-405

APPENDICES

APPENDIX A: ADDITIONAL RESULTS

Table 16: IARVs for the door included trials at ΔV = 16.1 km/h (10 mph) and grip strength = 0 N (0 lbf) with the respective injury threshold limits included

IARV	Peak Value	Limit
HIC_{36}	4	1,000
Omega [rad/s]	21	32
Alpha [rad/s^2]	1,257	1,700
NIC-tension neg. [N]	296	1,100
NIC-tension pos. [N]	362	1,100
NIC-shear neg. [N]	57	1,100
NIC-shear pos. [N]	76	1,100
NIC-bending neg. [Nm]	9.0	57.0
NIC-bending pos. [Nm]	8.0	57.0
ΣN_{ij}	0.2	1.0

Table 17: IARVs for door-absent trials at ΔV = 3.2 km/h and all grip strengths (0-678.9 N)

Velocity (km/h)		3.2								
Grip (N)		0.0	266.8	325.7	384.6	443.4	502.3	561.1	620.0	678.9
IARV	units									
HIC_{36}		164	185	71	69	70	0	0	0	0
Omega	rad/s	59	47	53	51	51	3	3	3	3
Alpha	rad/s^2	12,979	8,802	12,331	11,849	11,900	73	75	74	74
NIC-tension neg.	N	1,111	2,200	498	478	492	83	84	84	84
NIC-tension pos.	N	2,011	1,325	1,848	1,886	1,759	19	19	19	19
NIC-shear neg.	N	367	292	200	193	203	59	59	59	59
NIC-shear pos.	N	297	461	145	137	136	16	16	16	16
NIC-bending neg.	Nm	21.0	14.5	19.2	16.9	17.3	0.4	0.4	0.4	0.4
NIC-bending pos.	Nm	13.1	20.3	11.1	11.2	7.9	4.4	4.4	4.4	4.4
ΣN_{ij}		0.9	0.9	0.7	0.7	0.7	0.0	0.0	0.0	0.0

Table 18: IARVs for door-absent trials at ΔV = 6.4 km/h and all grip strengths (0-678.9 N)

Velocity (km/h)		6.4								
Grip (N)		**0.0**	**266.8**	**325.7**	**384.6**	**443.4**	**502.3**	**561.1**	**620.0**	**678.9**
IARV	*units*									
HIC$_{36}$		796	443	430	417	525	154	414	24	58
Omega	rad/s	47	46	46	45	43	50	44	21	17
Alpha	rad/s^2	20,684	13,534	13,300	13,243	14,520	10,793	12,923	6,163	2,506
NIC-tension neg.	N	5,085	3,688	3,439	3,338	3,662	1,081	2,212	1,588	580
NIC-tension pos.	N	2,032	1,754	1,615	1,545	1,657	1,894	1,744	210	349
NIC-shear neg.	N	420	393	395	379	408	361	381	150	401
NIC-shear pos.	N	1,150	960	1,002	822	848	176	340	824	215
NIC-bending neg.	Nm	23.4	19.9	19.4	17.5	19.3	19.3	20.5	3.8	29.3
NIC-bending pos.	Nm	19.6	38.6	42.3	36.4	38.6	20.7	20.6	46.1	19.2
ΣN$_{ij}$		2.2	1.4	1.3	1.2	1.6	0.7	1.1	0.5	0.6

Table 19: IARVs for door-absent trials at ΔV = 9.7 km/h and all grip strengths (0-678.9 N)

Velocity (km/h)		9.7								
Grip (N)		**0.0**	**266.8**	**325.7**	**384.6**	**443.4**	**502.3**	**561.1**	**620.0**	**678.9**
IARV	*units*									
HIC$_{36}$		267	1,435	1,261	1,133	1,020	1,126	1,029	261	409
Omega	rad/s	47	55	52	53	56	49	47	53	55
Alpha	rad/s^2	10,576	24,788	25,056	23,413	21,454	21,118	19,824	12,620	14,068
NIC-tens neg.	N	2,865	8,441	7,792	7,146	6,176	6,676	5,849	2,119	2,312
NIC-tens pos.	N	2,203	2,186	2,293	1,868	2,046	2,406	2,351	2,070	2,299
NIC-shear neg.	N	416	412	274	379	470	476	450	265	376
NIC-shear pos.	N	635	2,013	1,772	1,567	1,297	1,384	1,112	448	472
NIC-bend neg.	Nm	19.8	20.5	20.4	23.1	25.4	22.0	20.9	20.8	23.2
NIC-bend pos.	Nm	17.7	66.3	42.5	35.4	29.0	37.8	30.4	5.3	9.0
ΣN$_{ij}$		1.4	3.2	3.2	2.9	2.6	2.7	2.4	1.1	0.9

Table 20: IARVs for door-absent trials at ΔV = 12.9 km/h and all grip strengths (0-678.9 N)

Velocity (km/h)		12.9								
Grip (N)		**0.0**	**266.8**	**325.7**	**384.6**	**443.4**	**502.3**	**561.1**	**620.0**	**678.9**
IARV	*units*									
HIC$_{36}$		102	107	94	208	231	236	230	231	221
Omega	rad/s	49	49	50	45	41	40	38	38	40
Alpha	rad/s^2	5,131	5,226	5,867	7,209	7,980	7,665	7,224	6,855	6,713
NIC-tension neg.	N	638	511	1,024	5,277	5,094	4,970	4,833	4,710	4,597
NIC-tension pos.	N	1,988	1,955	2,156	1,117	1,064	1,068	980	948	1,152
NIC-shear neg.	N	397	440	330	173	189	170	157	173	315
NIC-shear pos.	N	97	112	314	662	643	614	604	579	543
NIC-bending neg.	Nm	12.3	11.0	10.3	14.8	14.9	17.1	21.0	41.7	53.6
NIC-bending pos.	Nm	8.7	8.0	8.6	14.0	11.7	12.1	13.0	20.1	23.3
ΣN$_{ij}$		0.6	0.5	0.7	1.4	1.3	1.3	1.3	1.6	1.6

Table 21: IARVs for door-absent trials at ΔV = 16.1 km/h and all grip strengths (0-678.9 N)

Velocity (km/h)		16.1								
Grip (N)		0.0	266.8	325.7	384.6	443.4	502.3	561.1	620.0	678.9
IARV	units									
HIC$_{36}$		172	217	213	313	588	484	456	359	337
Omega	rad/s	50	49	48	44	37	35	32	31	31
Alpha	rad/s^2	7,672	9,042	9,272	10,479	13,905	13,904	12,594	10,195	9,301
NIC-tension neg.	N	3,507	2,624	3,577	5,099	7,730	6,711	6,752	6,322	6,174
NIC-tension pos.	N	1,446	1,529	1,375	1,545	1,032	942	882	822	708
NIC-shear neg.	N	193	201	348	456	254	247	225	201	186
NIC-shear pos.	N	804	677	785	958	1,213	1,029	1,055	979	926
NIC-bending neg.	Nm	21.3	32.0	35.3	41.1	18.9	17.9	14.9	17.4	20.5
NIC-bending pos.	Nm	13.0	10.6	13.2	18.0	21.2	14.0	22.4	15.9	12.1
ΣN$_{ij}$		1.5	1.2	1.4	2.0	2.8	2.5	1.7	1.6	1.5

Table 22: Altered orientation outcome with ± 4 degrees of rigid transverse rotation of the ATD

Velocity (km/h)		9.7				
Grip (N)		443.4				
CCW Rotation (deg)		-4.0	-2.0	0.0	2.0	4.0
IARV	units					
HIC$_{36}$		90	218	1,020	977	394
Omega	rad/s	45	40	56	56	57
Alpha	rad/s^2	6,966	10,980	21,454	21,330	14,196
NIC-tension neg.	N	246	3,296	6,176	5,847	1,797
NIC-tension pos.	N	1,933	2,171	2,046	2,032	2,363
NIC-shear neg.	N	293	304	470	468	362
NIC-shear pos.	N	101	433	1,297	1,264	353
NIC-bending neg.	Nm	9.2	14.7	25.4	25.8	22.6
NIC-bending pos.	Nm	8.1	28.6	29.0	27.5	10.8
ΣNij		0.7	1.4	2.6	2.5	1.0

LINEAR REGRESSION
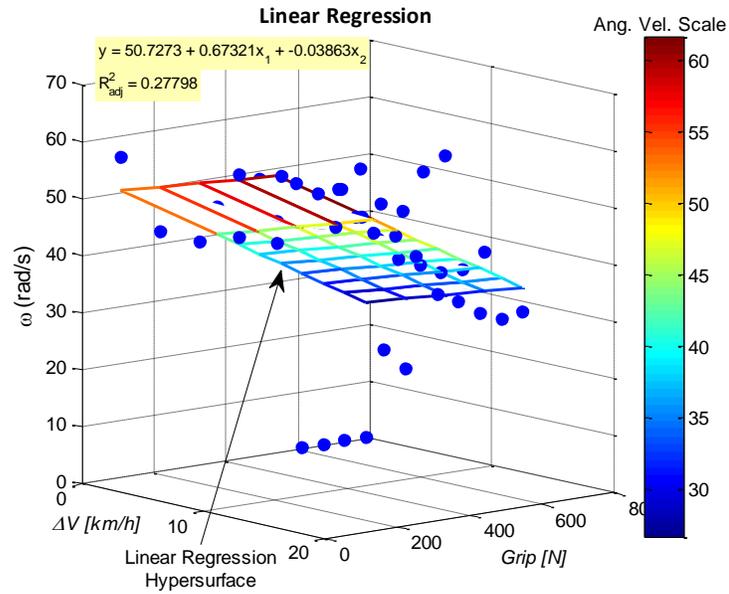
Figure 42: Linear regression surface fit for ω outputs with color scale, predictive equation, and adjusted R² value
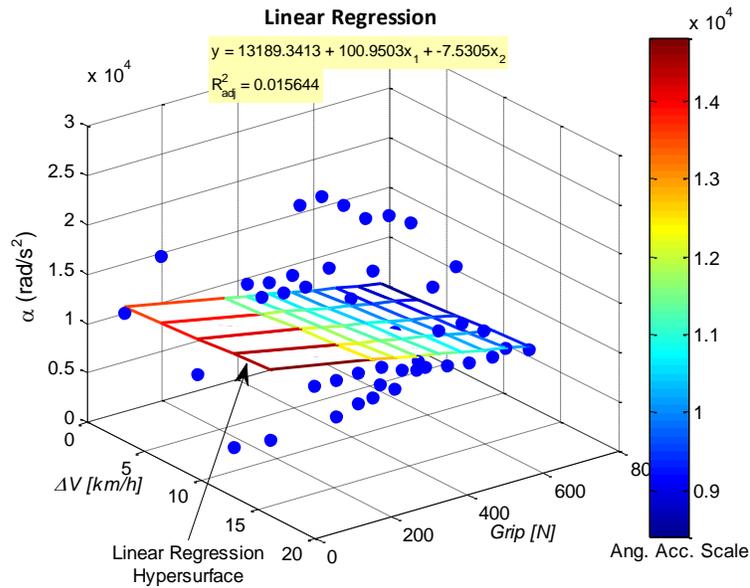
Figure 43: Linear regression surface fit for α outputs with color scale, predictive equation, and adjusted R² value
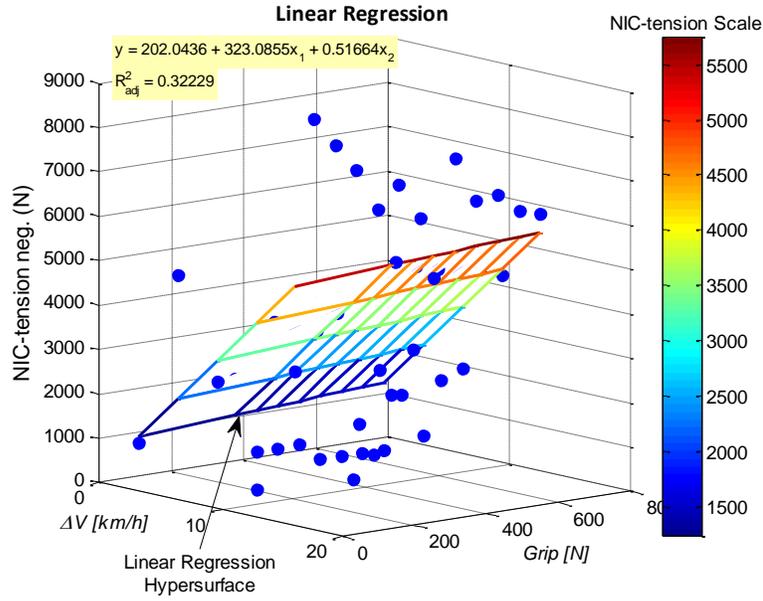
Figure 44: Linear regression surface fit for NIC-tension negative outputs with color scale, predictive equation, and adjusted R^2 value
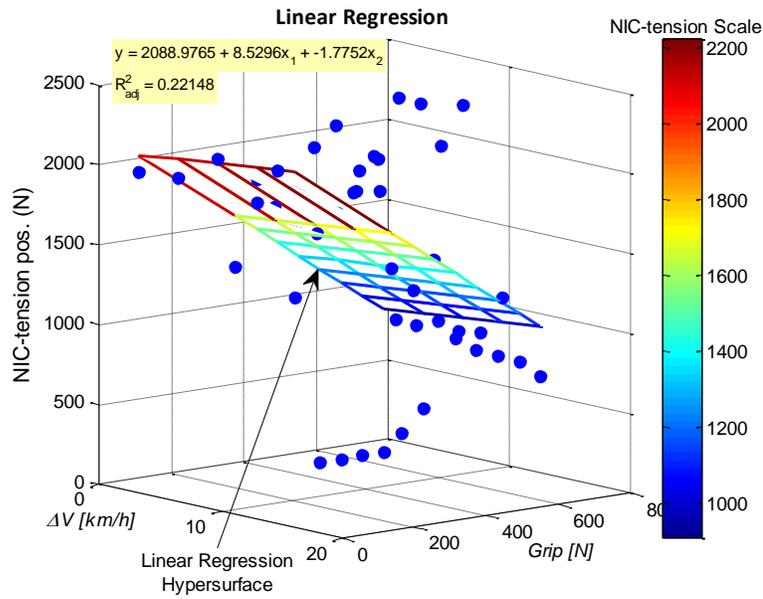
Figure 45: Linear regression surface fit for NIC-tension positive outputs with color scale, predictive equation, and adjusted R^2 value
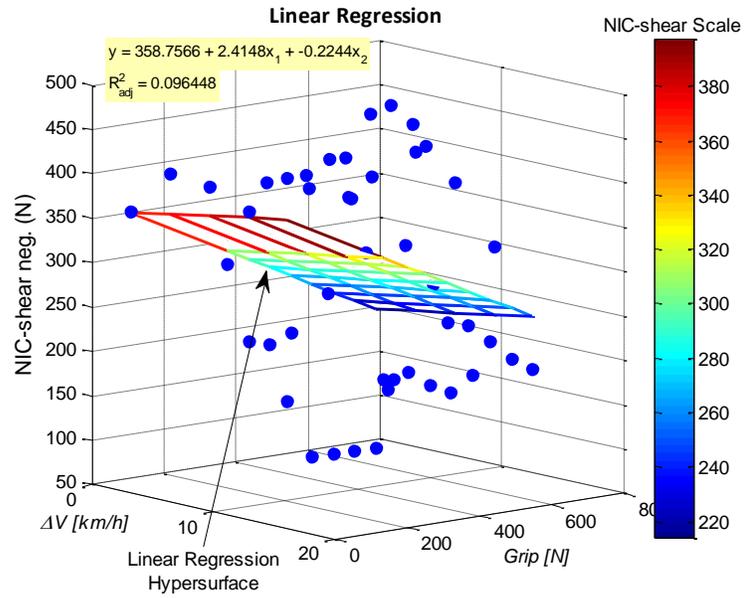
Figure 46: Linear regression surface fit for NIC-shear negative outputs with color scale, predictive equation, and adjusted R^2 value
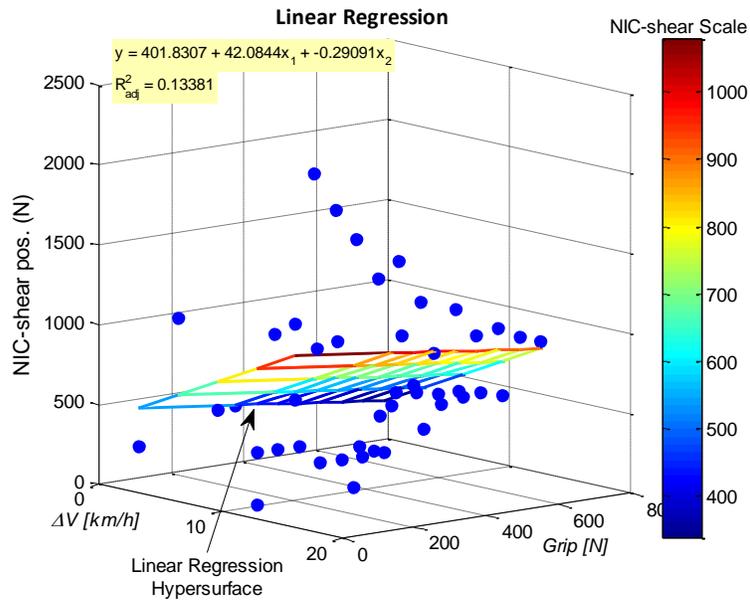
Figure 47: Linear regression surface fit for NIC-shear positive outputs with color scale, predictive equation, and adjusted R^2 value
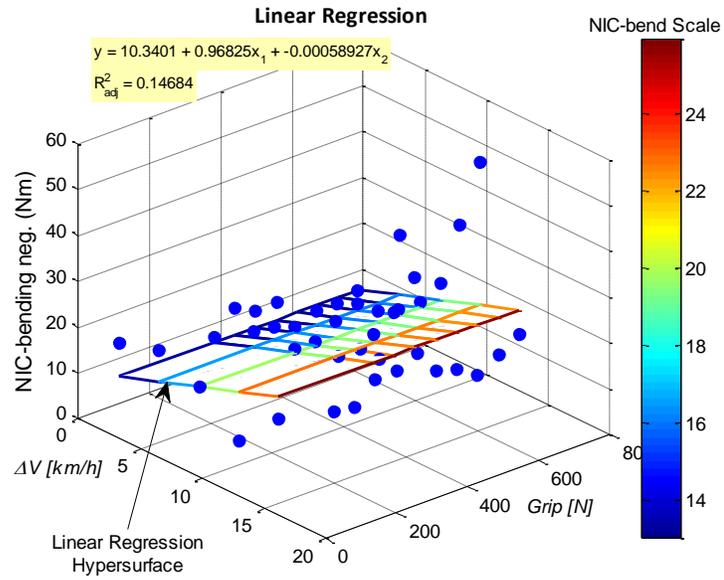
Figure 48: Linear regression surface fit for NIC-bending negative outputs with color scale, predictive equation, and adjusted R^2 value
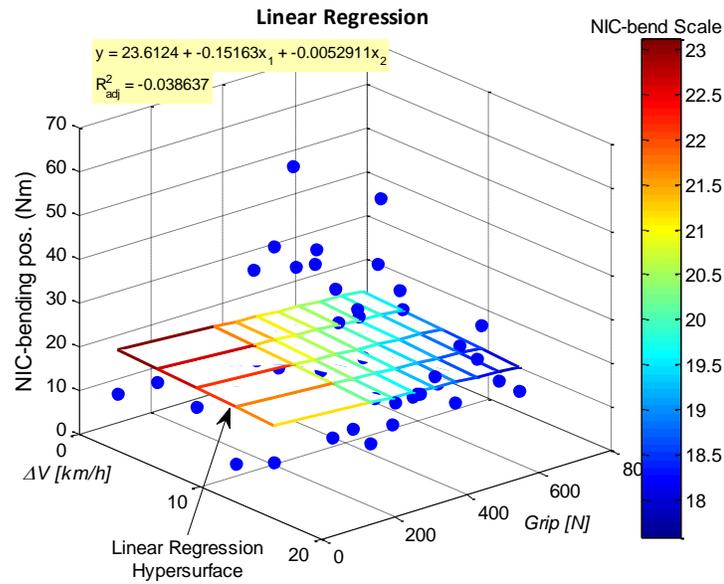
Figure 49: Linear regression surface fit for NIC-bending positive outputs with color scale, predictive equation, and adjusted R^2 value
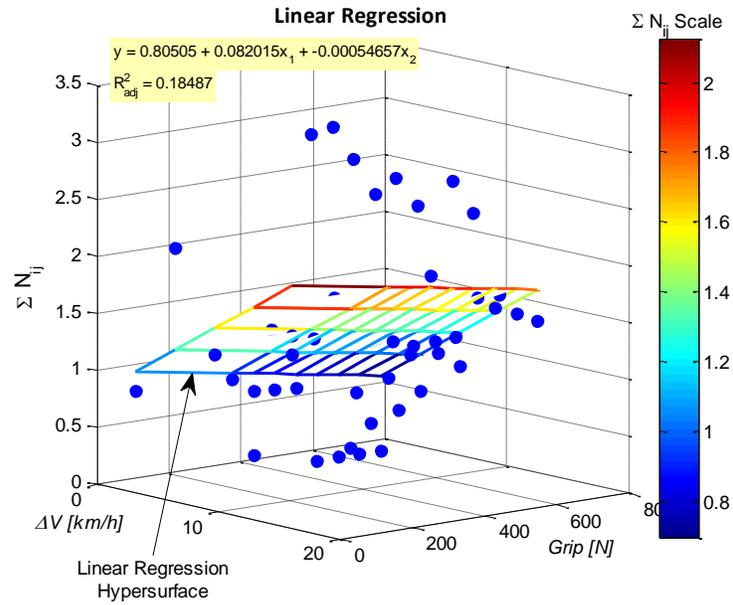
Figure 50: Linear regression surface fit for ΣN_{ij} outputs with color scale, predictive equation, and adjusted R^2 value

Table 23: IARV residuals for linear regression trials at $\Delta V = 3.2$ km/h and all grip strengths (0-678.9 N)

Velocity (km/h)		3.2								
Grip (N)		**0.0**	**266.8**	**325.7**	**384.6**	**443.4**	**502.3**	**561.1**	**620.0**	**678.9**
IARV	*units*									
HIC$_{36}$		-202	-133	-235	-227	-215	-275	-264	-254	-243
Omega	rad/s	6	5	12	13	15	-30	-28	-26	-24
Alpha	rad/s^2	-572	-2,740	1,233	1,194	1,688	-9,695	-9,251	-8,808	-8,365
NIC-tension neg.	N	-119	832	-901	-951	-967	-1,406	-1,436	-1,466	-1,497
NIC-tension pos.	N	-108	-320	308	451	428	-1,207	-1,103	-999	-894
NIC-shear neg.	N	1	-15	-93	-87	-64	-194	-181	-168	-155
NIC-shear pos.	N	-240	2	-297	-287	-272	-375	-357	-340	-323
NIC-bending neg.	Nm	7.6	1.3	6.1	3.8	4.2	-12.6	-12.6	-12.6	-12.5
NIC-bending pos.	Nm	-10.0	-1.3	-10.3	-9.8	-12.9	-16.0	-15.7	-15.4	-15.1
ΣN_{ij}		-0.2	-0.1	-0.1	-0.1	-0.1	-0.8	-0.7	-0.7	-0.7

Table 24: IARV residuals for linear regression trials at ΔV = 6.4 km/h and all grip strengths (0-678.9 N)

Velocity (km/h)		6.4								
Grip (N)		0.0	266.8	325.7	384.6	443.4	502.3	561.1	620.0	678.9
IARV	*units*									
HIC$_{36}$		390	85	83	81	199	-161	109	-270	-226
Omega	rad/s	-8	2	3	5	5	14	11	-11	-12
Alpha	rad/s^2	6,817	1,676	1,885	2,272	3,992	708	3,281	-3,036	-6,249
NIC-tension neg.	N	2,775	1,240	961	829	1,123	-1,489	-388	-1,042	-2,081
NIC-tension pos.	N	-114	82	47	82	298	640	594	-835	-592
NIC-shear neg.	N	46	78	94	91	133	99	133	-86	179
NIC-shear pos.	N	473	361	420	257	300	-355	-174	327	-264
NIC-bending neg.	Nm	6.7	3.4	2.9	1.1	3.0	3.0	4.2	-12.5	13.0
NIC-bending pos.	Nm	-3.0	17.4	21.4	15.8	18.4	0.7	1.0	26.8	0.2
ΣN$_{ij}$		0.9	0.2	0.1	0.1	0.5	-0.4	0.1	-0.5	-0.3

Table 25: IARV residuals for linear regression trials at ΔV = 9.7 km/h and all grip strengths (0-678.9 N)

Velocity (km/h)		9.7								
Grip (N)		0.0	266.8	325.7	384.6	443.4	502.3	561.1	620.0	678.9
IARV	*units*									
HIC$_{36}$		-176	1,039	877	759	657	773	687	-71	88
Omega	rad/s	-10	8	8	10	15	11	12	20	24
Alpha	rad/s^2	-3,584	12,637	13,349	12,150	10,633	10,741	9,890	3,129	5,021
NIC-tens neg.	N	-442	4,996	4,317	3,641	2,640	3,110	2,253	-1,508	-1,345
NIC-tens pos.	N	32	488	701	380	662	1,126	1,176	1,000	1,333
NIC-shear neg.	N	34	90	-35	83	188	207	194	23	147
NIC-shear pos.	N	-171	1,285	1,061	873	619	723	469	-177	-137
NIC-bend neg.	Nm	0.1	1.0	0.9	3.7	6.0	2.6	1.5	1.5	3.9
NIC-bend pos.	Nm	-4.5	45.5	22.0	15.2	9.1	18.3	11.2	-13.6	-9.5
ΣN$_{ij}$		-0.2	1.7	1.8	1.5	1.2	1.4	1.1	-0.2	-0.3

Table 26: IARV residuals for linear regression trials at ΔV = 12.9 km/h and all grip strengths (0-678.9 N)

Velocity (km/h)		12.9								
Grip (N)		0.0	266.8	325.7	384.6	443.4	502.3	561.1	620.0	678.9
IARV	*units*									
HIC$_{36}$		-381	-329	-330	-206	-173	-157	-152	-141	-140
Omega	rad/s	-10	0	3	1	-1	-1	0	2	7
Alpha	rad/s^2	-9,345	-7,242	-6,157	-4,371	-3,157	-3,029	-3,027	-2,952	-2,651
NIC-tens neg.	N	-3,749	-4,013	-3,531	692	478	324	157	4	-140
NIC-tens pos.	N	-210	230	536	-399	-347	-238	-222	-150	159
NIC-shear neg.	N	7	110	13	-131	-102	-108	-107	-78	77
NIC-shear pos.	N	-849	-757	-537	-172	-175	-186	-179	-187	-206
NIC-bend neg.	Nm	-10.6	-11.7	-12.4	-7.9	-7.7	-5.5	-1.6	19.2	31.1
NIC-bend pos.	Nm	-13.0	-12.3	-11.3	-5.6	-7.6	-6.9	-5.7	1.7	5.2
ΣN$_{ij}$		-1.3	-1.2	-1.0	-0.3	-0.3	-0.3	-0.2	0.1	0.1

Table 27: IARV residuals for linear regression trials at ΔV = 16.1 km/h and all grip strengths (0-678.9 N)

Velocity (km/h)		16.1								
Grip (N)		0.0	266.8	325.7	384.6	443.4	502.3	561.1	620.0	678.9
IARV	units									
HIC$_{36}$		-349	-256	-249	-138	147	54	37	-51	-61
Omega	rad/s	-12	-2	-1	-3	-8	-7	-8	-7	-4
Alpha	rad/s^2	-7,097	-3,717	-3,044	-1,393	2,476	2,918	2,051	96	-355
NIC-tension neg.	N	-1,876	-2,896	-1,974	-483	2,118	1,069	1,080	619	441
NIC-tension pos.	N	-778	-221	-271	4	-404	-389	-345	-300	-310
NIC-shear neg.	N	-205	-137	23	145	-44	-38	-47	-58	-59
NIC-shear pos.	N	-271	-321	-196	-6	266	99	143	84	48
NIC-bending neg.	Nm	-4.6	6.3	9.5	15.4	-6.7	-7.8	-10.7	-8.1	-5.0
NIC-bending pos.	Nm	-8.2	-9.2	-6.3	-1.1	2.4	-4.6	4.2	-2.0	-5.5
ΣN$_{ij}$		-0.6	-0.8	-0.6	0.1	1.0	0.7	-0.2	-0.2	-0.3

PURE QUADRATIC REGRESSION

$$z = a + bx + cy + dx^2 + ey^2 \qquad (17)$$

Table 28: Pure quadratic regression results for predicted IARVs including the regression coefficients (a-e) and the goodness of fit measurements (R^2 and $\overline{R}^2$)

IARV	a	b	c	d	e	R^2	$\overline{R}^2$
HIC$_{36}$	-4.6E+02	1.6E+02	9.4E-01	-7.8E+00	-1.5E-03	0.30	0.23
Omega [rad/s]	2.2E+01	5.5E+00	2.9E-02	-2.5E-01	-8.4E-05	0.49	0.44
Alpha [rad/s^2]	-2.7E+03	3.0E+03	2.6E+01	-1.4E+02	-4.9E-02	0.30	0.23
NIC-tension neg. [N]	-4.2E+03	1.1E+03	8.2E+00	-4.1E+01	-1.1E-02	0.45	0.39
NIC-tension pos. [N]	3.8E+02	3.7E+02	6.5E-01	-1.9E+01	-3.1E-03	0.54	0.50
NIC-shear neg. [N]	-5.8E+01	9.8E+01	2.0E-01	-4.9E+00	-4.7E-04	0.34	0.28
NIC-shear pos. [N]	-3.0E+02	1.8E+02	1.6E+00	-7.2E+00	-3.0E-03	0.34	0.27
NIC-bending neg. [Nm]	1.6E+01	1.3E+00	-1.3E-02	-5.8E-02	1.7E-05	0.72	0.69
NIC-bending pos. [Nm]	-1.5E+01	7.8E+00	3.3E-02	-3.9E-01	-5.3E-05	0.31	0.24
ΣN$_{ij}$	-4.5E-01	2.8E-01	2.8E-03	-9.5E-03	-4.8E-06	0.35	0.29
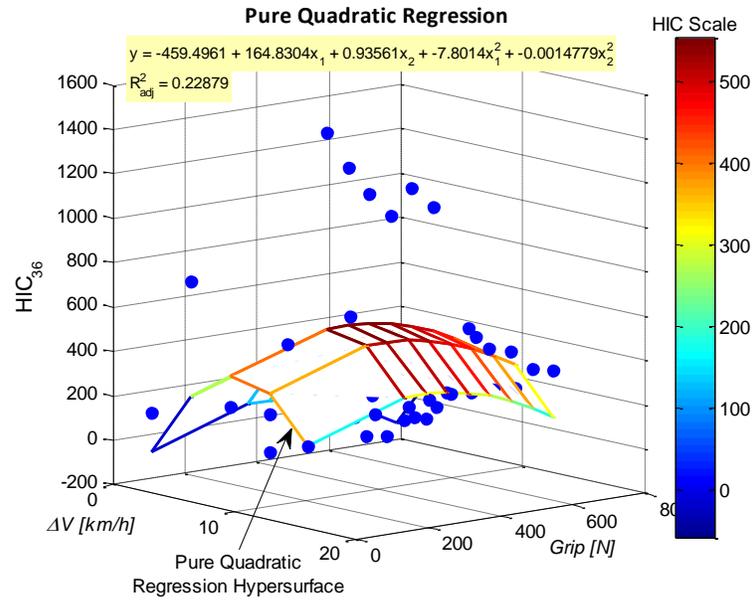
Figure 51: Pure quadratic regression surface fit for HIC outputs with color scale, predictive equation, and adjusted R^2 value
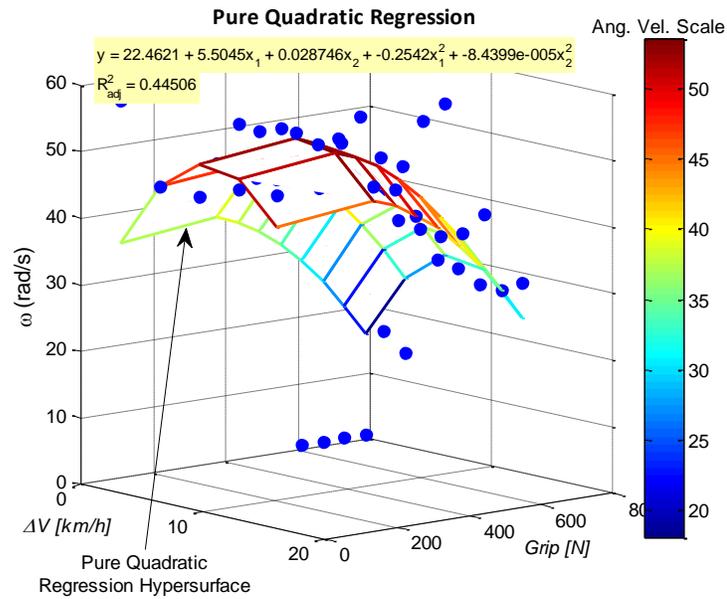

Figure 52: Pure quadratic regression surface fit for ω outputs with color scale, predictive equation, and adjusted R^2 value
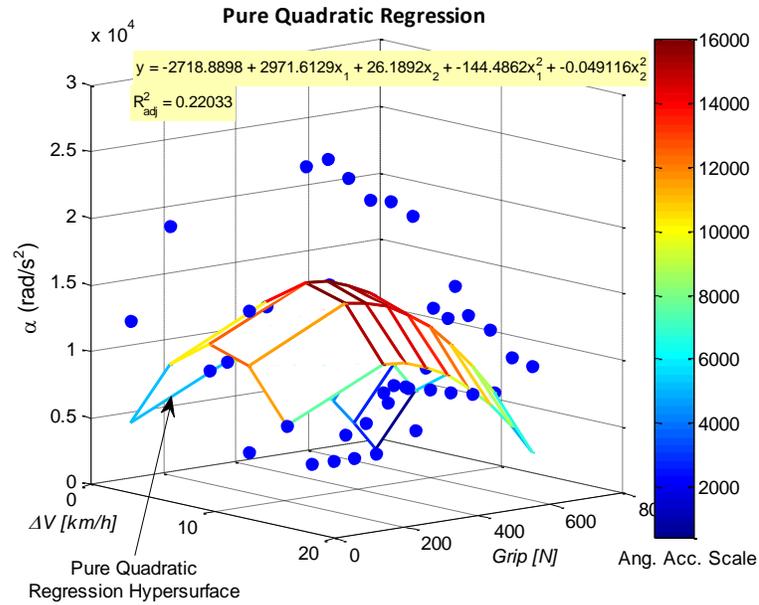
Figure 53: Pure quadratic regression surface fit for α outputs with color scale, predictive equation, and adjusted R^2 value
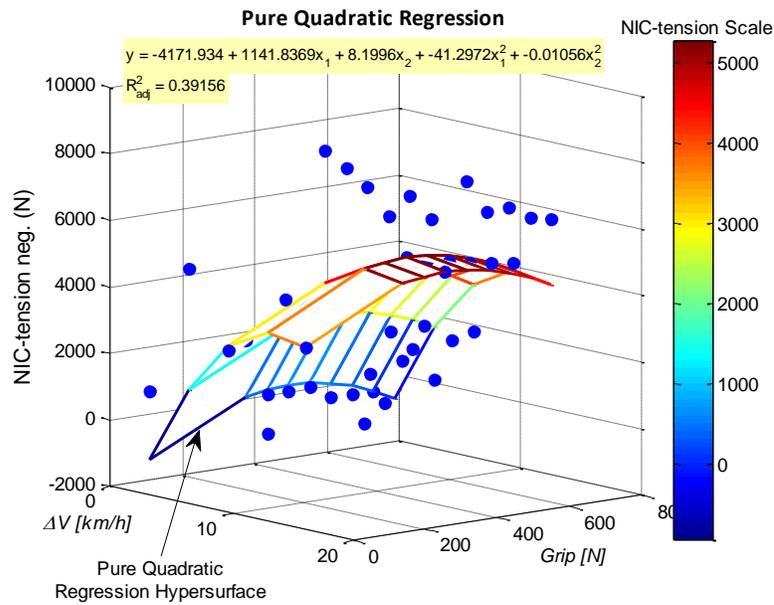
Figure 54: Pure quadratic regression surface fit for NIC-tension negative outputs with color scale, predictive equation, and adjusted R^2 value
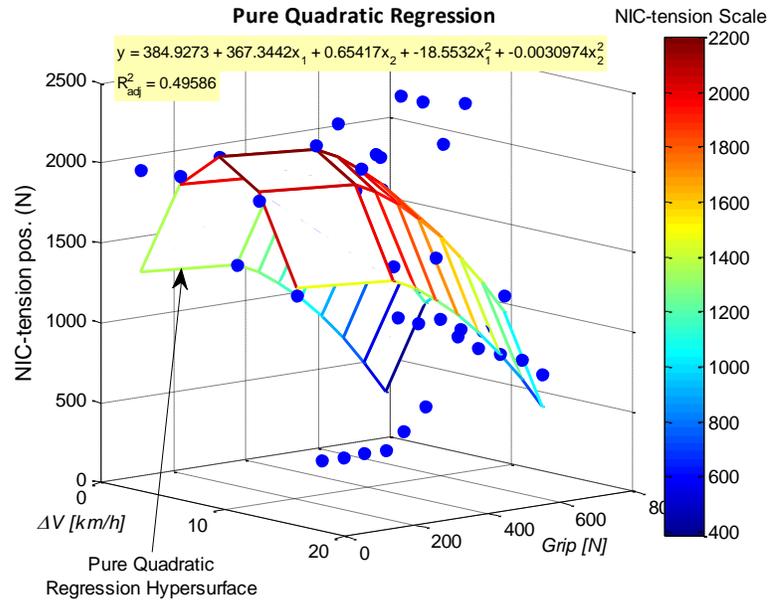
Figure 55: Pure quadratic regression surface fit for NIC-tension positive outputs with color scale, predictive equation, and adjusted R^2 value
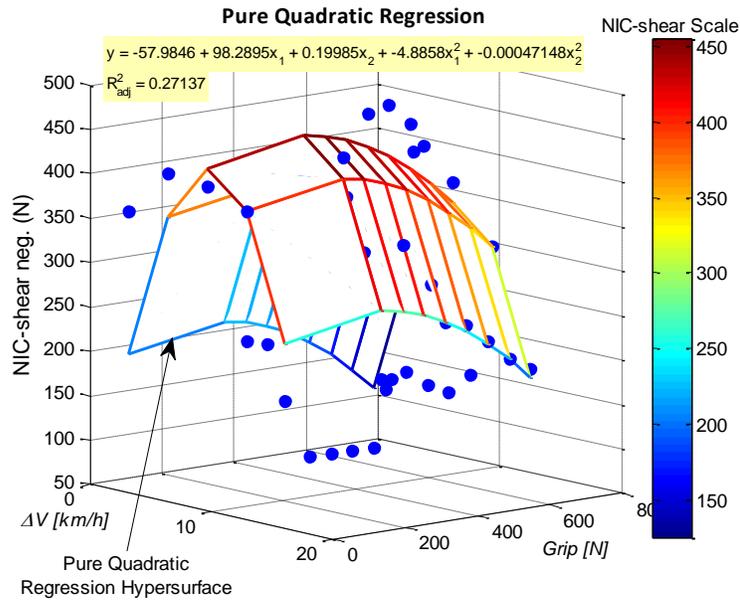
Figure 56: Pure quadratic regression surface fit for NIC-shear negative outputs with color scale, predictive equation, and adjusted R^2 value
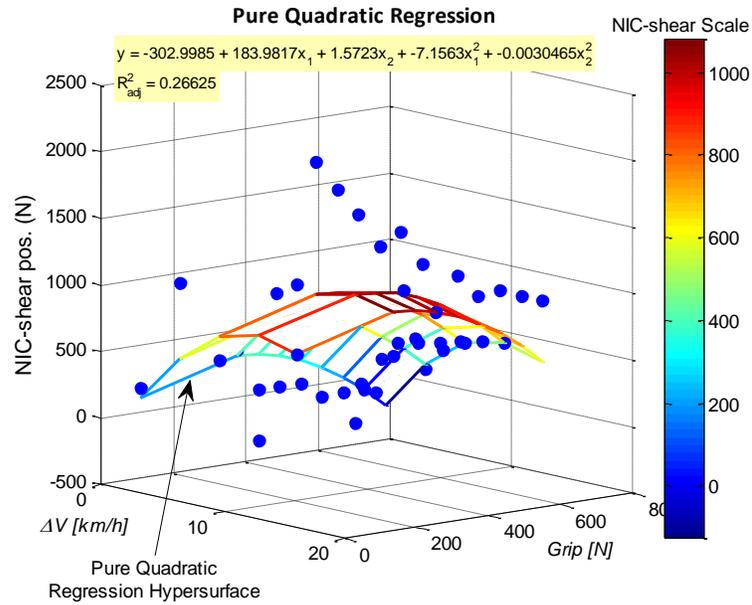
Figure 57: Pure quadratic regression surface fit for NIC-shear positive outputs with color scale, predictive equation, and adjusted R^2 value
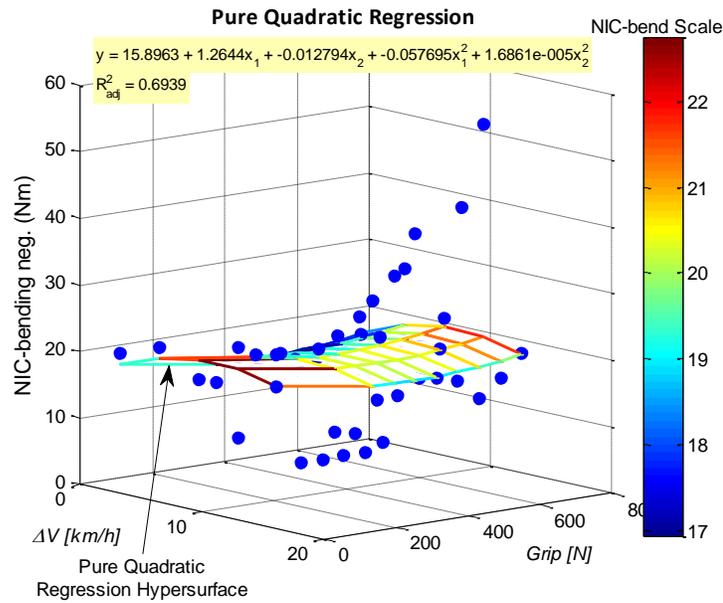

Figure 58: Pure quadratic regression surface fit for NIC-bending negative outputs with color scale, predictive equation, and adjusted R^2 value
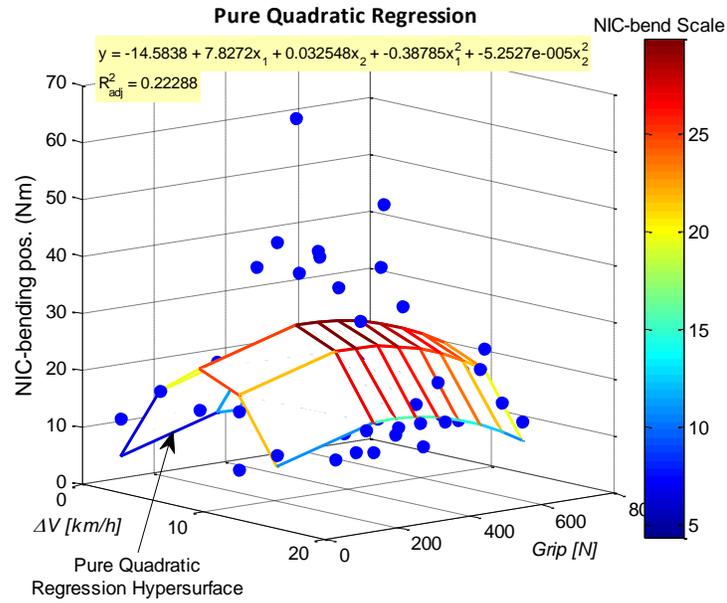
Figure 59: Pure quadratic regression surface fit for NIC-bending positive outputs with color scale, predictive equation, and adjusted R^2 value
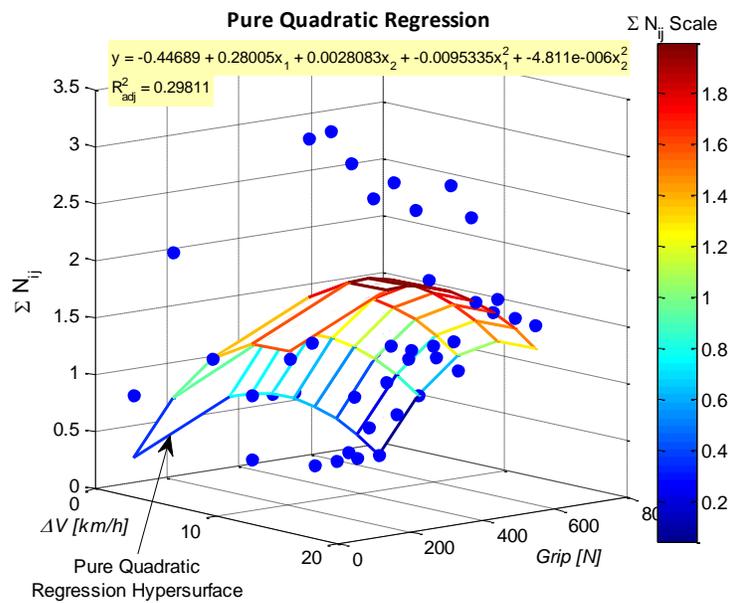

Figure 60: Pure quadratic regression surface fit for ΣN_{ij} outputs with color scale, predictive equation, and adjusted R^2 value

Table 29: IARV residuals for pure quadratic regression trials at ΔV = 3.2 km/h and all grip strengths (0-678.9 N)

Velocity (km/h)		3.2								
Grip (N)		0.0	266.8	325.7	384.6	443.4	502.3	561.1	620.0	678.9
IARV	units									
HIC$_{36}$		202	86	-33	-32	-19	-69	-39	0	48
Omega	rad/s	22	9	15	15	18	-27	-24	-20	-15
Alpha	rad/s^2	7,636	0	3,688	3,699	4,575	-6,093	-4,601	-2,775	-615
NIC-tension neg.	N	2,052	1,705	-112	-173	-127	-430	-252	0	325
NIC-tension pos.	N	622	0	595	727	713	-892	-737	-560	-363
NIC-shear neg.	N	175	80	-6	-5	15	-114	-96	-75	-51
NIC-shear pos.	N	68	26	-275	-245	-188	-227	-125	0	147
NIC-bending neg.	Nm	1.7	-2.6	2.3	0.0	0.4	-16.7	-17.0	-17.4	-18.0
NIC-bending pos.	Nm	7.0	9.0	-0.4	0.0	-2.7	-5.2	-3.8	-2.1	0.0
ΣN$_{ij}$		0.5	0.1	0.0	0.0	0.1	-0.5	-0.4	-0.2	0.0

Table 30: IARV residuals for pure quadratic regression trials at ΔV = 6.4 km/h and all grip strengths (0-678.9 N)

Velocity (km/h)		6.4								
Grip (N)		0.0	266.8	325.7	384.6	443.4	502.3	561.1	620.0	678.9
IARV	units									
HIC$_{36}$		519	28	10	0	120	-230	60	-291	-210
Omega	rad/s	0	-3	-2	-1	0	9	7	-12	-11
Alpha	rad/s^2	10,249	-360	-435	1	2,102	-465	3,155	-1,779	-3,276
NIC-tension neg.	N	3,555	722	359	216	572	-1,904	-595	-967	-1,650
NIC-tension pos.	N	32	-182	-249	-226	0	371	376	-981	-644
NIC-shear neg.	N	48	1	8	0	40	7	45	-165	110
NIC-shear pos.	N	523	127	184	41	126	-465	-199	409	-53
NIC-bending neg.	Nm	1.7	0.4	0.0	-1.7	0.0	-0.2	0.6	-16.4	8.5
NIC-bending pos.	Nm	0.0	13.7	17.3	11.6	14.4	-2.5	-1.2	26.1	1.3
ΣN$_{ij}$		1.2	0.0	-0.1	-0.1	0.3	-0.4	0.1	-0.3	0.0

Table 31: IARV residuals for pure quadratic regression trials at ΔV = 9.7 km/h and all grip strengths (0-678.9 N)

Velocity (km/h)		9.7								
Grip (N)		0.0	266.8	325.7	384.6	443.4	502.3	561.1	620.0	678.9
IARV	units									
HIC$_{36}$		-139	891	712	587	487	613	546	-183	13
Omega	rad/s	-4	1	0	2	8	4	6	16	23
Alpha	rad/s^2	-1,761	8,992	9,419	8,269	7,134	7,958	8,154	2,776	6,384
NIC-tension neg.	N	-126	4,014	3,250	2,564	1,625	2,231	1,582	-1,897	-1,379
NIC-tension pos.	N	0	47	227	-106	186	680	781	677	1,103
NIC-shear neg.	N	-21	-44	-177	-65	37	58	50	-114	21
NIC-shear pos.	N	-204	967	742	574	362	529	360	-179	-9
NIC-bending neg.	Nm	-3.0	0.0	0.0	2.8	5.0	1.4	0.0	-0.5	1.4
NIC-bending pos.	Nm	-6.7	36.6	12.7	5.8	0.0	9.9	3.8	-19.6	-13.7
ΣN$_{ij}$		0.0	1.4	1.5	1.2	0.9	1.1	1.0	-0.1	-0.1

Table 32: IARV residuals for pure quadratic regression trials at ΔV = 12.9 km/h and all grip strengths (0-678.9 N)

Velocity (km/h)		12.9								
Grip (N)		0.0	266.8	325.7	384.6	443.4	502.3	561.1	620.0	678.9
IARV	units									
HIC$_{36}$		-266	-399	-418	-301	-266	-239	-216	-176	-138
Omega	rad/s	-1	-4	-2	-4	-6	-5	-3	1	9
Alpha	rad/s^2	-6,235	-9,600	-8,799	-6,965	-5,369	-4,524	-3,475	-2,018	0
NIC-tens neg.	N	-3,048	-4,611	-4,212	0	-152	-170	-128	0	212
NIC-tens pos.	N	-43	-12	261	-685	-624	-485	-418	-274	128
NIC-shear neg.	N	0	24	-82	-231	-204	-208	-204	-166	0
NIC-shear pos.	N	-804	-996	-778	-394	-355	-302	-210	-110	0
NIC-bend neg.	Nm	-10.2	-9.3	-9.9	-5.4	-5.3	-3.4	0.3	20.6	31.9
NIC-bend pos.	Nm	-12.5	-18.5	-18.0	-12.3	-14.0	-12.7	-10.3	-1.5	3.8
ΣN$_{ij}$		-1.0	-1.5	-1.3	-0.6	-0.6	-0.4	-0.3	0.2	0.4

Table 33: IARV residuals for pure quadratic regression trials at ΔV = 16.1 km/h and all grip strengths (0-678.9 N)

Velocity (km/h)		16.1								
Grip (N)		0.0	266.8	325.7	384.6	443.4	502.3	561.1	620.0	678.9
IARV	units									
HIC$_{36}$		0	-92	-102	1	288	205	207	148	175
Omega	rad/s	5	2	2	0	-5	-4	-3	0	5
Alpha	rad/s^2	0	-2,089	-1,699	0	4,251	5,409	5,590	5,017	6,282
NIC-tension neg.	N	0	-2,319	-1,481	0	2,663	1,750	1,969	1,790	1,968
NIC-tension pos.	N	-65	83	0	263	-136	-91	4	121	204
NIC-shear neg.	N	-65	-77	74	191	0	8	3	0	9
NIC-shear pos.	N	0	-334	-211	0	314	210	339	388	481
NIC-bending neg.	Nm	0.0	12.9	16.3	22.2	0.0	-1.3	-4.6	-2.4	0.1
NIC-bending pos.	Nm	2.5	-5.1	-2.7	2.4	6.3	0.0	9.8	5.0	3.3
ΣN$_{ij}$		-0.1	-0.8	-0.6	0.1	0.9	0.7	0.0	0.1	0.2

MODIFIED QUADRATIC REGRESSION
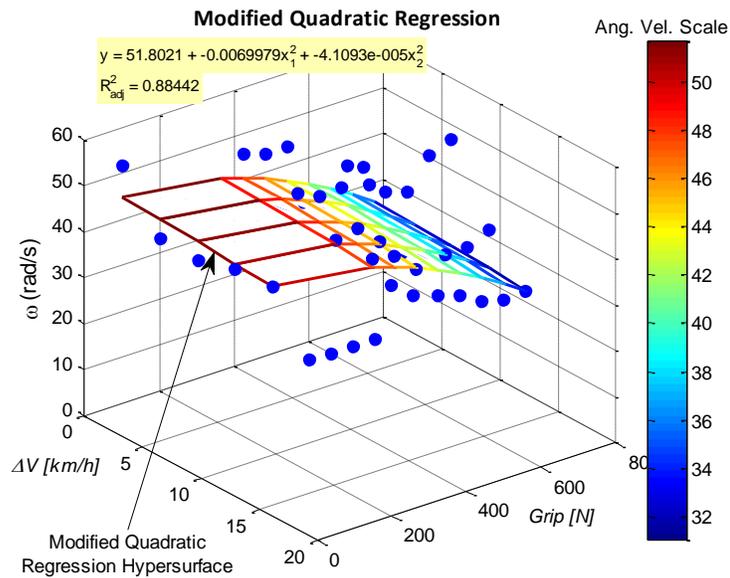
Figure 61: Modified quadratic regression surface fit for ω outputs with color scale, predictive equation, and adjusted R^2 value
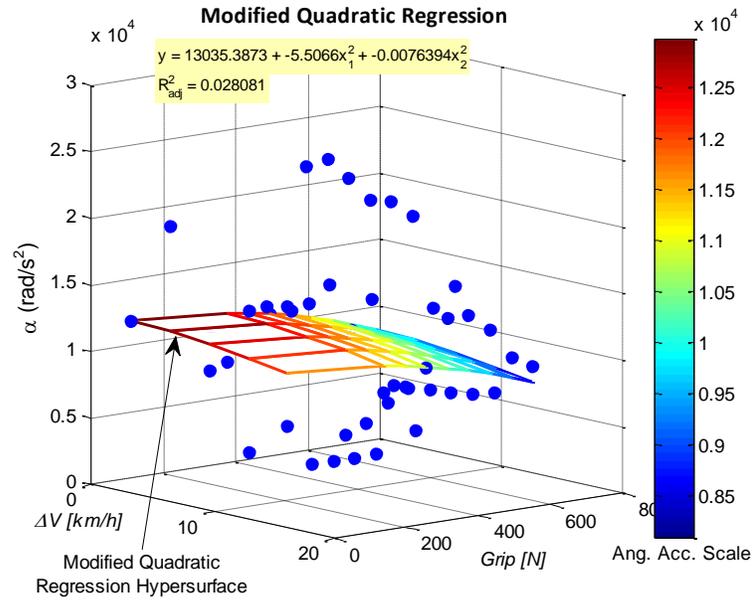
**Figure 62: Modified quadratic regression surface fit for α outputs with color scale, predictive equation, and adjusted R² value**
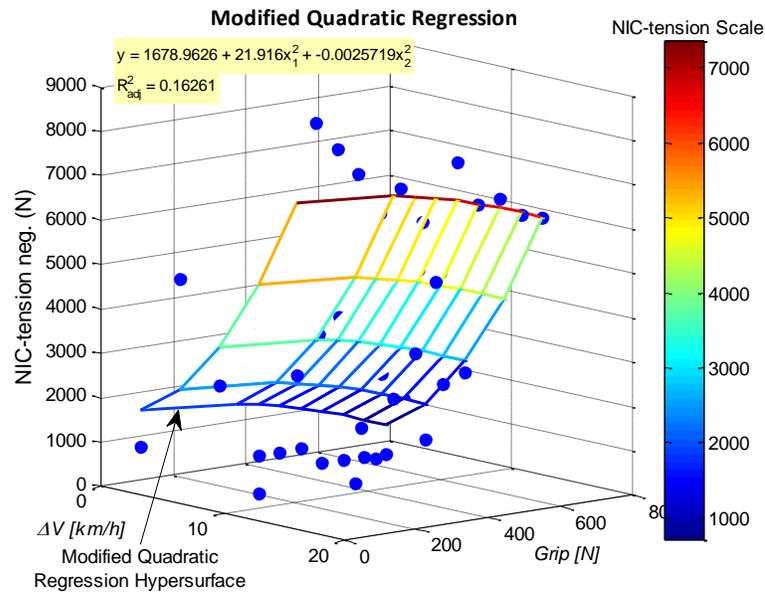
Figure 63: Modified quadratic regression surface fit for NIC-tension negative outputs with color scale, predictive equation, and adjusted R² value
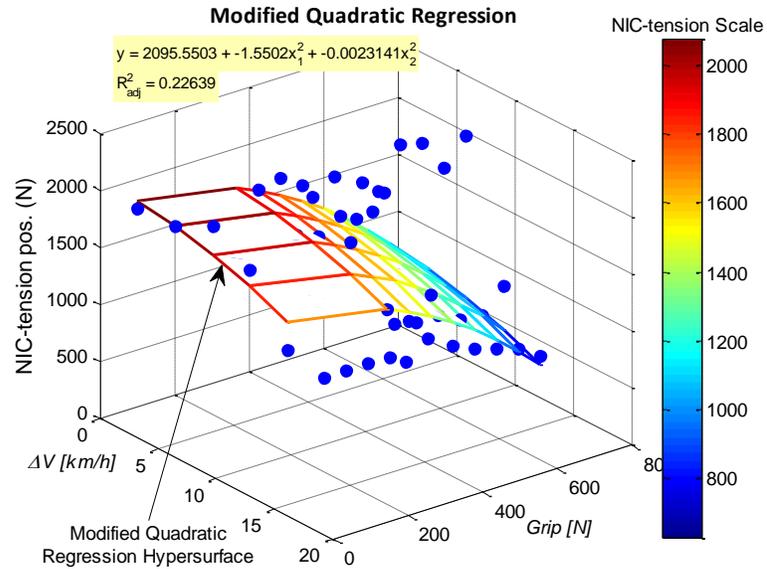
Figure 64: Modified quadratic regression surface fit for NIC-tension positive outputs with color scale, predictive equation, and adjusted R^2 value
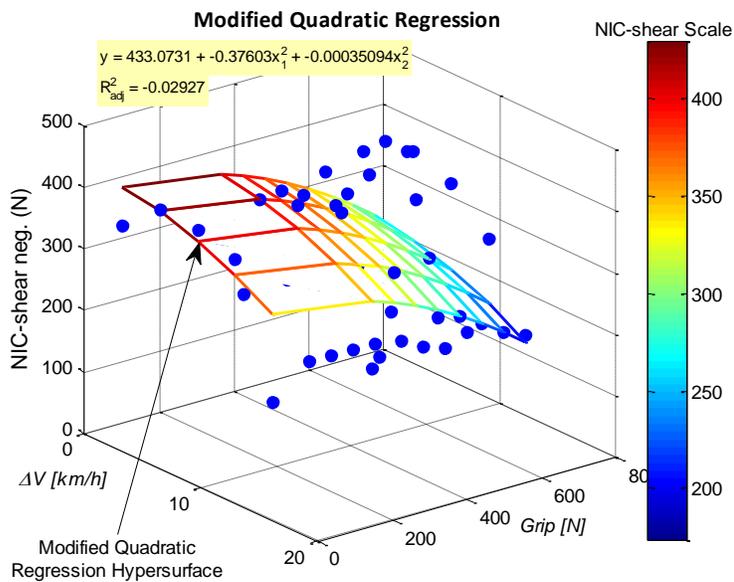
Figure 65: Modified quadratic regression surface fit for NIC-shear negative outputs with color scale, predictive equation, and adjusted R^2 value
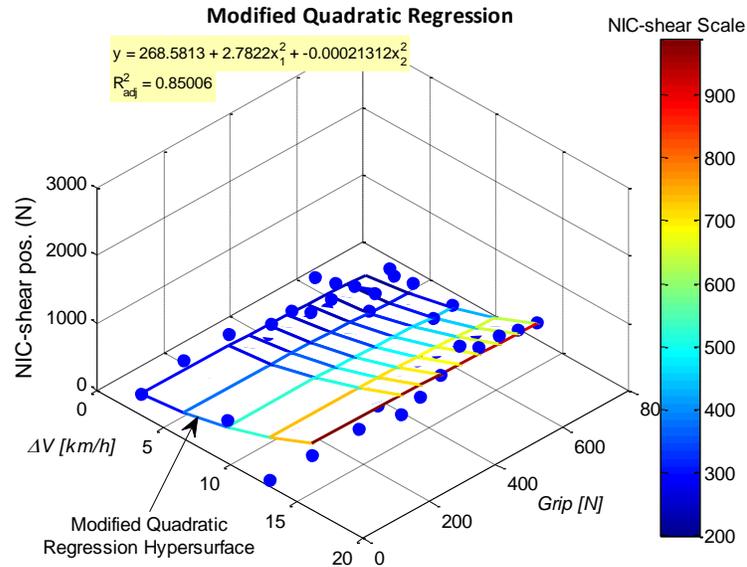
Figure 66: Modified quadratic regression surface fit for NIC-shear positive outputs with color scale, predictive equation, and adjusted R^2 value
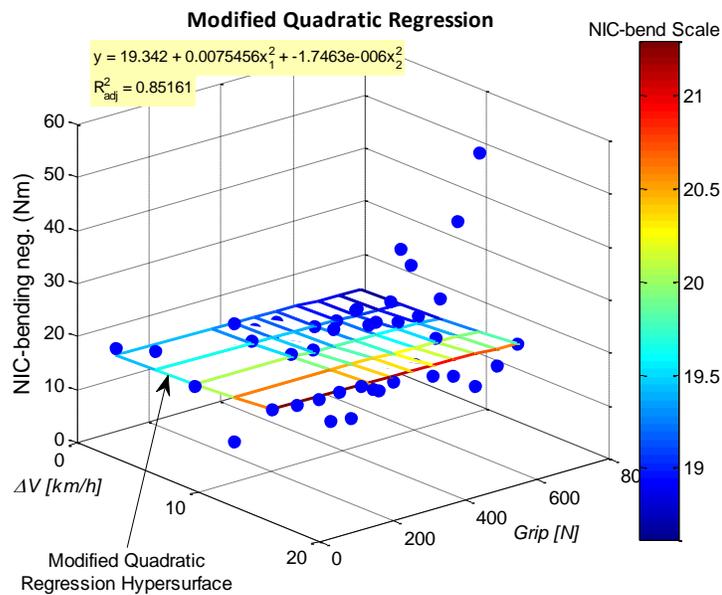
Figure 67: Modified quadratic regression surface fit for NIC-bending negative outputs with color scale, predictive equation, and adjusted R^2 value
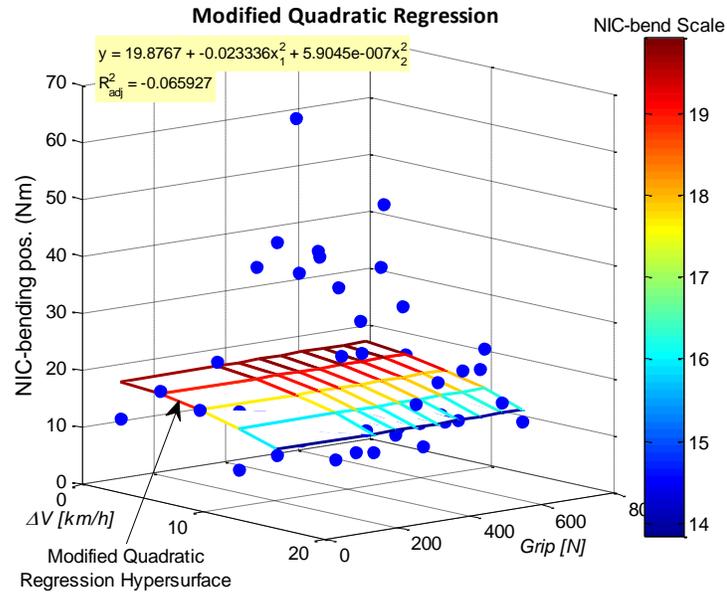
**Figure 68: Modified quadratic regression surface fit for NIC-bending positive outputs with color scale, predictive equation, and adjusted R^2 value**
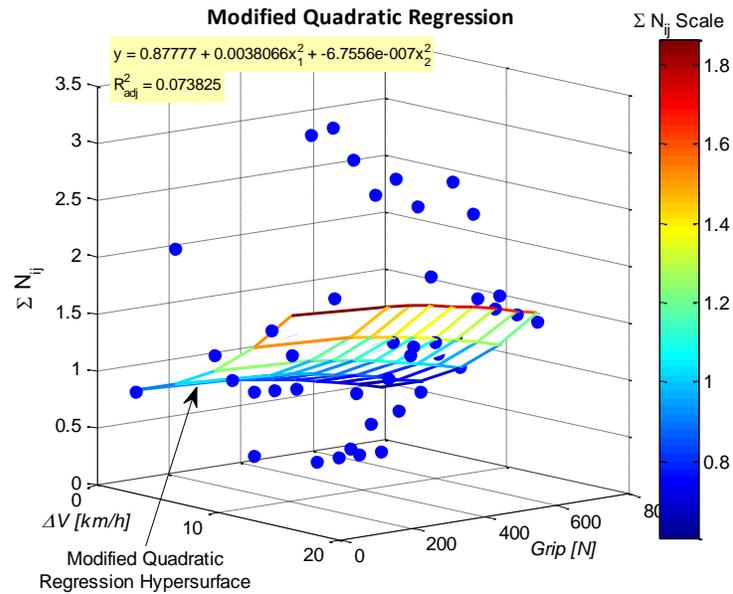

Figure 69: Modified quadratic regression surface fit for ΣN_{ij} outputs with color scale, predictive equation, and adjusted R^2 value

Table 34: IARV residuals for modified quadratic regression trials at ΔV = 3.2 km/h and all grip strengths (0-678.9 N)

Velocity (km/h)		3.2								
Grip (N)		0.0	266.8	325.7	384.6	443.4	502.3	561.1	620.0	678.9
IARV	units									
HIC$_{36}$		0	28	-82	-80	-74	-139	-133	-126	-118
Omega	rad/s	7	-1	5	6	7	-38	-36	-33	-30
Alpha	rad/s^2	0	-3,634	162	0	423	-10,978	-10,499	-9,968	-9,384
NIC-tens neg.	N	-751	521	-1,091	-1,004	-864	-1,130	-968	-789	-593
NIC-tens pos.	N	-77	-598	6	141	126	-1,485	-1,340	-1,179	-1,003
NIC-shear neg.	N	-63	-113	-193	-185	-158	-282	-261	-236	-209
NIC-shear pos.	N	-6	174	-135	-134	-125	-233	-219	-205	-188
NIC-bend neg.	Nm	1.6	-4.8	0.0	-2.2	-1.8	-18.5	-18.4	-18.3	-18.2
NIC-bend pos.	Nm	-6.5	0.7	-8.6	-8.5	-11.9	-15.4	-15.4	-15.5	-15.6
ΣN_{ij}		0.0	0.0	-0.1	-0.1	-0.1	-0.7	-0.7	-0.6	-0.6

Table 35: IARV residuals for modified quadratic regression trials at ΔV = 6.4 km/h and all grip strengths (0-678.9 N)

Velocity (km/h)		6.4								
Grip (N)		0.0	266.8	325.7	384.6	443.4	502.3	561.1	620.0	678.9
IARV	units									
HIC$_{36}$		611	265	255	247	360	-6	260	-123	-82
Omega	rad/s	-4	-2	-1	0	0	9	6	-15	-16
Alpha	rad/s^2	7,926	1,320	1,352	1,615	3,264	-38	2,570	-3,659	-6,731
NIC-tension neg.	N	2,509	1,294	1,135	1,141	1,591	-847	445	0	-811
NIC-tension pos.	N	-4	-117	-176	-149	75	441	435	-938	-622
NIC-shear neg.	N	3	0	15	13	59	31	74	-133	145
NIC-shear pos.	N	758	583	633	461	498	-162	15	514	-79
NIC-bending neg.	Nm	3.7	0.4	-0.1	-1.9	0.0	0.1	1.3	-15.2	10.4
NIC-bending pos.	Nm	0.8	19.7	23.4	17.4	19.6	1.6	1.6	27.0	0.0
ΣN_{ij}		1.2	0.4	0.3	0.3	0.7	-0.2	0.3	-0.3	-0.1

Table 36: IARV residuals for modified quadratic regression trials at ΔV = 9.7 km/h and all grip strengths (0-678.9 N)

Velocity (km/h)		9.7								
Grip (N)		0.0	266.8	325.7	384.6	443.4	502.3	561.1	620.0	678.9
IARV	units									
HIC$_{36}$		48	1,223	1,053	929	821	932	842	80	236
Omega	rad/s	-4	6	6	8	12	8	9	18	23
Alpha	rad/s^2	-1,840	12,916	13,450	12,127	10,540	10,629	9,813	3,140	5,173
NIC-tension neg.	N	-817	4,942	4,382	3,844	2,999	3,643	2,977	-575	-185
NIC-tension pos.	N	246	393	582	253	544	1,032	1,121	1,002	1,407
NIC-shear neg.	N	17	38	-87	32	140	166	162	2	139
NIC-shear pos.	N	105	1,498	1,265	1,069	808	907	649	0	39
NIC-bending neg.	Nm	-0.3	0.6	0.5	3.3	5.7	2.4	1.4	1.4	3.9
NIC-bending pos.	Nm	0.0	48.5	24.7	17.6	11.1	19.9	12.5	-12.7	-9.0
ΣN$_{ij}$		0.1	2.0	2.0	1.8	1.5	1.6	1.4	0.1	0.0

Table 37: IARV residuals for modified quadratic regression trials at ΔV = 12.9 km/h and all grip strengths (0-678.9 N)

Velocity (km/h)		12.9								
Grip (N)		0.0	266.8	325.7	384.6	443.4	502.3	561.1	620.0	678.9
IARV	units									
HIC$_{36}$		-166	-155	-164	-46	-18	-7	-7	0	-2
Omega	rad/s	-1	1	3	1	-1	-1	0	3	8
Alpha	rad/s^2	-6,765	-6,127	-5,219	-3,558	-2,415	-2,304	-2,268	-2,105	-1,663
NIC-tens neg.	N	-4,725	-4,669	-4,066	295	237	256	280	336	420
NIC-tens pos.	N	152	283	564	-378	-318	-185	-129	0	381
NIC-shear neg.	N	27	95	-3	-145	-112	-112	-102	-62	107
NIC-shear pos.	N	-643	-613	-403	-47	-56	-73	-69	-79	-99
NIC-bend neg.	Nm	-8.3	-9.5	-10.1	-5.6	-5.4	-3.1	0.9	21.8	33.7
NIC-bend pos.	Nm	-7.2	-8.0	-7.3	-2.0	-4.3	-4.0	-3.1	3.9	7.0
ΣN$_{ij}$		-0.9	-1.0	-0.8	0.0	-0.1	0.0	0.0	0.4	0.4

Table 38: IARV residuals for modified quadratic regression trials at ΔV = 16.1 km/h and all grip strengths (0-678.9 N)

Velocity (km/h)		16.1								
Grip (N)		0.0	266.8	325.7	384.6	443.4	502.3	561.1	620.0	678.9
IARV	units									
HIC$_{36}$		-156	-104	-105	-1	279	181	159	68	54
Omega	rad/s	0	2	2	0	-5	-5	-5	-4	0
Alpha	rad/s^2	-3,607	-1,694	-1,197	330	4,128	4,552	3,720	1,852	1,542
NIC-tension neg.	N	-3,853	-4,553	-3,510	-1,881	876	0	202	-50	0
NIC-tension pos.	N	-248	0	-74	193	-207	-168	-84	17	80
NIC-shear neg.	N	-143	-109	49	172	-13	0	0	0	12
NIC-shear pos.	N	-185	-298	-182	0	265	93	132	71	34
NIC-bending neg.	Nm	0.0	10.8	14.2	20.1	-2.0	-3.0	-5.9	-3.2	0.0
NIC-bending pos.	Nm	-0.8	-3.2	-0.6	4.2	7.3	0.0	8.4	1.8	-2.0
ΣN$_{ij}$		-0.3	-0.6	-0.4	0.3	1.1	0.8	0.0	0.0	-0.1

QUADRATIC REGRESSION

$$z = a + bx + cy + dx^2 + exy + fy^2 \qquad (18)$$

Table 39: Quadratic regression results for predicted IARVs including the regression coefficients (a-f) and the goodness of fit measurements (R^2 and $\bar{R}^2$)

IARV	a	b	c	d	e	f	R^2	$\bar{R}^2$
HIC$_{36}$	-2.3E+02	1.8E+02	3.8E-01	-1.0E+01	8.4E-02	-2.0E-03	0.38	0.31
Omega [rad/s]	4.0E+01	4.9E+00	-2.9E-02	-3.2E-01	4.7E-03	-8.0E-05	0.60	0.55
Alpha [rad/s^2]	9.2E+03	2.0E+03	-4.6E+00	-1.6E+02	2.6E+00	-4.0E-02	0.47	0.40
NIC-tension neg. [N]	6.4E+02	6.2E+02	-1.1E+00	-3.7E+01	9.7E-01	-1.1E-02	0.58	0.52
NIC-tension pos. [N]	1.0E+03	3.3E+02	-1.2E+00	-2.0E+01	1.5E-01	-2.9E-03	0.59	0.53
NIC-shear neg. [N]	1.6E+02	6.7E+01	-3.1E-01	-3.9E+00	2.5E-02	-2.2E-04	0.49	0.43
NIC-shear pos. [N]	2.4E+01	1.7E+02	3.4E-01	-9.6E+00	1.3E-01	-2.7E-03	0.42	0.34
NIC-bending neg. [Nm]	1.6E+01	1.7E+00	-3.8E-02	-1.1E-01	3.1E-03	1.1E-05	0.30	0.21
NIC-bending pos. [Nm]	-1.9E+00	6.4E+00	3.3E-02	-3.9E-01	2.2E-03	-8.6E-05	0.37	0.29
ΣN$_{ij}$	3.7E-01	2.8E-01	-6.3E-05	-1.6E-02	2.6E-04	-4.4E-06	0.47	0.40
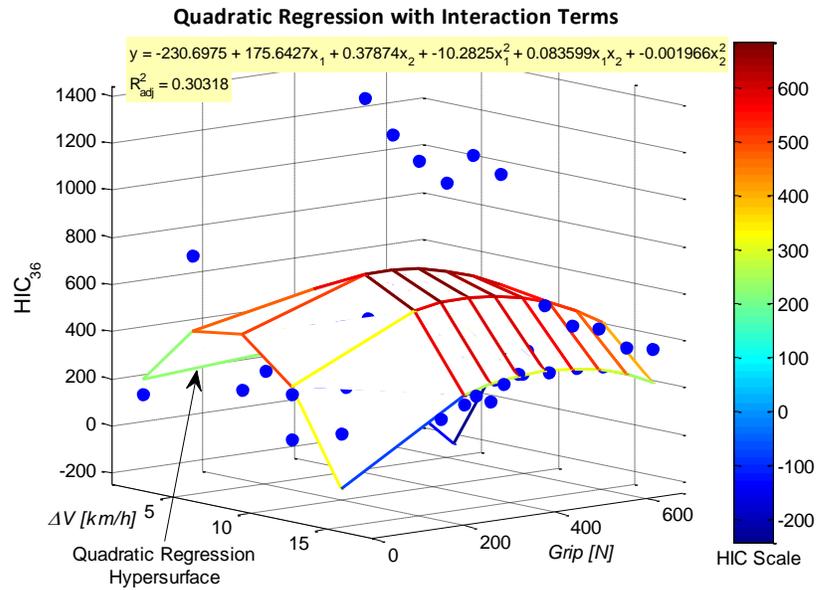
Figure 70: Quadratic regression surface fit for HIC outputs with color scale, predictive equation, and adjusted R^2 value
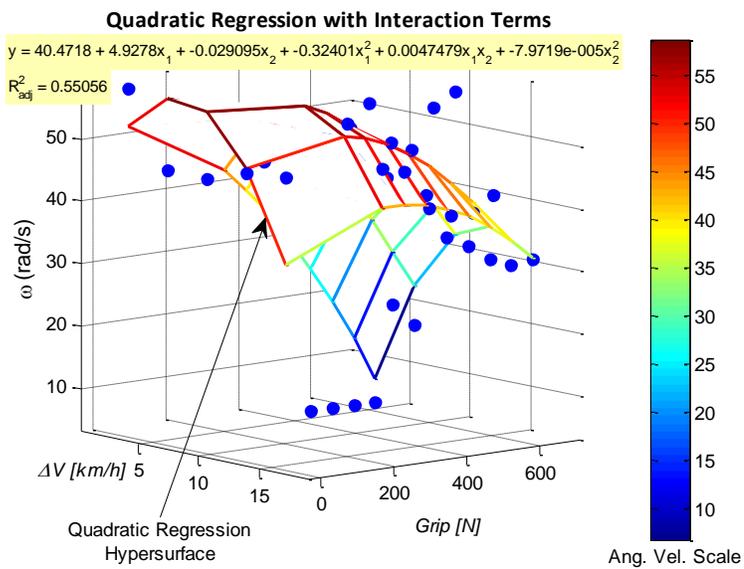
**Figure 71: Quadratic regression surface fit for ω outputs with color scale, predictive equation, and adjusted R^2 value**
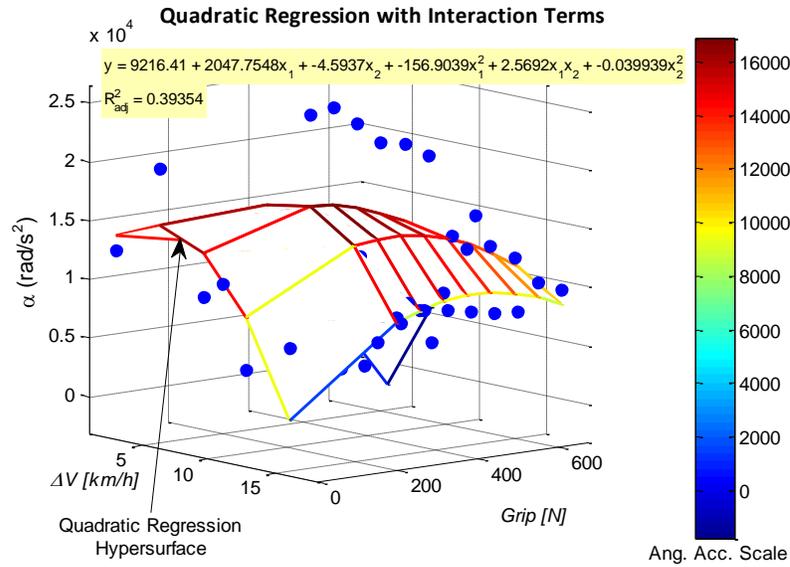
Figure 72: Quadratic regression surface fit for α outputs with color scale, predictive equation, and adjusted R² value
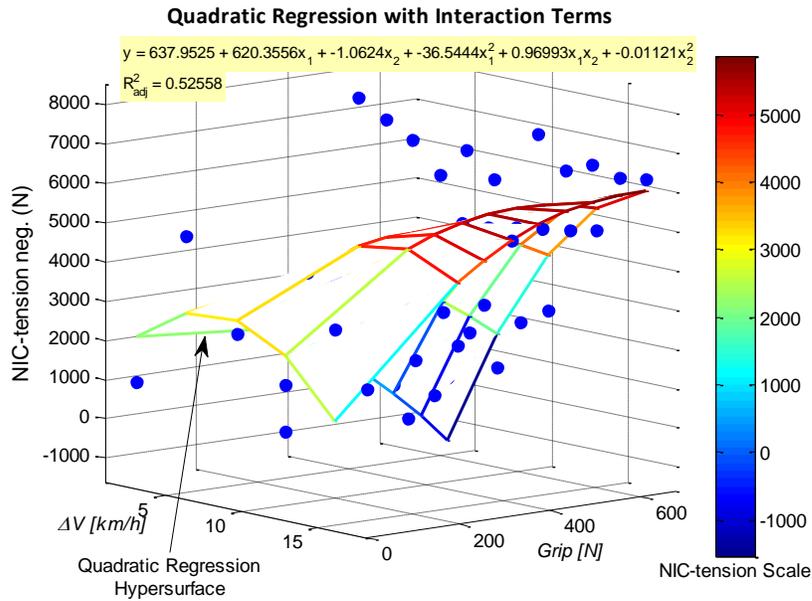
Figure 73: Quadratic regression surface fit for NIC-tension negative outputs with color scale, predictive equation, and adjusted R² value

**Quadratic Regression with Interaction Terms**

$y = 1028.0414 + 333.3941x_1 + -1.2281x_2 + -20.1526x_1^2 + 0.15198x_1x_2 + -0.0028999x_2^2$

$R_{adj}^2 = 0.53573$

NIC-tension pos. (N)

ΔV [km/h]

Grip [N]

Quadratic Regression Hypersurface
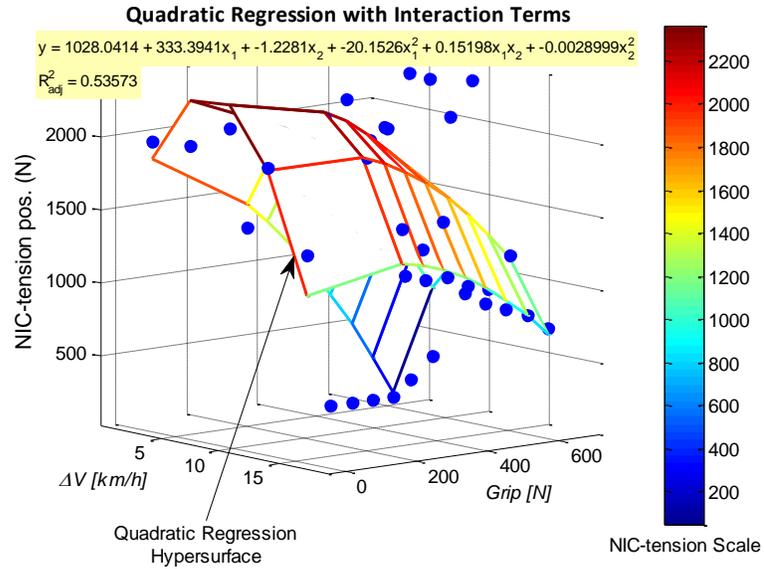
NIC-tension Scale

Figure 74: Quadratic regression surface fit for NIC-tension positive outputs with color scale, predictive equation, and adjusted R^2 value

Quadratic Regression with Interaction Terms

$y = 162.521 + 66.7758x_1 + -0.30876x_2 + -3.8778x_1^2 + 0.024842x_1x_2 + -0.00022392x_2^2$

$R_{adj}^2 = 0.41531$

NIC-shear neg. (N)

ΔV [km/h]

Grip [N]

Quadratic Regression Hypersurface
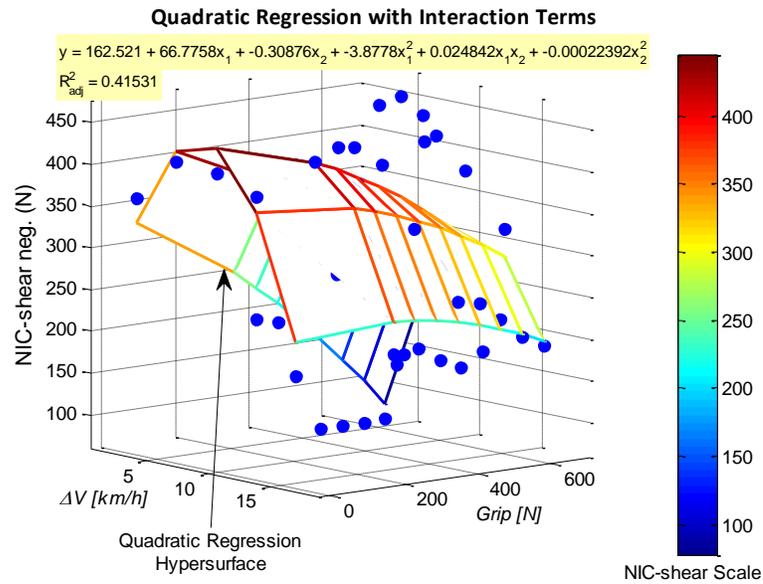
NIC-shear Scale

Figure 75: Quadratic regression surface fit for NIC-shear negative outputs with color scale, predictive equation, and adjusted R^2 value
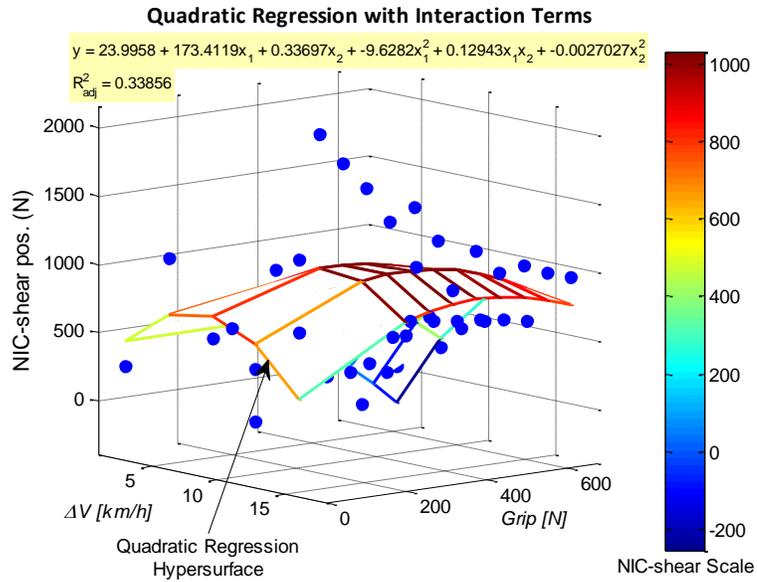
Figure 76: Quadratic regression surface fit for NIC-shear positive outputs with color scale, predictive equation, and adjusted R^2 value
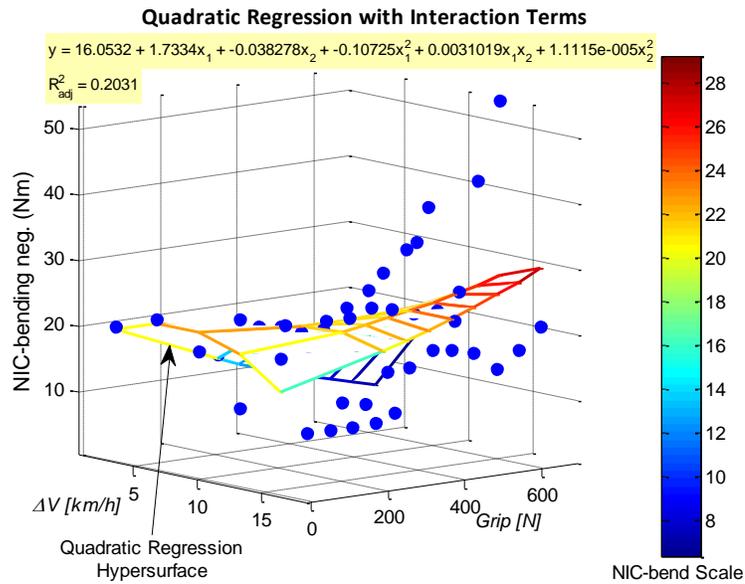
Figure 77: Quadratic regression surface fit for NIC-bending negative outputs with color scale, predictive equation, and adjusted R^2 value
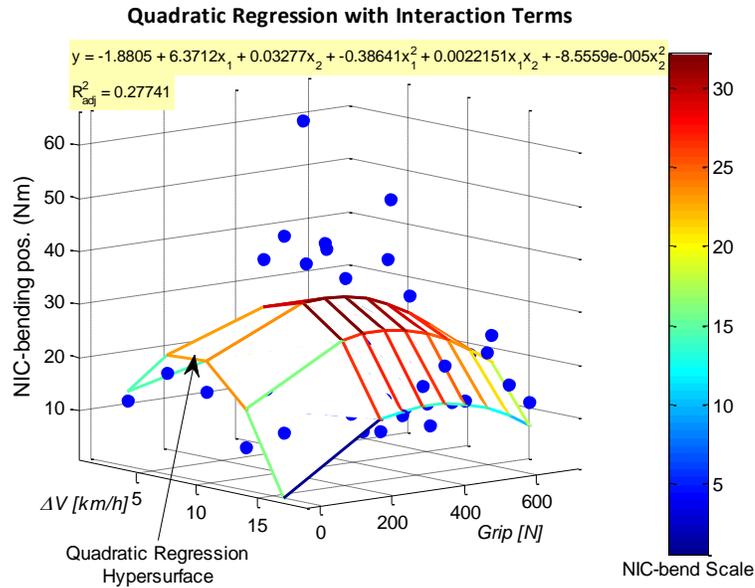
Figure 78: Quadratic regression surface fit for NIC-bending positive outputs with color scale, predictive equation, and adjusted R^2 value
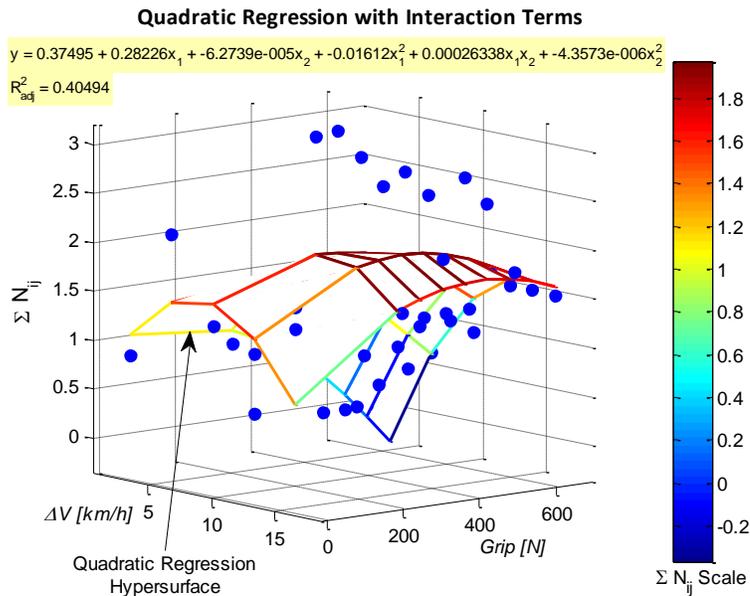
Figure 79: Quadratic regression surface fit for ΣN_{ij} outputs with color scale, predictive equation, and adjusted R^2 value

Table 40: IARV residuals for quadratic regression trials at ΔV = 3.2 km/h and all grip strengths (0-678.9 N)

Velocity (km/h)		3.2								
Grip (N)		0.0	266.8	325.7	384.6	443.4	502.3	561.1	620.0	678.9
IARV	units									
HIC$_{36}$		-60	-72	-154	-112	-54	-52	32	131	243
Omega	rad/s	6	4	13	15	20	-23	-17	-10	-4
Alpha	rad/s^2	-1,161	-3,445	1,268	2,247	4,033	-5,779	-3,489	-921	1,924
NIC-tension neg.	N	-1,140	215	-1,213	-881	-438	-340	245	908	1,648
NIC-tension pos.	N	125	-157	511	715	772	-763	-538	-293	-27
NIC-shear neg.	N	33	35	-36	-20	14	-103	-76	-47	-16
NIC-shear pos.	N	-180	-22	-288	-226	-140	-153	-28	117	280
NIC-bending neg.	Nm	0.4	0.8	6.9	5.8	7.3	-8.5	-7.5	-6.6	-5.7
NIC-bending pos.	Nm	-1.4	1.5	-7.1	-5.7	-7.2	-8.2	-5.2	-1.6	2.6
ΣN$_{ij}$		-0.2	-0.1	-0.2	0.0	0.1	-0.4	-0.1	0.1	0.4

Table 41: IARV residuals for quadratic regression trials at ΔV = 6.4 km/h and all grip strengths (0-678.9 N)

Velocity (km/h)		6.4								
Grip (N)		0.0	266.8	325.7	384.6	443.4	502.3	561.1	620.0	678.9
IARV	units									
HIC$_{36}$		317	-143	-142	-127	23	-294	35	-273	-143
Omega	rad/s	-12	-7	-5	-3	-1	10	9	-9	-7
Alpha	rad/s^2	4,737	-2,814	-2,370	-1,472	1,034	-1,184	2,729	-1,969	-3,287
NIC-tension neg.	N	1,947	-53	-220	-162	400	-1,866	-343	-496	-955
NIC-tension pos.	N	-313	-322	-346	-281	-14	398	443	-875	-500
NIC-shear neg.	N	-13	14	33	35	84	57	100	-107	170
NIC-shear pos.	N	401	89	156	19	108	-483	-220	383	-89
NIC-bending neg.	Nm	0.5	1.1	1.3	0.0	2.4	2.8	4.3	-12.0	13.7
NIC-bending pos.	Nm	-3.8	8.8	12.7	7.5	11.2	-4.8	-2.2	26.5	3.3
ΣN$_{ij}$		0.7	-0.3	-0.3	-0.3	0.2	-0.6	0.0	-0.4	0.0

Table 42: IARV residuals for quadratic regression trials at ΔV = 9.7 km/h and all grip strengths (0-678.9 N)

Velocity (km/h)		9.7								
Grip (N)		0.0	266.8	325.7	384.6	443.4	502.3	561.1	620.0	678.9
IARV	units									
HIC$_{36}$		-242	751	576	461	374	520	476	-225	4
Omega	rad/s	-11	-2	-2	0	6	3	5	16	23
Alpha	rad/s^2	-3,865	7,830	8,308	7,152	5,957	6,662	6,684	1,075	4,395
NIC-tension neg.	N	-360	3,811	3,066	2,404	1,493	2,132	1,521	-1,916	-1,352
NIC-tension pos.	N	-166	-38	157	-161	145	652	765	672	1,109
NIC-shear neg.	N	-31	0	-126	-8	98	121	113	-52	80
NIC-shear pos.	N	-169	979	740	555	323	467	272	-297	-160
NIC-bending neg.	Nm	-3.1	-0.8	-0.9	1.9	4.2	0.6	-0.7	-1.0	1.0
NIC-bending pos.	Nm	-6.1	34.1	10.1	3.4	-2.0	8.4	3.2	-19.2	-12.0
ΣN$_{ij}$		-0.2	1.2	1.3	1.0	0.7	0.9	0.8	-0.4	-0.3

Table 43: IARV residuals for quadratic regression trials at ΔV = 12.9 km/h and all grip strengths (0-678.9 N)

Velocity (km/h)		12.9								
Grip (N)		0.0	266.8	325.7	384.6	443.4	502.3	561.1	620.0	678.9
IARV	units									
HIC$_{36}$		-214	-459	-489	-379	-346	-317	-287	-235	-180
Omega	rad/s	0	-4	-2	-5	-7	-6	-5	-2	5
Alpha	rad/s^2	-4,238	-8,955	-8,610	-7,287	-6,258	-6,038	-5,669	-4,949	-3,725
NIC-tens neg.	N	-1,888	-4,289	-4,064	-19	-334	-512	-625	-646	-580
NIC-tens pos.	N	29	5	264	-697	-652	-530	-480	-354	28
NIC-shear neg.	N	21	76	-27	-176	-150	-157	-156	-125	33
NIC-shear pos.	N	-555	-885	-708	-366	-372	-369	-328	-284	-232
NIC-bend neg.	Nm	-8.1	-10.7	-12.0	-8.1	-8.6	-7.2	-4.1	15.7	26.6
NIC-bend pos.	Nm	-7.0	-18.1	-18.1	-12.8	-14.5	-13.0	-10.4	-1.0	5.1
ΣN$_{ij}$		-0.7	-1.4	-1.3	-0.6	-0.6	-0.6	-0.5	-0.1	0.0

Table 44: IARV residuals for quadratic regression trials at ΔV = 16.1 km/h and all grip strengths (0-678.9 N)

Velocity (km/h)		16.1								
Grip (N)		0.0	266.8	325.7	384.6	443.4	502.3	561.1	620.0	678.9
IARV	units									
HIC$_{36}$		240	-33	-70	11	281	185	179	117	145
Omega	rad/s	14	6	5	1	-5	-5	-5	-4	0
Alpha	rad/s^2	6,158	600	67	787	4,004	4,071	3,105	1,327	1,331
NIC-tension neg.	N	2,358	-1,601	-1,113	23	2,346	1,096	984	478	333
NIC-tension pos.	N	266	234	110	331	-111	-111	-60	11	47
NIC-shear neg.	N	-40	-40	109	222	25	26	12	-2	-5
NIC-shear pos.	N	488	-92	-32	112	356	181	233	204	215
NIC-bending neg.	Nm	5.2	12.0	14.2	18.8	-4.6	-7.0	-11.4	-10.3	-8.8
NIC-bending pos.	Nm	12.6	-2.0	-0.5	3.9	7.2	0.7	10.5	5.8	4.5
ΣN$_{ij}$		0.8	-0.3	-0.3	0.3	1.1	0.8	-0.1	-0.1	-0.1

CUBIC REGRESSION

$$z = a + bx + cy + dx^2 + exy + fy^2 + gx^3 + hx^2y + ixy^2 + jy^3 \qquad (19)$$

Table 45: Cubic regression results for predicted IARVs including the regression coefficients (a-g)

IARV	a	b	c	d	e	f	g
HIC_{36}	-1.4E+03	6.4E+02	3.2E-01	-6.0E+01	-8.8E-02	6.9E-04	1.6E+00
Omega [rad/s]	7.5E+01	-5.6E+00	-9.0E-03	1.8E-01	2.7E-02	-4.1E-04	5.6E-03
Alpha [rad/s^2]	-8.9E+03	1.0E+04	-1.7E+01	-1.2E+03	3.5E+00	9.3E-03	3.6E+01
NIC-tension neg. [N]	-6.4E+03	3.3E+03	-4.3E+00	-3.0E+02	-8.3E-01	3.1E-02	8.1E+00
NIC-tension pos. [N]	1.7E+03	1.6E+02	-3.0E-01	-1.9E+01	6.8E-01	-1.2E-02	5.5E-01
NIC-shear neg. [N]	-1.2E+02	2.2E+02	-3.4E-01	-2.4E+01	1.3E-01	-1.9E-03	7.4E-01
NIC-shear pos. [N]	-2.1E+03	1.0E+03	1.6E+00	-1.1E+02	-1.2E-01	-3.8E-03	3.2E+00
NIC-bending neg. [Nm]	3.5E+01	-1.7E+00	-1.7E-02	-2.8E-01	2.3E-02	-3.6E-04	2.2E-02
NIC-bending pos. [Nm]	-7.1E+01	3.4E+01	1.5E-01	-3.5E+00	-4.7E-03	-4.0E-04	1.1E-01
ΣN_{ij}	-1.6E+00	1.2E+00	-3.2E-03	-1.2E-01	2.2E-04	8.7E-06	3.5E-03

Table 46: Cubic regression results for predicted IARVs including the regression coefficients (h-j) and the goodness of fit measurements (R^2 and $\bar{R}^2$)

IARV	h	i	j	R^2	$\bar{R}^2$
HIC_{36}	9.8E-03	-2.4E-05	-2.4E-06	0.45	0.31
Omega [rad/s]	-1.6E-03	1.2E-05	2.0E-07	0.77	0.71
Alpha [rad/s^2]	-1.1E-01	1.7E-03	-6.4E-05	0.58	0.48
NIC-tension neg. [N]	8.3E-02	3.0E-04	-4.4E-05	0.64	0.54
NIC-tension pos. [N]	-4.1E-02	3.8E-04	5.2E-06	0.64	0.55
NIC-shear neg. [N]	-3.7E-03	-4.5E-05	2.1E-06	0.63	0.54
NIC-shear pos. [N]	1.3E-02	1.0E-05	9.7E-07	0.56	0.45
NIC-bending neg. [Nm]	-1.1E-03	2.2E-06	3.4E-07	0.49	0.36
NIC-bending pos. [Nm]	1.3E-04	6.3E-06	2.5E-07	0.59	0.48
ΣN_{ij}	3.6E-06	-3.6E-08	-1.2E-08	0.54	0.42
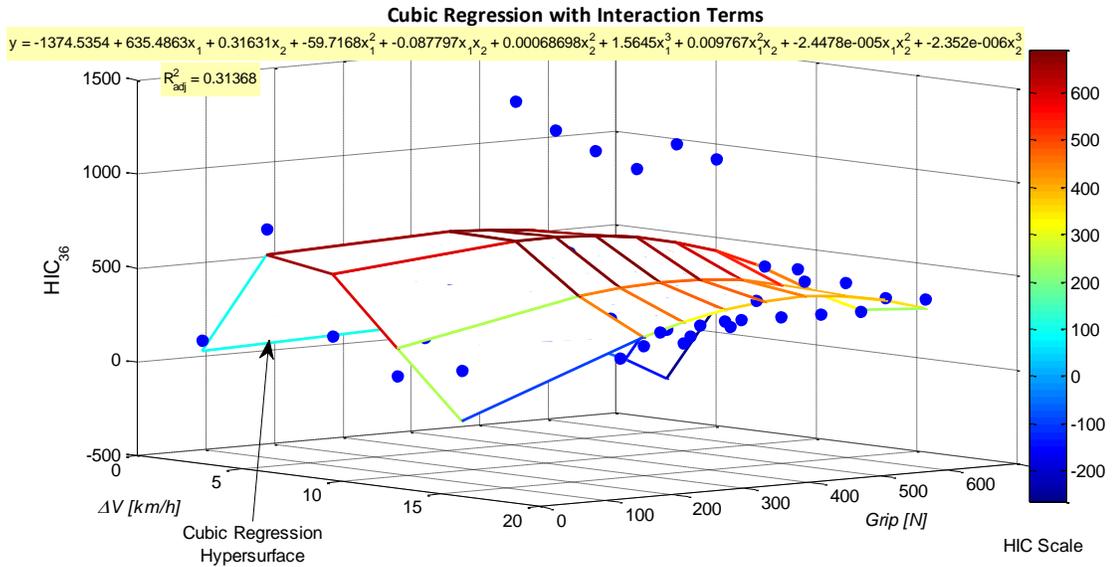
Figure 80: Cubic regression surface fit for HIC outputs with color scale, predictive equation, and adjusted R² value
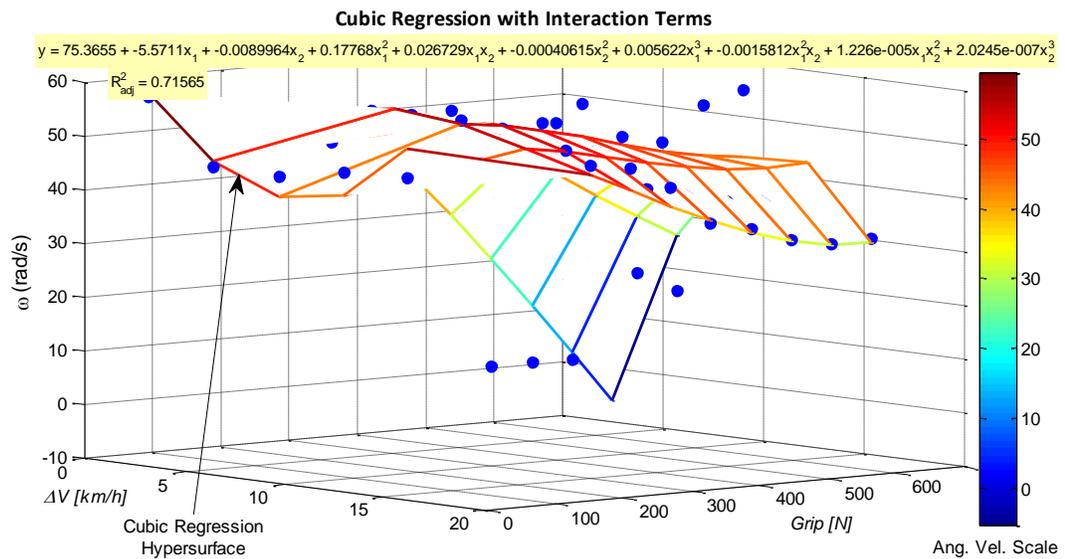
Figure 81: Cubic regression surface fit for ω outputs with color scale, predictive equation, and adjusted R² value
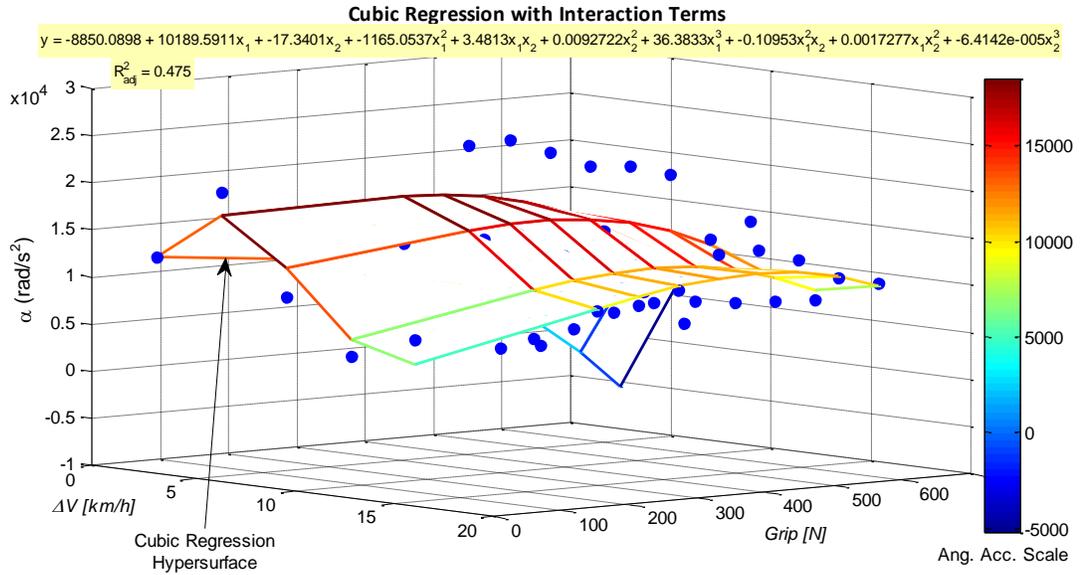
Figure 82: Cubic regression surface fit for α outputs with color scale, predictive equation, and adjusted R^2 value
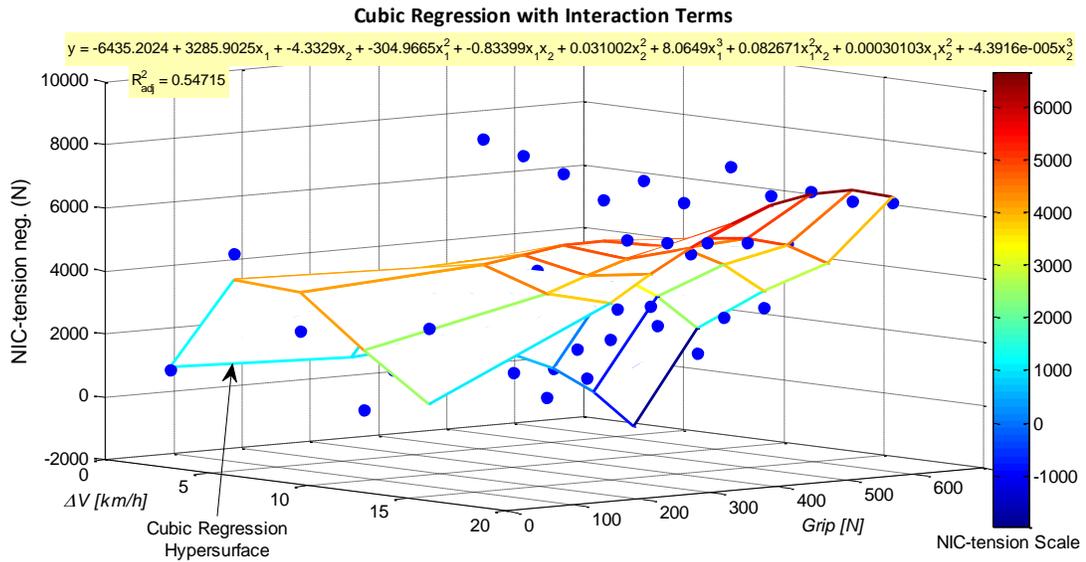
Figure 83: Cubic regression surface fit for NIC-tension negative outputs with color scale, predictive equation, and adjusted R^2 value

Cubic Regression with Interaction Terms

$y = 1664.3494 + 163.2629x_1 + -0.29881x_2 + -18.7424x_1^2 + 0.67979x_1x_2 + -0.011918x_2^2 + 0.54883x_1^3 + -0.041189x_1^2x_2 + 0.00038382x_1x_2^2 + 5.1685e{-}006x_2^3$

$R_{adj}^2 = 0.5561$
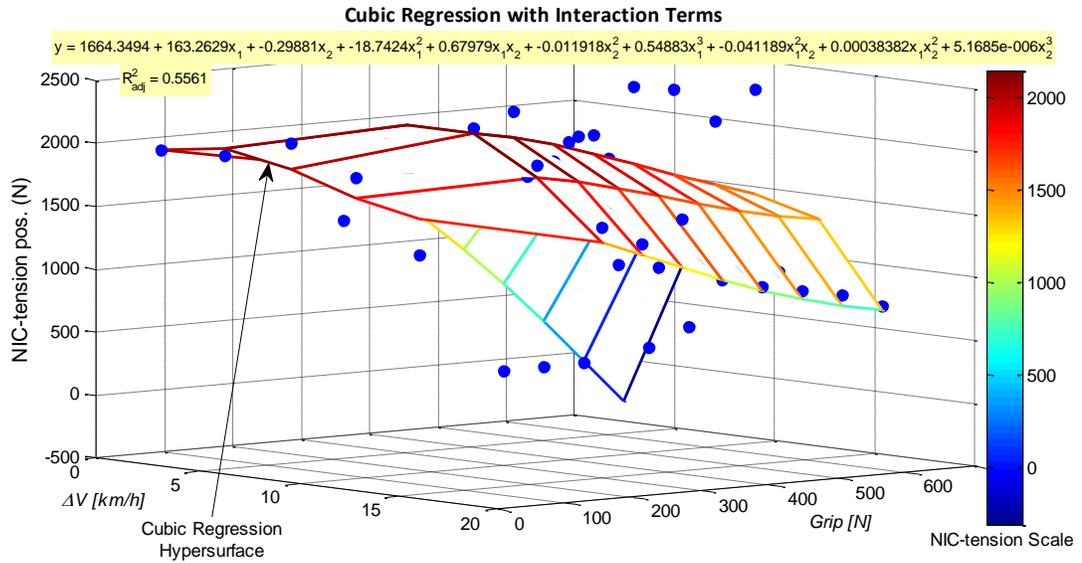
Figure 84: Cubic regression surface fit for NIC-tension positive outputs with color scale, predictive equation, and adjusted R^2 value

Cubic Regression with Interaction Terms

$y = -116.6068 + 215.4772x_1 + -0.34138x_2 + -23.9047x_1^2 + 0.12717x_1x_2 + -0.0019318x_2^2 + 0.74485x_1^3 + -0.0036991x_1^2x_2 + -4.4569e{-}005x_1x_2^2 + 2.0813e{-}006x_2^3$

$R_{adj}^2 = 0.53597$
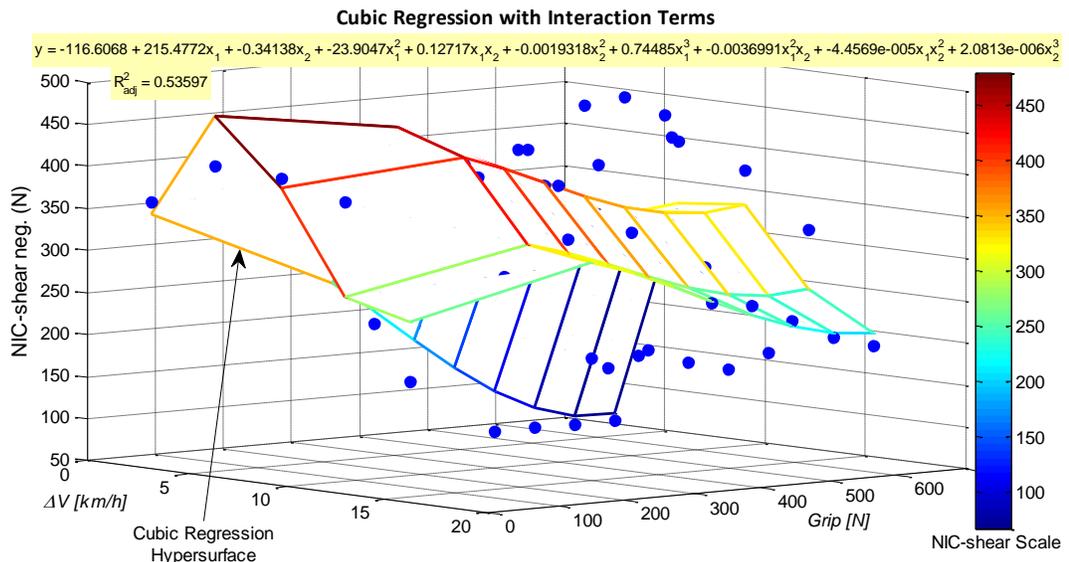
Figure 85: Cubic regression surface fit for NIC-shear negative outputs with color scale, predictive equation, and adjusted R^2 value
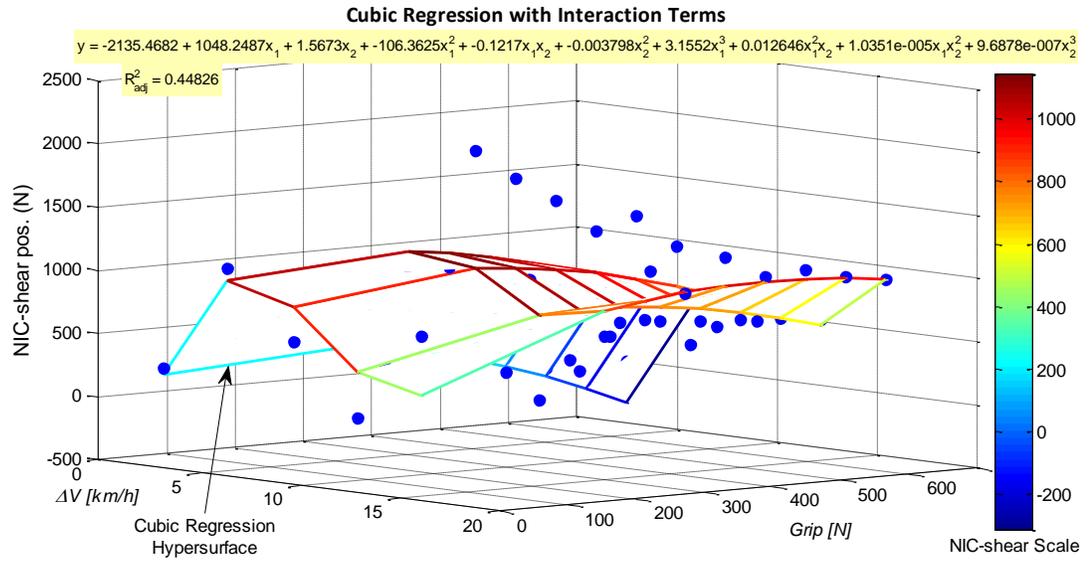
Figure 86: Cubic regression surface fit for NIC-shear positive outputs with color scale, predictive equation, and adjusted R^2 value
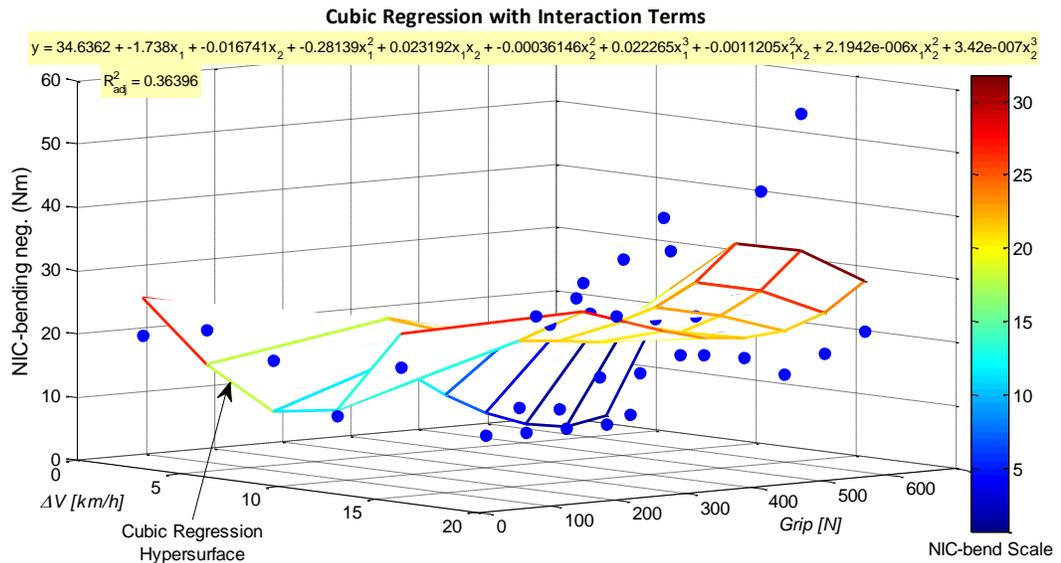
Figure 87: Cubic regression surface fit for NIC-bending negative outputs with color scale, predictive equation, and adjusted R^2 value
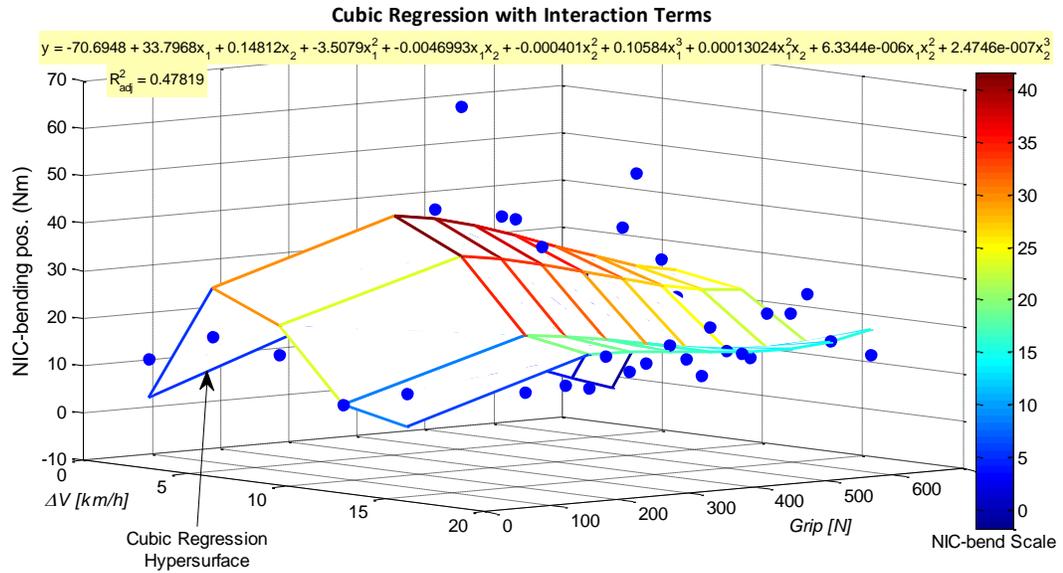
Figure 88: Cubic regression surface fit for NIC-bending positive outputs with color scale, predictive equation, and adjusted R^2 value
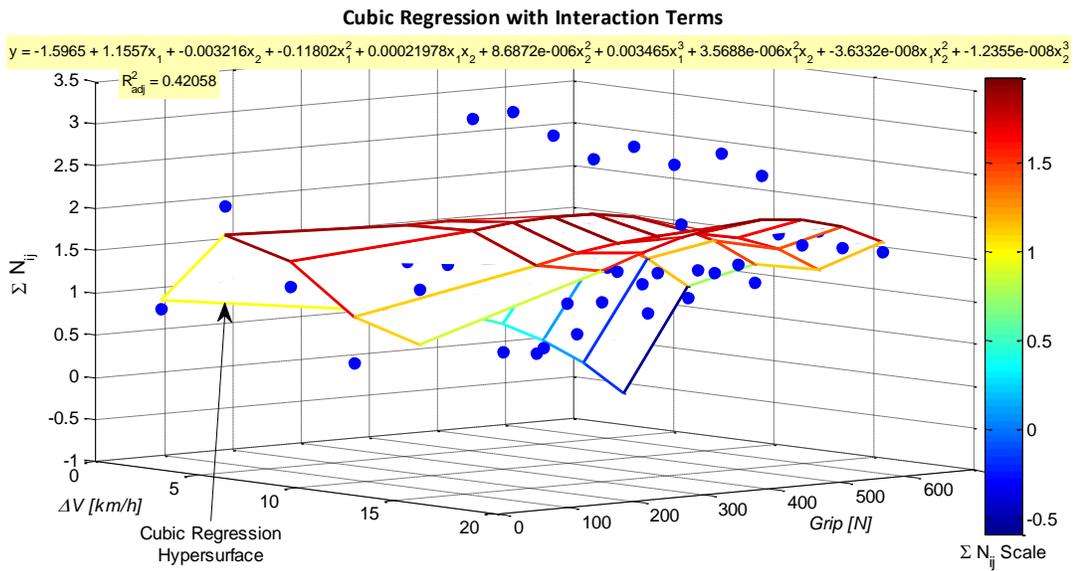
Figure 89: Cubic regression surface fit for ΣN_{ij} outputs with color scale, predictive equation, and adjusted R^2 value

Table 47: IARV residuals for cubic regression trials at ΔV = 3.2 km/h and all grip strengths (0-678.9 N)

Velocity (km/h)		3.2								
Grip (N)		**0.0**	**266.8**	**325.7**	**384.6**	**443.4**	**502.3**	**561.1**	**620.0**	**678.9**
IARV	*units*									
HIC$_{36}$		71	48	-59	-42	-8	-27	44	140	261
Omega	rad/s	-1	-6	5	11	19	-20	-11	-1	8
Alpha	rad/s^2	-4	-2,169	2,264	3,023	4,727	-4,949	-2,230	1,144	5,247
NIC-tension neg.	N	-66	1,175	-603	-621	-473	-564	-7	842	2,039
NIC-tension pos.	N	-9	-418	313	598	749	-685	-359	-20	327
NIC-shear neg.	N	12	39	-14	18	64	-48	-23	-9	-7
NIC-shear pos.	N	71	126	-152	-101	-26	-52	59	185	325
NIC-bending neg.	Nm	-5.9	-6.1	3.0	5.2	9.8	-3.5	-1.1	-0.2	-1.2
NIC-bending pos.	Nm	8.0	1.7	-6.0	-3.3	-3.5	-3.5	0.2	3.5	6.3
ΣN$_{ij}$		-0.1	0.1	0.1	0.1	0.2	-0.3	-0.1	0.2	0.6

Table 48: IARV residuals for cubic regression trials at ΔV = 6.4 km/h and all grip strengths (0-678.9 N)

Velocity (km/h)		6.4								
Grip (N)		**0.0**	**266.8**	**325.7**	**384.6**	**443.4**	**502.3**	**561.1**	**620.0**	**678.9**
IARV	*units*									
HIC$_{36}$		135	-255	-259	-250	-106	-422	-86	-376	-215
Omega	rad/s	-1	-8	-7	-4	-2	9	8	-11	-11
Alpha	rad/s^2	2,565	-5,030	-5,021	-4,540	-2,354	-4,718	-699	-4,959	-5,428
NIC-tens neg.	N	825	-410	-754	-881	-458	-2,764	-1,127	-960	-838
NIC-tens pos.	N	-43	-385	-416	-348	-74	342	382	-956	-623
NIC-shear neg.	N	-55	-53	-24	-14	41	15	51	-173	73
NIC-shear pos.	N	99	-193	-113	-235	-133	-712	-439	169	-302
NIC-bend neg.	Nm	5.9	-2.5	-1.4	-1.4	1.9	2.6	3.3	-15.4	6.1
NIC-bend pos.	Nm	-10.0	-3.0	2.2	-1.5	3.6	-11.3	-8.4	19.6	-5.5
ΣN$_{ij}$		0.3	-0.4	-0.5	-0.6	-0.2	-0.9	-0.3	-0.7	-0.1

Table 49: IARV residuals for cubic regression trials at ΔV = 9.7 km/h and all grip strengths (0-678.9 N)

Velocity (km/h)		9.7								
Grip (N)		**0.0**	**266.8**	**325.7**	**384.6**	**443.4**	**502.3**	**561.1**	**620.0**	**678.9**
IARV	*units*									
HIC$_{36}$		-338	745	571	454	370	522	492	-184	84
Omega	rad/s	4	1	0	1	6	2	2	10	13
Alpha	rad/s^2	-3,168	8,869	8,889	7,254	5,636	6,054	6,002	612	4,522
NIC-tension neg.	N	-1,283	3,998	3,133	2,334	1,326	1,960	1,489	-1,607	-448
NIC-tension pos.	N	216	39	211	-129	151	621	680	511	841
NIC-shear neg.	N	11	-8	-128	-3	108	131	117	-64	41
NIC-shear pos.	N	-278	931	713	550	339	502	322	-235	-92
NIC-bending neg.	Nm	7.9	-0.9	-0.5	2.9	5.4	1.4	-1.5	-5.0	-8.1
NIC-bending pos.	Nm	-6.2	31.3	8.7	3.5	-0.6	10.7	5.4	-18.1	-13.5
ΣN$_{ij}$		-0.3	1.3	1.3	1.0	0.7	0.9	0.7	-0.4	-0.2

Table 50: IARV residuals for cubic regression trials at ΔV = 12.9 km/h and all grip strengths (0-678.9 N)

Velocity (km/h)		12.9								
Grip (N)		**0.0**	**266.8**	**325.7**	**384.6**	**443.4**	**502.3**	**561.1**	**620.0**	**678.9**
IARV	*units*									
HIC$_{36}$		-136	-327	-364	-261	-233	-204	-164	-93	-4
Omega	rad/s	4	-2	0	-3	-5	-5	-6	-5	-3
Alpha	rad/s^2	-1,615	-4,988	-4,997	-4,093	-3,467	-3,559	-3,330	-2,501	-839
NIC-tens neg.	N	-1,856	-3,278	-3,224	625	146	-111	-165	64	627
NIC-tens pos.	N	154	94	364	-593	-556	-463	-468	-428	-172
NIC-shear neg.	N	114	113	18	-121	-87	-88	-88	-67	72
NIC-shear pos.	N	-356	-659	-468	-113	-108	-95	-49	-4	42
NIC-bend neg.	Nm	-1.2	-10.7	-10.7	-5.5	-5.2	-3.6	-1.5	15.6	21.8
NIC-bend pos.	Nm	0.1	-11.6	-10.1	-3.4	-4.1	-2.2	-0.1	7.4	10.1
ΣN$_{ij}$		-0.5	-1.0	-0.9	-0.3	-0.4	-0.4	-0.3	0.2	0.5

Table 51: IARV residuals for cubic regression trials at ΔV = 16.1 km/h and all grip strengths (0-678.9 N)

Velocity (km/h)		16.1								
Grip (N)		**0.0**	**266.8**	**325.7**	**384.6**	**443.4**	**502.3**	**561.1**	**620.0**	**678.9**
IARV	*units*									
HIC$_{36}$		264	-45	-106	-51	196	84	69	10	56
Omega	rad/s	-5	2	4	4	0	1	0	0	1
Alpha	rad/s^2	2,621	-131	-804	-327	2,622	2,473	1,424	-226	195
NIC-tension neg.	N	2,451	-1,119	-952	-169	1,826	325	93	-349	-191
NIC-tension pos.	N	-277	122	90	387	-1	28	71	95	37
NIC-shear neg.	N	-74	-114	49	178	-2	12	8	-4	-16
NIC-shear pos.	N	468	-186	-137	-4	228	36	69	15	-5
NIC-bending neg.	Nm	-5.0	4.7	10.0	17.9	-2.7	-3.1	-6.8	-6.6	-8.1
NIC-bending pos.	Nm	7.1	-7.0	-4.0	1.5	5.5	-1.2	7.3	0.0	-5.6
ΣN$_{ij}$		0.7	-0.3	-0.3	0.2	0.9	0.5	-0.3	-0.3	-0.1

APPENDIX B: MATLAB CODE

---

multivar_reg3.m

```matlab
% Multivariate Nonlinear and Linear Regression
% Braden Cripe
% 3.16.11

clear all
close all

% Read in data file
[num,txt,RAW]=XLSREAD('NoDoor_Compiled.xlsx',...
    'ALL DATA - Grip by Vel','E4:AW17');

% Input velocity (mph) and grip values (lbf)
% velocity = [2 4 6 8 10]';
% gripstr = [0 59.8 73.0 86.2 99.4 112.6 125.8 139.0 152.2]';

% Input velocity (km/h) and grip values (N)
velocity = [3.2 6.4 9.7 12.9 16.1]';
gripstr = [0 266.8 325.7 384.6 443.4 502.3 561.1 620.0 678.9]';

% Create appropriate vectors for regression models
vel = [];
for i = 1:length(gripstr)
    vel = [vel velocity];
end
grip = [];
for i = 1:length(velocity)
    grip = [grip;gripstr];
end
vel = reshape(vel',1,length(velocity)*length(gripstr))';
data = [num(1:9,:);num(14,:)]';

% IARVs in TeX format (13 total):
names(1) = {'HIC_3_6'};
names(2) = {'\omega (rad/s)'};
names(3) = {'\alpha (rad/s^2)'};
names(4) = {'NIC-tension neg. (N)'};
names(5) = {'NIC-tension pos. (N)'};
names(6) = {'NIC-shear neg. (N)'};
names(7) = {'NIC-shear pos. (N)'};
names(8) = {'NIC-bending neg. (Nm)'};
names(9) = {'NIC-bending pos. (Nm)'};
names(10) = {'\Sigma N_i_j'};

% Color Scale names in TeX format
scale(1) = {'HIC Scale'};
scale(2) = {'Ang. Vel. Scale'};
scale(3) = {'Ang. Acc. Scale'};
scale(4) = {'NIC-tension Scale'};
scale(5) = {'NIC-tension Scale'};
scale(6) = {'NIC-shear Scale'};
scale(7) = {'NIC-shear Scale'};
scale(8) = {'NIC-bend Scale'};
scale(9) = {'NIC-bend Scale'};
scale(10) = {'\Sigma N_i_j Scale'};

for i = 1:size(data,2)
```

```matlab
% Send data one column (IARV) at a time to regression
[fitresult, gof] = SurFitReg3(vel, grip, data(:,i))

%% Regression coefficients, confidence intervals and goodness of fit tests
% Coefficients
a = coeffvalues(fitresult{1});
b = coeffvalues(fitresult{2});
c = coeffvalues(fitresult{3});
d = coeffvalues(fitresult{4});
e = coeffvalues(fitresult{5});

coeff1(i,:) = a;
coeff2(i,:) = b;
coeff3(i,:) = c;
coeff4(i,:) = d;
coeff5(i,:) = e;

% Confidence intervals
int1 = confint(fitresult{1});
int2 = confint(fitresult{2});
int3 = confint(fitresult{3});
int4 = confint(fitresult{4});
int5 = confint(fitresult{5});

inv1(i,:) = reshape(int1,1,2*length(int1));
inv2(i,:) = reshape(int2,1,2*length(int2));
inv3(i,:) = reshape(int3,1,2*length(int3));
inv4(i,:) = reshape(int4,1,2*length(int4));
inv5(i,:) = reshape(int5,1,2*length(int5));

% Sum of the squared error
sse1 = gof(1).sse;
sse2 = gof(2).sse;
sse3 = gof(3).sse;
sse4 = gof(4).sse;
sse5 = gof(5).sse;

SSE1(i) = sse1;
SSE2(i) = sse2;
SSE3(i) = sse3;
SSE4(i) = sse4;
SSE5(i) = sse5;

% R-squared statistic
rsquare1 = gof(1).rsquare;
rsquare2 = gof(2).rsquare;
rsquare3 = gof(3).rsquare;
rsquare4 = gof(4).rsquare;
rsquare5 = gof(5).rsquare;

RSQ1(i) = rsquare1;
RSQ2(i) = rsquare2;
RSQ3(i) = rsquare3;
RSQ4(i) = rsquare4;
RSQ5(i) = rsquare5;

% Degree of freedom in the error
dfe1 = gof(1).dfe;
dfe2 = gof(2).dfe;
dfe3 = gof(3).dfe;
dfe4 = gof(4).dfe;
dfe5 = gof(5).dfe;
```

```matlab
    DOF1(i) = dfe1;
    DOF2(i) = dfe2;
    DOF3(i) = dfe3;
    DOF4(i) = dfe4;
    DOF5(i) = dfe5;

    % Adjusted R-squared
    adjrsquare1 = gof(1).adjrsquare;
    adjrsquare2 = gof(2).adjrsquare;
    adjrsquare3 = gof(3).adjrsquare;
    adjrsquare4 = gof(4).adjrsquare;
    adjrsquare5 = gof(5).adjrsquare;

    AdjRSQ1(i) = adjrsquare1;
    AdjRSQ2(i) = adjrsquare2;
    AdjRSQ3(i) = adjrsquare3;
    AdjRSQ4(i) = adjrsquare4;
    AdjRSQ5(i) = adjrsquare5;

    % Root mean squared error
    rmse1 = gof(1).rmse;
    rmse2 = gof(2).rmse;
    rmse3 = gof(3).rmse;
    rmse4 = gof(4).rmse;
    rmse5 = gof(5).rmse;

    RMSE1(i) = rmse1;
    RMSE2(i) = rmse2;
    RMSE3(i) = rmse3;
    RMSE4(i) = rmse4;
    RMSE5(i) = rmse5;

    %% Forming TeX coded output for equation
    uistr1 = ['y = ',num2str(a(1)),' + ',num2str(a(2)),'x_1 + ',...
        num2str(a(3)),'x_2'];
    uistr2 = ['y = ',num2str(b(1)),' + ',num2str(b(2)),'x_1 + ',...
        num2str(b(3)),'x_2 + ',num2str(b(4)),'x_1^2 + ',num2str(b(5)),'x_2^2'];
    uistr3 = ['y = ',num2str(c(1)),' + ',num2str(c(2)),'x_1^2 + ',...
        num2str(c(3)),'x_2^2'];
    uistr4 = ['y = ',num2str(d(1)),' + ',num2str(d(2)),'x_1 + ',...
        num2str(d(3)),'x_2 + ',num2str(d(4)),'x_1^2 + ',...
        num2str(d(5)),'x_1x_2 + ',num2str(d(6)),'x_2^2'];
    uistr5 = ['y = ',num2str(e(1)),' + ',num2str(e(2)),'x_1 + ',...
        num2str(e(3)),'x_2 + ',num2str(e(4)),'x_1^2 + ',...
        num2str(e(5)),'x_1x_2 + ',num2str(e(6)),'x_2^2 + '...
        ,num2str(e(7)),'x_1^3 + ',num2str(e(8)),'x_1^2x_2 + ',...
        num2str(e(9)),'x_1x_2^2 + ',num2str(e(10)),'x_2^3'];
    uistr1 = cellstr(uistr1);
    uistr2 = cellstr(uistr2);
    uistr3 = cellstr(uistr3);
    uistr4 = cellstr(uistr4);
    uistr5 = cellstr(uistr5);

    %% Linear1 regression graphs
    figure(i)
    % Scatterplot of the measured data
    scatter3(vel,grip,data(:,i),'filled')
    hold on
    % Mesh surface of the predicted IARVs
    [X1FIT,X2FIT] = meshgrid(velocity,gripstr);
    YFIT = a(1) + a(2)*X1FIT + a(3)*X2FIT;
    mesh(X1FIT,X2FIT,YFIT,'LineWidth',1.5)
    xlabel('\DeltaV [km/h]','FontAngle','oblique')
```

```matlab
ylabel('Grip [N]','FontAngle','italic')
zlabel(names(i),'FontName','Baskerville','FontSize',11)
title('Linear Regression','FontName','Calibri','FontWeight','Bold',...
    'FontSize',12)
text(.03,.97,.9,uistr1,'Units','normalized','FontSize',8,...
    'BackgroundColor',[1 1 .7])
colorbar('location','eastoutside')

% Regression Statistics
arsq = ['R_a_d_j^2 = ',num2str(adjrsquare1)];
arsq = cellstr(arsq);
text(.03,.91,.9,arsq,'Units','normalized','FontSize',8,...
    'BackgroundColor',[1 1 .7])

% Colorbar Title
text(.96,1.03,.9,scale(i),'Units','normalized','FontSize',10)

view(50,10)
hold off

%% Nonlinear2 regression graphs
figure(i+10)
% Scatterplot of the measured data
scatter3(vel,grip,data(:,i),'filled')
hold on
% Mesh surface of the predicted IARVs
[X1FIT,X2FIT] = meshgrid(velocity,gripstr);
YFIT = b(1) + b(2)*X1FIT + b(3)*X2FIT + b(4)*X1FIT.^2 + b(5)*X2FIT.^2;
mesh(X1FIT,X2FIT,YFIT,'LineWidth',1.5)
xlabel('\DeltaV [km/h]','FontAngle','oblique')
ylabel('Grip [N]','FontAngle','italic')
zlabel(names(i),'FontName','Baskerville','FontSize',11)
title('Pure Quadratic Regression','FontName','Calibri',...
    'FontWeight','Bold','FontSize',12)
text(.03,.97,.9,uistr2,'Units','normalized','FontSize',8,...
    'BackgroundColor',[1 1 .7])
colorbar('location','eastoutside')

% Regression Statistics
arsq = ['R_a_d_j^2 = ',num2str(adjrsquare2)];
arsq = cellstr(arsq);
text(.03,.91,.9,arsq,'Units','normalized','FontSize',8,...
    'BackgroundColor',[1 1 .7])

% Colorbar Title
text(.96,1.03,.9,scale(i),'Units','normalized','FontSize',10)

view(50,10)
hold off

%% Nonlinear3 regression graphs
figure(i+20)
% Scatterplot of the measured data
scatter3(vel,grip,data(:,i),'filled')
hold on
% Mesh surface of the predicted IARVs
[X1FIT,X2FIT] = meshgrid(velocity,gripstr);
YFIT = c(1) + c(2)*X1FIT.^2 + c(3)*X2FIT.^2;
mesh(X1FIT,X2FIT,YFIT,'LineWidth',1.5)
xlabel('\DeltaV [km/h]','FontAngle','oblique')
ylabel('Grip [N]','FontAngle','italic')
zlabel(names(i),'FontName','Baskerville','FontSize',11)
title('Modified Quadratic Regression','FontName','Calibri',...
```

```matlab
    'FontWeight','Bold','FontSize',12)
text(.03,.97,.9,uistr3,'Units','normalized','FontSize',8,...
    'BackgroundColor',[1 1 .7])
colorbar('location','eastoutside')

% Regression Statistics
arsq = ['R_a_d_j^2 = ',num2str(adjrsquare3)];
arsq = cellstr(arsq);
text(.03,.91,.9,arsq,'Units','normalized','FontSize',8,...
    'BackgroundColor',[1 1 .7])

% Colorbar Title
text(.96,1.03,.9,scale(i),'Units','normalized','FontSize',10)

view(50,10)
hold off

%% Nonlinear4 regression graph
figure(i+30)
% Scatterplot of the measured data
scatter3(vel,grip,data(:,i),'filled')
hold on
% Mesh surface of the predicted IARVs
[X1FIT,X2FIT] = meshgrid(velocity,gripstr);
YFIT = d(1) + d(2)*X1FIT + d(3)*X2FIT + d(4)*X1FIT.^2 + d(5)*X1FIT.*X2FIT...
    + d(6)*X2FIT.^2;
mesh(X1FIT,X2FIT,YFIT,'LineWidth',1.5)
xlabel('\DeltaV [km/h]','FontAngle','oblique')
ylabel('Grip [N]','FontAngle','italic')
zlabel(names(i),'FontName','Baskerville','FontSize',11)
title('Quadratic Regression with Interaction Terms','FontName','Calibri',...
    'FontWeight','Bold','FontSize',12)
text(.03,.97,.9,uistr4,'Units','normalized','FontSize',8,...
    'BackgroundColor',[1 1 .7])
colorbar('location','eastoutside')

% Regression Statistics
arsq = ['R_a_d_j^2 = ',num2str(adjrsquare4)];
arsq = cellstr(arsq);
text(.03,.91,.9,arsq,'Units','normalized','FontSize',8,...
    'BackgroundColor',[1 1 .7])

% Colorbar Title
text(.96,1.03,.9,scale(i),'Units','normalized','FontSize',10)

view(50,10)
hold off

%% Nonlinear5 regression graph
figure(i+40)
% Scatterplot of the measured data
scatter3(vel,grip,data(:,i),'filled')
hold on
% Mesh surface of the predicted IARVs
[X1FIT,X2FIT] = meshgrid(velocity,gripstr);
YFIT = e(1) + e(2)*X1FIT + e(3)*X2FIT + e(4)*X1FIT.^2 + e(5)*X1FIT.*X2FIT...
    + e(6)*X2FIT.^2 + e(7)*X1FIT.^3 + e(8)*X1FIT.^2.*X2FIT...
    + e(9)*X1FIT.*X2FIT.^2 + e(10)*X2FIT.^3;
mesh(X1FIT,X2FIT,YFIT,'LineWidth',1.5)
xlabel('\DeltaV [km/h]','FontAngle','oblique')
ylabel('Grip [N]','FontAngle','italic')
zlabel(names(i),'FontName','Baskerville','FontSize',11)
title('Cubic Regression with Interaction Terms','FontName','Calibri',...
```

```matlab
    'FontWeight','Bold','FontSize',12)
text(.03,.97,.9,uistr5,'Units','normalized','FontSize',8,...
    'BackgroundColor',[1 1 .7])
colorbar('location','eastoutside')

% Regression Statistics
arsq = ['R_a_d_j^2 = ',num2str(adjrsquare5)];
arsq = cellstr(arsq);
text(.03,.91,.9,arsq,'Units','normalized','FontSize',8,...
    'BackgroundColor',[1 1 .7])

% Colorbar Title
text(.96,1.03,.9,scale(i),'Units','normalized','FontSize',10)

view(50,10)
hold off
end

% Building output data columns of the goodness of fit statistics by IARV
coeff = {coeff1 coeff2 coeff3 coeff4 coeff5};
SSE = {SSE1' SSE2' SSE3' SSE4' SSE5'};
RSQ = {RSQ1' RSQ2' RSQ3' RSQ4' RSQ5'};
AdjRSQ = {AdjRSQ1' AdjRSQ2' AdjRSQ3' AdjRSQ4' AdjRSQ5'};
DOF = {DOF1' DOF2' DOF3' DOF4' DOF5'};
RMSE = {RMSE1' RMSE2' RMSE3' RMSE4' RMSE5'};
IARV = {'HIC','Omega','Alpha','NIC ten neg','NIC ten pos',...
    'NIC shear neg','NIC shear pos','NIC bend neg', ...
    'NIC ben pos','Sum Nij'};
regName = {'LinReg1','Nonlin2','Nonlin3','Nonlin4','Nonlin5'};

%% Write to Excel file
for i = 1:5
build = [coeff{i},SSE{i},RSQ{i},AdjRSQ{i},DOF{i},RMSE{i}];
xlswrite('Regression Results2.xlsx',build,char(regName(i)));
end
```

SurFitReg3.m

```matlab
function [fitresult, gof] = SurFitReg3(vel, grip, outputs)
%CREATESURFACEFITS(VEL,GRIP,OUTPUTS)
%  Fit surfaces to data.
%
%  Data for 'Linear1' fit:
%      X Input : vel
%      Y Input : grip
%      Z Output: outputs
%  Data for 'Nonlinear2' fit:
%      X Input : vel
%      Y Input : grip
%      Z Output: outputs
%  Data for 'Nonlinear3' fit:
%      X Input : vel
%      Y Input : grip
%      Z Output: outputs
%  Data for 'Nonlinear4' fit:
%      X Input : vel
%      Y Input : grip
%      Z Output: outputs
%  Data for 'Nonlinear5' fit:
%      X Input : vel
%      Y Input : grip
%      Z Output: outputs
%  Output:
%      fitresult : a cell-array of sfit objects representing the fits.
%      gof : structure array with goodness-of fit info.
%
%  See also FIT, SFIT.

%  Auto-generated by MATLAB on 30-Mar-2011 00:02:46

%% Initialization.

% Initialize arrays to store fits and goodness-of-fit.
fitresult = cell( 6, 1 );
gof = struct( 'sse', cell( 6, 1 ), ...
    'rsquare', [], 'dfe', [], 'adjrsquare', [], 'rmse', [] );

%% Fit: 'Linear1'.
[xInput, yInput, zOutput] = prepareSurfaceData( vel, grip, outputs );

% Set up fittype and options.
ft = fittype( 'poly11' );
opts = fitoptions( ft );

% Fit model to data.
[fitresult{1}, gof(1)] = fit( [xInput, yInput], zOutput, ft, opts );

%% Fit: 'Nonlinear2'.
[xInput, yInput, zOutput] = prepareSurfaceData( vel, grip, outputs );

% Set up fittype and options.
ft = fittype( 'a + b*x + c*y + d*x^2 + e*y^2', 'indep', {'x', 'y'},...
    'depend', 'z' );
opts = fitoptions( ft );
opts.Algorithm = 'Levenberg-Marquardt';
```

```matlab
opts.Display = 'Off';
opts.Lower = [-Inf -Inf -Inf -Inf -Inf];
opts.Robust = 'LAR';
opts.StartPoint = [0.430523507828261 0.351644439514934...
    0.383101294733604 0.53526728749686 0.965677560444338];
opts.Upper = [Inf Inf Inf Inf Inf];

% Fit model to data.
[fitresult{2}, gof(2)] = fit( [xInput, yInput], zOutput, ft, opts );

%% Fit: 'Nonlinear3'.
[xInput, yInput, zOutput] = prepareSurfaceData( vel, grip, outputs );

% Set up fittype and options.
ft = fittype( 'a + b*x^2 + c*y^2', 'indep', {'x', 'y'},...
    'depend', 'z' );
opts = fitoptions( ft );
opts.Algorithm = 'Levenberg-Marquardt';
opts.Display = 'Off';
opts.Lower = [-Inf -Inf -Inf];
opts.Robust = 'LAR';
opts.StartPoint = [0.0471362399179591 0.88993761404486...
    0.29668767002079];
opts.Upper = [Inf Inf Inf];

% Fit model to data.
[fitresult{3}, gof(3)] = fit( [xInput, yInput], zOutput, ft, opts );

%% Fit: 'Nonlinear4'.
[xInput, yInput, zOutput] = prepareSurfaceData( vel, grip, outputs );

% Set up fittype and options.
ft = fittype( 'poly22' );
opts = fitoptions( ft );
opts.Lower = [-Inf -Inf -Inf -Inf -Inf -Inf];
opts.Upper = [Inf Inf Inf Inf Inf Inf];

% Fit model to data.
[fitresult{4}, gof(4)] = fit( [xInput, yInput], zOutput, ft, opts );

%% Fit: 'Nonlinear5'.
[xInput, yInput, zOutput] = prepareSurfaceData( vel, grip, outputs );

% Set up fittype and options.
ft = fittype( 'poly33' );
opts = fitoptions( ft );
opts.Lower = [-Inf -Inf -Inf -Inf -Inf -Inf -Inf -Inf -Inf -Inf];
% opts.Robust = 'Bisquare';
opts.Upper = [Inf Inf Inf Inf Inf Inf Inf Inf Inf Inf];

% Fit model to data.
[fitresult{5}, gof(5)] = fit( [xInput, yInput], zOutput, ft, opts );
```